



SENIOR DESIGN:  
MAE 4351 Project

Ref.: MAE 4351-001-2021  
Date: 09. Jul. 2023  
Name: **Gayathri Kola**  
Status: In Progress

Designing a Hypersonic Spirit of St. Louis: Aerodynamics, Stability and Control Study

**Signatures:**

	Name:	Signature:	Dept.:	Date:
Author:	Gayathri Kola		MAE	7/9/2023
Seen:	Dr. Bernd Chudoba		MAE	

**Summary:**

Summarize your report here (This will be your abstract). Use this document as a template if you are using Microsoft Word 2001 or later for Windows, or Word X or later for Mac OS X. The style for this paragraph should be the “Abstract” style. Otherwise, use this document as an instruction set. Anywhere between five and one hundred articles might appear in a volume of an academic journal, so it is important to have a concise abstract that outlines your work so people will read it. There are several questions that you will want to answer in the abstract. What is the report about? What is the objective of the study/project? In a few sentences, what were the major results obtained? What are your conclusions from the study/project? Define all symbols used in the abstract. The abstract should be self-contained (i.e. it should not contain references to sources, figures, tables, or equations). It can contain numerical results. It is also left-right justified with 0.5" margins. Make sure the bottom of the table in this page does not cross into the next page. You will have to delete some lines below.

Replace the Maverick Aero Space logo in the upper right-hand corner with your team’s logo.

**Distribution:**

Institution:	Dept.:	Name:
The University of Texas at Arlington	MAE	Dr. Bernd Chudoba



SENIOR DESIGN:  
MAE 4351 Project

Ref.: MAE 4351-001-2021  
Date: 09. Jul. 2023  
Name: **Gayathri Kola**  
Status: In Progress

### Work Disclosure Statement

The work I performed to document the results presented in this report was performed by me, or it is otherwise acknowledged.

**Date:** 7/9/2023

**Signature:**

A handwritten signature in black ink, appearing to read "Gayathri".



## Table of Contents

WORK DISCLOSURE STATEMENT .....	2
LIST OF FIGURES.....	5
LIST OF TABLES.....	6
NOMENCLATURE .....	7
1 INTRODUCTION .....	8
1.1 BACKGROUND ON PLANES .....	8
1.2 PROJECT OVERVIEW .....	11
1.3 TEAM STRUCTURE AND BREAKDOWN.....	12
2 LITERATURE REVIEW .....	13
2.1 HYPERSONIC REVIEW.....	13
2.2 STABILITY AND CONTROL RESOURCE LIST.....	14
2.3 AERODYNAMICS RESOURCE LIST .....	15
3 CONCEPTUAL DESIGN BREAKDOWN .....	16
3.1 PARAMETRIC SIZING .....	17
3.2 CONFIGURATION LAYOUT .....	18
3.3 CONFIGURATION EVALUATION .....	19
4 STABILITY AND CONTROL.....	20
4.1 BACKGROUND .....	20
4.2 VOLUME COEFFICIENT APPROACH .....	22
4.3 CONTROL SURFACE SIZING .....	23
4.4 FLIGHT CONDITIONS TO ADDRESS .....	25
4.5 AXIS SYSTEMS .....	29
4.6 STATIC STABILITY .....	30
4.7 DYNAMIC STABILITY .....	31
4.8 LONGITUDINAL STABILITY.....	31
4.9 METHODOLOGY FOR STABILITY AND CONTROL DERIVATIVES .....	32
4.10 VALIDATION METHODS.....	37
4.11 RESULTS, VERIFICATION AND DISCUSSION FOR S&C.....	37
5 AERODYNAMICS.....	37
5.1 BACKGROUND .....	37
5.2 METHODOLOGY FOR AERODYNAMICS IN PS.....	40
5.3 METHODOLOGY FOR CL AND CE .....	50
5.4 VALIDATION METHODS.....	50
5.5 RESULTS, VERIFICATION AND DISCUSSION FOR AERODYNAMICS.....	52
6 HISTORICAL DEVELOPMENT.....	52
6.1 WEEK 1.....	52
6.2 WEEK 2.....	53
6.3 WEEK 3.....	53
6.4 WEEK 4.....	53
6.5 WEEK 5.....	53
APPENDIX .....	53
APPENDIX A .....	53
APPENDIX B.....	56



APPENDIX C .....	56
APPENDIX D .....	62
REFERENCES .....	67

## List of Figures

Fig. 1 The Spirit of St. Louis was built back in 1927 [1].....	8
Fig. 2 The Gulfstream G700 was launched in 2020 [3].....	9
Fig. 3 The SR-71 Blackbird was built in 1964 [4].....	9
<b>Fig. 4 Hermeus Quarterhorse, expected flight in 2024 [5].</b>	10
Fig. 5 Hermeus Darkhorse, expected to launch in 2025 [7].....	10
Fig. 6 Hermeus Halcyon with drooped wings is expected to launch in 2029 [9].	11
<b>Fig. 7 Hypersonic Spirit of St. Louis progression [10].</b>	12
Fig. 8 Atlantix logo created by Wesley Junell [11].	12
Fig. 9 Atlantix team structure by Noah Blakely [12].....	13
<b>Fig. 10 Different aircraft configurations for hypersonic vehicle concepts [HYFAC]</b>	13
<b>Fig. 11 Concorde and Tupolev Tu-144 [13].</b>	14
Fig. 12 Aircraft design phases [20].....	17
Fig. 13 Wight and volume budgets for convergence [36].....	18
<b>Fig. 14 Stability and Control IDA for CL.</b>	19
<b>Fig. 15 Stability and Control CE IDA.</b>	20
<b>Fig. 16 Stable, unstable, and neutral equilibrium [27].</b>	21
<b>Fig. 17 Stability and Control overview.</b>	21
<b>Fig. 18 Types of tail configurations available to the designer [29].</b>	22
<b>Fig. 19 Canard designs on supersonic aircraft.</b>	24
<b>Fig. 20 Elevons features in supersonic and hypersonic aircraft.</b>	24
<b>Fig. 21 High-speed aircrafts with twin vertical tails.</b>	25
<b>Fig. 22 Single vertical tail used in high-speed aircraft.</b>	25
<b>Fig. 23 Ground clearance required for takeoff rotation [23].</b>	26
<b>Fig. 24 Forces and moments during takeoff rotation [23].</b>	27
<b>Fig. 25 Asymmetric thrust condition [23].</b>	28
<b>Fig. 26 Control surface sizing IDA for CE</b>	29
<b>Fig. 27 Axis Systems with body frame</b>	30
<b>Fig. 28 Static stability requirements overview [30].</b>	31
<b>Fig. 29 Interactions between disciplines for longitudinal stability.</b>	32
<b>Fig. 30 Static stability assessment roadmap [30].</b>	33
<b>Fig. 31 Axis system and forces acting on a tailless wing-body [20].</b>	35
<b>Fig. 32 Spectrum of aerodynamic issues to address [53].</b>	38
<b>Fig. 33 Common types of delta wings [54].</b>	39
<b>Fig. 34 Lift formation due to free vortices on various aircraft bodies [Nicolai].</b>	40
<b>Fig. 35 Chart for determining constant for non-linear lift coefficient [20].</b>	41
<b>Fig. 36 Empirical charts to estimate maximum lift coefficient [25].</b>	43
<b>Fig. 37 Correlation for supersonic lift-curve-slope of delta wing-body configuration [HYFAC]</b>	44
<b>Fig. 38 Lift-to-drag relations for Mach numbers 2, 5 and 12.</b>	46
<b>Fig. 39 Concorde aerodynamic analysis geometric parameters [58].</b>	47
<b>Fig. 40 Mission profile chosen for PS phase created by Noah Blakely [12].</b>	50
<b>Fig. 41 Subsonic lift-curve-slope of Nicolai's method.</b>	51
<b>Fig. 42 XB-70 parasite drag test using Raymer's method.</b>	51
<b>Fig. 43 Zero-lift drag coefficient verification of XB-70 [Raymer].</b>	52
<b>Fig. 44 Assumptions to calculate pitching moment as a function of angle of attack from DATCOM [24].</b>	54
<b>Fig. 45 Specific wing-body geometry for calculating 3D lift-curve slope of the wing [24].</b>	54
<b>Fig. 46 Wing geometry parameter definitions [24].</b>	55
<b>Fig. 47 Method to find lift ratio for estimating pitching moments [24].</b>	55
<b>Fig. 48 Wing geometries presented to estimate the lift-curve slope [24].</b>	55

	<b>SENIOR DESIGN:</b> MAE 4351 Project	Ref.: MAE 4351-001-2021 Date: 09. Jul. 2023 Name: <b>Gayathri Kola</b> Status: In Progress
---	---	---

## List of Tables

Table 1. Selected Aircraft Characteristics .....	11
Table 2. Literature Review for Stability and Control. ....	14
Table 3. Literature Review for Aerodynamics. ....	15
Table 4. Important longitudinal and lateral stability derivatives .....	22
Table 5. Similar aircraft control surface dimensions [19,43–45].....	23
Table 6. Sign requirements for main stability derivatives [20].....	32
Table 7. Stability and Control derivatives in Jan Roskam [15,32,49] .....	35
Table 8. Stability and Control Verification Literature.....	37
Table 9. Concept vehicles aerodynamic estimates for PS phase. ....	39
Table 10. Aircraft with similar TOGW as our conceptual vehicles.....	42
Table 11. Data using Raymer's method for subsonic maximum lift coefficient [57].....	43
Table 12. The XB-70 data used for parasite drag verification [57]. .....	52

**Nomenclature**

$f_0$	= systems engineering and integration factor	$OEI$	= one engine inoperative
$f_1$	= technical development standard factor	$SM$	= static margin
$f_2$	= technical quality correlation factor	$LEX$	= leading edge extensions
$f_6$	= cost growth factor for schedule deviation	$AR$	= aspect ratio
$g$	= Earth's gravitational constant, m/s <sup>2</sup>	$TO$	= takeoff
$I_{sp}$	= specific impulse, sec	$T&P$	= trajectory and performance
$m$	= mass, kg	$T&P$	= trajectory and performance
$MR$	= mass ratio of stage	$T&P$	= trajectory and performance
$N$	= number of launch vehicles used	$T&P$	= trajectory and performance
$S$	= implementation strategy factor		
$\Delta V$	= change in velocity, m/s		
$\chi$	= mass split ratio		
$\varepsilon$	= stage structure factor		
$0$	= initial state		
$f$	= final state		

$HTHL$	= horizontal takeoff horizontal landing
$VTHL$	= vertical takeoff horizontal landing
$UAS$	= unmanned aerial system
$PAX$	= number of passengers
$IC$	= industry capability
$RBCC$	= rocket-based combined cycle
$TBCC$	= turbine-based combined cycle
$SSTC$	= single stage to cruise
$SSTO$	= single stage to orbit
$TSTO$	= two stage to orbit
$AB$	= all-body configuration
$WB$	= wing-body configuration
$BB$	= blended-body configuration
$SAS$	= stability augmentation system
$ACS$	= active control system
$FCS$	= flight control system
$HGV$	= hypersonic glide vehicle
$DOF$	= degree of freedom
$EOM$	= equations of motion
$PS$	= parametric sizing
$CL$	= configuration layout
$CE$	= configuration evaluation
$CD$	= conceptual design
$PD$	= preliminary design
$DD$	= detailed design
$C.G.$	= center of gravity
$COP$	= center of pressure
$TOGW$	= takeoff gross weight
$OEW$	= operating empty weight
$OWE$	= operating weight empty
$TPS$	= thermal protection system
$S&C$	= stability and control
$W&B$	= weights and balance
$T&P$	= trajectory and performance

	<b>SENIOR DESIGN:</b> MAE 4351 Project	Ref.: MAE 4351-001-2021 Date: 09. Jul. 2023 Name: <b>Gayathri Kola</b> Status: In Progress
---	---	---

## 1 Introduction

Hypersonic vehicle concepts are frequently emerging in today's market. This quest for a high-speed transport vehicle whether it be supersonic or hypersonic is rampant among commercial companies all over the world. While these vehicles do achieve top speeds, their range is often compromised due to their high fuel consumption.

The goal of this project is to perform a feasibility study for a hypothetical hypersonic Spirit of St. Louis with a wing-body configuration. The other competing teams will be addressing an all-body and a blended body configuration. For this reason, it is important to understand the background of the plane and the characteristics that made it possible to fly from New York to Paris, with a range of 4,100 miles, without any additional refueling back in 1927. Then, we will look into the progression of planes from the Spirit of St. Louis to hypersonic planes that are under development today.

### 1.1 Background on planes

#### 1.1.1 Spirit of St. Louis [1].

The Spirit of St. Louis, designed in 1927 by Donald A. Hall was one of a kind back in its era [2]. Piloted by Charles Lindbergh on a single-fueled flight from New York to Paris over the North Atlantic Ocean, this plane stayed in flight for an incredible 33 hours. It flew at a very low speed of 133 nautical miles (Mach 0.173) with a radial piston engine named Wright J-5C. This was a propeller-driven airplane with two blades and a rectangular wing connected to the fuselage by trusses. It had its landing gear intact with an aft tail containing elevators, a single vertical tail, and a rudder. The horizontal stabilizer was supported by smaller trusses. This tail dragger was a lightweight structure with a gross weight of approximately 2,888 lb.



Fig. 1 The Spirit of St. Louis was built back in 1927 [1].

#### 1.1.2 Gulfstream G700 [3]

The private jet Gulfstream G700 is a subsonic aircraft cruising at Mach 0.90 with a long range of 7,500 nautical miles. Its swept wing with winglets reduces aerodynamic drag thus improving its fuel efficiency and critical Mach number making flight close to sonic speed possible. Its slender fuselage is built to hold up to 13 passengers and sleeps 8 passengers. Its maximum cruise altitude is 51,000 ft. It has a T-tail configuration that helps avoid the downwash from the wing's plane. It has two Rolls-Royce Pearl 700 engines mounted at the aft section of the fuselage above the centerline. This has several benefits: reduces cabin noise, improves longitudinal stability at high speeds, the landing gear can be shorter, and if an engine fails, it wouldn't immediately harm the passengers.

	<b>SENIOR DESIGN:</b> MAE 4351 Project	Ref.: MAE 4351-001-2021 Date: 09. Jul. 2023 Name: <b>Gayathri Kola</b> Status: In Progress
---	---	---



**Fig. 2 The Gulfstream G700 was launched in 2020 [3].**

### 1.1.3 SR-71 Blackbird

This legendary aircraft set the speed record in 1964 at Mach 3.2 with its maximum speed capability classified. To this day, many projects are trying to beat this record with a Horizontal-Takeoff-Horizontal-Landing (HTHL) vehicle. Designed by the infamous Skunk Works chief engineer Clarence (Kelly) Johnson, new design thinking and re-engineering manufacturing made this reconnaissance plane possible. Its lightweight titanium alloy structure allowed it to withstand an incredible amount of heat generated while cruising at Mach 3.0. Its engines had to be combined: turbojet and ramjet in order to takeoff at a conventional runway. Its engine featured a 3D circular inlet with spikes that controlled the location of the normal shock wave. The addition of chines did a lot: they added lift, contributed to directional stability, and helped with avoiding the radar. Its high service ceiling and long-range kept it mostly undetectable.



**Fig. 3 The SR-71 Blackbird was built in 1964 [4].**

### 1.1.4 Darkhorse [5,6]

Hermeus is an aerospace startup based in Atlanta, Georgia with a target to make reusable hypersonic transport aircraft. The Hermeus Darkhorse will be the second iteration of the hypersonic Unmanned-Aerial-System (UAS), after its test iteration named Quarterhorse. The Quarterhorse, which is currently in development with an expected launch in 2024, also features a remote piloting capability [5]. Its expected maximum speed is at Mach 4+ intending to break the speed 50-year-old speed record set by the SR-71. Its propulsion system features a single Turbojet/Ramjet engine combination named Chimera. This engine contains a repurposed J85 turbojet engine to allow for takeoff at

runways before switching to ramjet at Mach 3.0. The Chimera is housed in the fuselage of the Quarterhorse, and the design features a wing-body configuration with an aft-tail section, single vertical tail, and highly swept delta wing.

The Darkhorse has a few distinguishable features compared to Quarterhorse. There is no aft tail, instead, the fuselage is extended further to mount twin vertical tails canted outward. The wing features multiple sweeps, with a high sweep on the front fuselage section (somewhat like chines) with a reduced sweep at the rear. Looks like a normal delta wing in the back with elevons on either side of the fuselage. Its propulsion system utilizes a Turbofan/Ramjet configuration instead of the turbojet, increasing its speed to Mach 5.0.

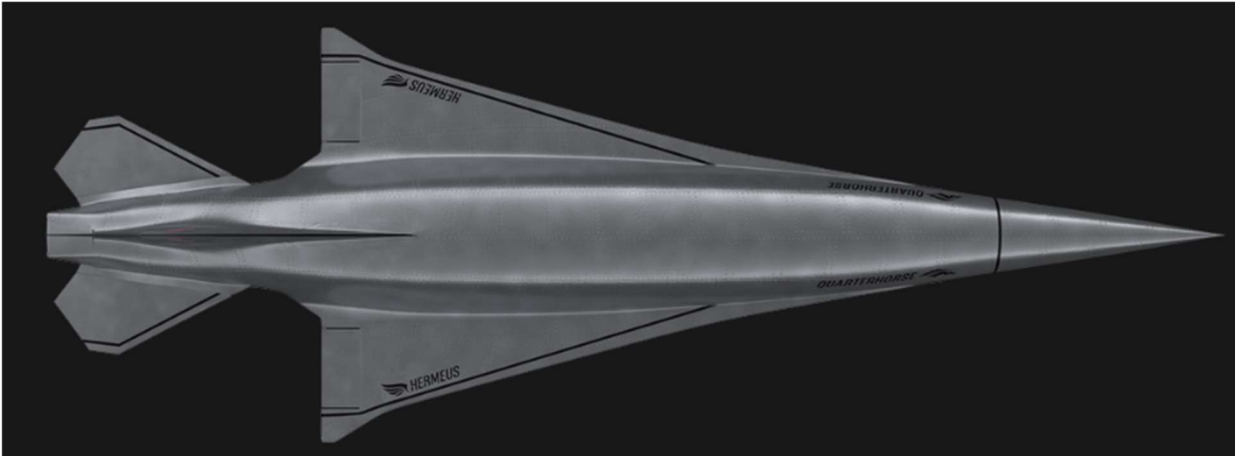


Fig. 4 Hermeus Quarterhorse, expected flight in 2024 [5].



Fig. 5 Hermeus Darkhorse, expected to launch in 2025 [7].

### 1.1.5 Halycon [8].

The last concept of Hermeus is the reusable hypersonic transport with a payload of 20 passengers and 2 crew as shown in Fig. 6. The unique design features a flat bottom and a slender bulged fuselage. It has a double delta wing with a high sweep in the forward fuselage section. Additionally, it also has drooped wing tips that add to directional stability and gives additional lift due to shock waves. It is to have two engines propelling to a speed of Mach 5.0, flying at an altitude of 90,000 ft. Its expected range is 4,600 miles, expected to make a flight from New York to Paris in 90 minutes. Its structure is made of titanium alloy with twin vertical tails similar to the Darkhorse. It is currently in development with an expected launch in 2029.

	<b>SENIOR DESIGN:</b> MAE 4351 Project	Ref.: MAE 4351-001-2021 Date: 09. Jul. 2023 Name: <b>Gayathri Kola</b> Status: In Progress
---	---	---



**Fig. 6 Hermeus Halcyon with drooped wings is expected to launch in 2029 [9].**

**Table 1. Selected Aircraft Characteristics**

Aircraft Name	Max Speed [mph]	Range [nmi]	Engine Type	Year	Crew, Passengers	Gross Weight [lb]
Spirit of St. Louis	133 (Mach 0.173)	3,600	Radial piston engine	1927	1, 0 PAX	2,888
Gulfstream	611 (Mach 0.925)	7,500	Pearl 700 Turbofan	2021	2, 13 PAX	56,365
SR-71 Blackbird	2,500 (Mach 3.00+)	2,824	J-58, TBCC	1964	1-2, 0 PAX	152,000
Darkhorse (UAS)	3,850 (Mach 5.000)		Turbofan-Ramjet	2025	0, 0 PAX	
Halcyon	3,850 (Mach 5.000)	4,600	"Ramburner"	2029	2, 20 PAX	

## 1.2 Project Overview

As mentioned earlier, the goal of this capstone project is to design a hypersonic aircraft that has the same range as the Spirit of St. Louis. Our team Atlantix is tasked with creating a wing-body hypersonic demonstrator that is of Industry Capability (IC). The aim is to create a solution space topology using a convergence methodology that screens all possible designs and produces a feasible baseline configuration. This solution space topology must also include the aircraft Gulfstream G700, Hermeus Darkhorse, and Halcyon. Finally, an overall market assessment of these vehicle designs must be conducted in terms of cost and technology available [10]. A mission profile must be made in agreement with the other two competing teams. The project's progress will be documented with weekly reports and presentations.

### 1.2.1 Mission Details [10]

The following are the mission details:

- The flight path must be similar to that of the Spirit of St. Louis.
- Has two main crew members: the pilot and the co-pilot. No additional crew members.
- Payload: 20 military personnel.
- Required solution spaces must be screened for designated trades. These are Mach numbers 5, 7.5, and 10.
- No rocket acceleration. That means the vehicle cannot be powered by either a rocket engine or Rocket-Based-Combined-Cycle (RBCC) engine.

### 1.2.2 Vehicle Details [10]

The following are the vehicle details:

- The engine must be of Turbine-Based-Combined-Cycle (TBCC). There are two vehicle designs: one with a single engine and the other with a twin engine. Both vehicles must have a 3D engine intake.
- Horizontal-Takeoff-Horizontal-Landing (HTHL) capability with Single-Stage-To-Cruise (SSTC).
- Fuel must be any form of Kerosene.
- Wing-body configuration for Atlantix.

<b>ATLANTIX</b>		SENIOR DESIGN: MAE 4351 Project	Ref.: MAE 4351-001-2021 Date: 09. Jul. 2023 Name: <b>Gayathri Kola</b> Status: In Progress
-----------------	--	------------------------------------	---

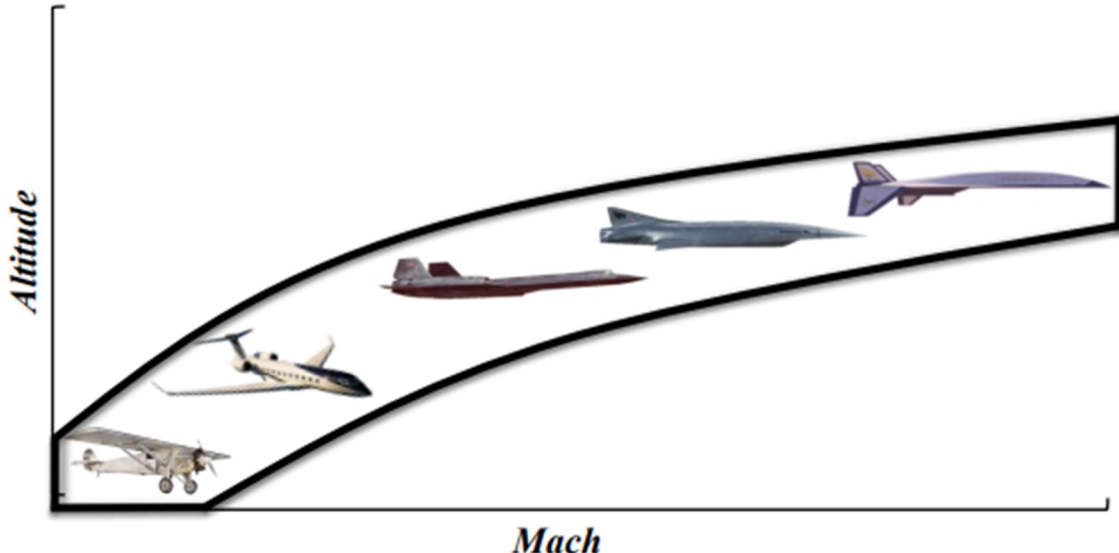


Fig. 7 Hypersonic Spirit of St. Louis progression [10].

### 1.3 Team Structure and Breakdown

The team name “Atlantix” was inspired by the transatlantic route the designed vehicle will take from New York to Paris over the North Atlantic Ocean. The following team logo was created by the Chief Engineer, Wesley Junell.



Fig. 8 Atlantix logo created by Wesley Junell [11].

The following in Fig. 9 below is the team structure and discipline breakdown created by team member Noah Blakely. There are 9 disciplines in total with some disciplines that have additional sub-disciplines such as Structures & Materials and Geometry & Weights. The focus of this report will be on Stability and Control, and Aerodynamics. The author is the Stability and Control team lead; hence this will be the primary discipline and Aerodynamics is the secondary discipline.

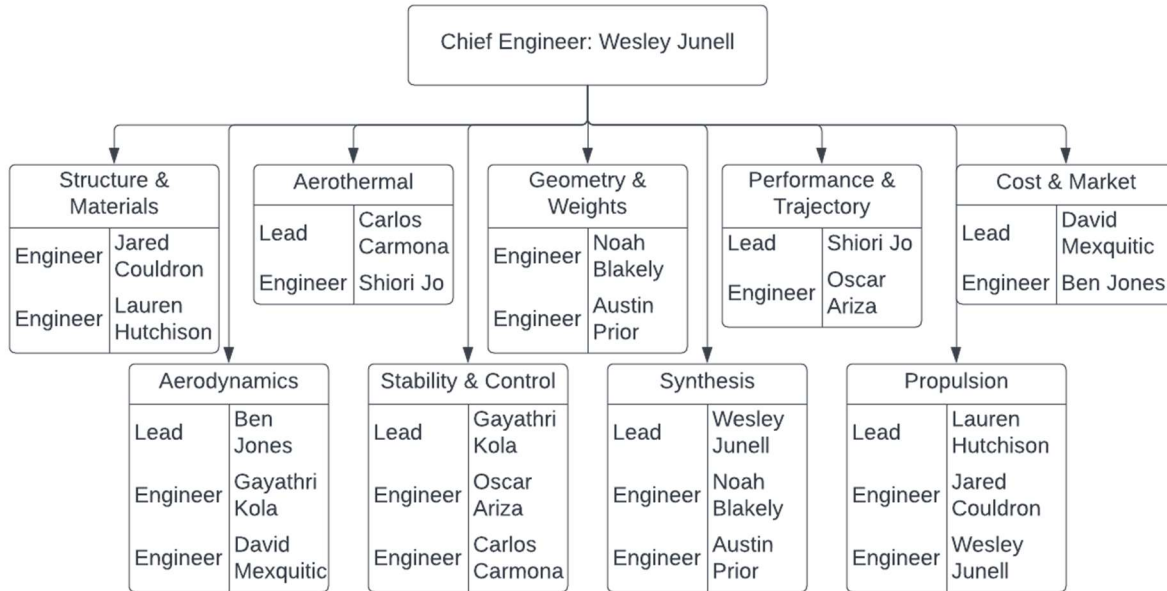


**Fig. 9** Atlantix team structure by Noah Blakely [12].

## 2 Literature Review

Before designing any new aircraft, it is essential to first perform an extensive literature review in order to find any similar aircraft configurations that can aid with the design process and validation. In this section, we will first have a brief review of Hypersonics, followed by past hypersonic aircraft programs, particularly the U.S. Air Force X planes.

### 2.1 Hypersonic Review

The following in Fig. 10 gives the distinction between Wing-Body (WB), Blended-Body (BB), and All-Body (AB). As illustrated, the WB configuration is less integrated with a set of distinct wings, engines, and fuselage. We will review the characteristics of an AB configuration aircraft – X-43A Hyper X, along with a WB configuration vehicle namely the Space Shuttle Orbiter. The weight of the Orbiter alone is significantly less compared to our concept aircraft, hence, other supersonic WB aircraft within similar weight categories will also be discussed.

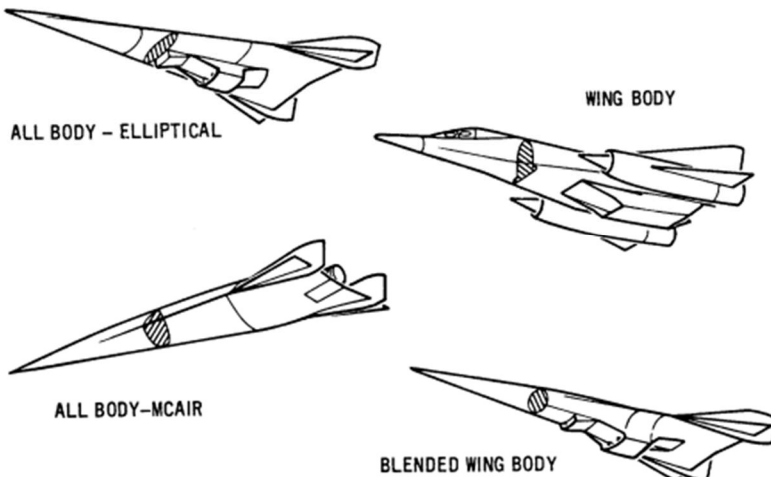


**Fig. 10** Different aircraft configurations for hypersonic vehicle concepts [HYFAC]

	<b>SENIOR DESIGN:</b> MAE 4351 Project	Ref.: MAE 4351-001-2021 Date: 09. Jul. 2023 Name: <b>Gayathri Kola</b> Status: In Progress
---	---	---

## 2.1.1 X-15

## 2.1.2 X-43A Hyper X

Pratt & Whitney scramjet engine SJY61.

## 2.1.3 Space Shuttle Orbiter

## 2.1.4 Wing-body Supersonic Transport

Apart from the Space Shuttle Orbiter, WB aircraft transport aircraft can be found in the supersonic regime. The most successful supersonic passenger aircraft was the Concorde.

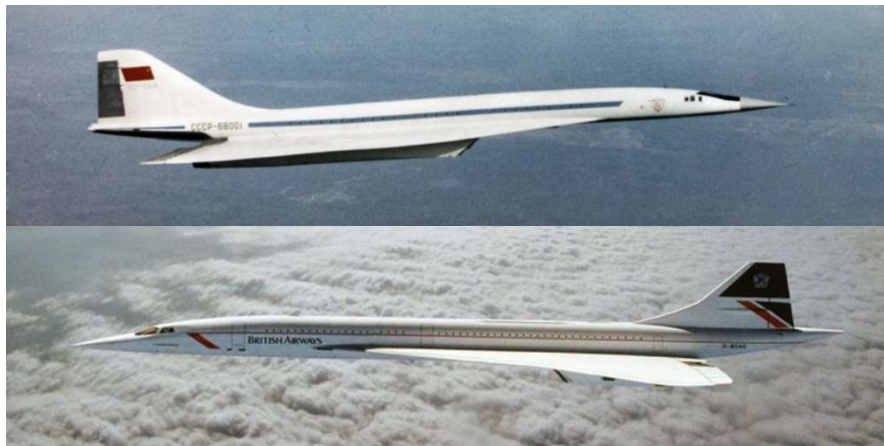


**Fig. 11 Concorde and Tupolev Tu-144 [13].**

## 2.2 Stability and Control Resource List

As mentioned in the mission details section, it is important to first build a Data-Base (DB) to begin the literature review process. To start, that means collecting all the relevant books, articles, journals, and conference papers for a particular aircraft, configuration, or component. Here, an initial search is performed for each discipline.

**Table 2. Literature Review for Stability and Control.**

Serial No.	Title	Author	Year	Category
1	Stability & Control of Conventional & Unconventional Aerospace Vehicle Configurations [14]	Chudoba, B.	2019	Book
2	Airplane Design Part VII: Determination of Stability, Control, and Performance Characteristics [15]	Roskam, J.	2017	Book
3	Stability and Control Estimation Flight Test Results for the SR-71 Aircraft with Externally Mounted Experiments [16]	Moes, T. R.	2002	Book
4	Flight Stability and Control and Performance Results from the Linear Aerospike SR-71 Experiment (LASRE) [17]	Moes, T. Et al.	1998	Conference Paper
5	Longitudinal Handling Qualities of the Tu-144LL Airplane and Comparisons with Other Large, Supersonic Aircraft [18]	Cox, T. H Marshall, A.	2000	Journal Article
6	Development of the Vehicle Configuration Compendium: A Comprehensive Data-Information-Knowledge System to Aid in High-Speed Vehicle Design [19]	Simon, S.	2021	Master's Thesis
7	Fundamentals of Aircraft and Airship Design. Volume I – Aircraft Design [20]	Nicolai, L. M. Carichner, G.	2010	Book
8	Aircraft Performance and Design [21]	Anderson, J.D	1999	Book
9	Introduction to Aircraft Flight Mechanics, Performance, Static Stability, Dynamic Stability, and Classical Feedback Control [22]	Yechout, T. R. Et al.	2003	Book
10	Aircraft Design: A Systems Engineering Approach [23]	Sadrrey, M. Hoak, D. E.	2013	Book
11	USAF Stability and Control DATCOM [24]	Finck, R. D	1978	Data Sheets

	<b>SENIOR DESIGN:</b> <b>MAE 4351 Project</b>	Ref.: MAE 4351-001-2021 Date: 09. Jul. 2023 Name: <b>Gayathri Kola</b> Status: In Progress
---	--	---

12	Aircraft Design: A Conceptual Approach [25]	Raymer, D.	2018	Book
13	Airplane Flight Dynamics and Automatic Flight Controls [26]	Roskam, J.	1998	Book
14	Mechanics of Flight [27]	Philips, W. F	2004	Book
15	On Stability and Control of Hypersonic Vehicles [28]	Coleman, C. C	2009	Review
16	A Generic Stability and Control Tool for Conceptual Design Prototype System Overview [29]	Faruqi, F. A		Paper
17	A Generic Stability and Control Tool for Flight Vehicle Conceptual Design: AeroMech Software Development [30].	Coleman, G.	2007	Conference
		Chudoba, B.		Paper
		Coleman, G.	2007	Master's thesis

### 2.2.1 USAF Stability and Control DATCOM [24].

This document is a database containing equations for stability and control derivatives at various speed regimes ranging from subsonic to hypersonic. However, upon further review, it appears that coverage for hypersonic equations is fairly limited, only two derivatives were found to have equations solely for hypersonic speeds. Further, these equations are for wing and tail-body configurations only. A software version of this database is available online which requires knowledge of the programming language: FORTRAN. The author is currently looking into the way this resource can be used.

### 2.2.2 On Stability and Control of Hypersonic Vehicles [28].

This paper explains the most common issues associated with the stability and control of hypersonic vehicles and emphasizes the need for an Active-Control-System (ACS) or Stability-Augmentation-System (SAS). One caveat is that this paper primarily discusses hypersonic missiles and Hypersonic Glide Vehicle (HGV). It gives basic information on the range for L/D for supersonic and hypersonic vehicles and also explains how lift and drag coefficients remain constant for speeds over Mach 6.

### 2.2.3 A Generic Stability & Control Tool for Conceptual Design Prototype System Overview [30].

The author of this thesis acknowledges the fact that stability and control analysis for novel designs is difficult, especially with limited data, and also time-consuming. A generic solution for stability and control analysis is presented called *AeroMech* and the software development and integration process are described. Techniques for analyzing control power for control surface sizing, static and dynamic stability derivatives, and 6-degree-of-freedom (DOF) trimmed equations-of-motion (EOM) are presented. Various tailplane configurations are presented, and critical flight conditions are discussed. Finally, the Appendix B of this thesis contains a user guide to Digital DATCOM that is simpler to read and follow.

### 2.2.4 Jan Roskam's Design Books

The author discovered simpler methodology that could be implemented within time in Jan Roskam's design books for S&C. The Part VI for the series gives extensive methods for calculating several types of steady state, stability, and control derivatives. This resource is being used currently to develop the S&C code for Configuration Evaluation (CE). If some of the methods are not applicable for supersonic and hypersonic flight, then DATCOM will be used to sort for the derivatives. The Part VII of the series gives flight conditions to address and methods for computation.

### 2.2.5 Resource 5

There was a need for understanding what types of control surfaces are suitable for hypersonic flight and how these can vary for Mach numbers of 5, 7.5 and 10. Additionally, since our vehicles are of two types: single and double flow path intakes, we wanted to see if there is any justification for what control surfaces to use.

## 2.3 Aerodynamics Resource List

Cross-reference is crucial when you are working with long reports and editing many different sections at once.

**Table 3. Literature Review for Aerodynamics.**

Serial No.	Title	Author	Year	Category
1	Fundamentals of Aerodynamics [31]	Anderson, J. D	2017	Book
2	Airplane Design Part VI: Preliminary Calculation of Aerodynamic, Thrust, and Power Characteristics, Vol 1 [32]	Roskam, J.	1987	Book
3	Aircraft Conceptual Design: An Adaptable Parametric Sizing Methodology [33]	Coleman, G.	2010	Thesis

	<b>SENIOR DESIGN:</b> <b>MAE 4351 Project</b>	Ref.: MAE 4351-001-2021 Date: 09. Jul. 2023 Name: <b>Gayathri Kola</b> Status: In Progress
---	--	---

4	Transatlantic Launcher Sizing (Chapter 16): Scramjet Propulsion [34]	Czysz, P. Jean, V.	2000	Book
5	Future Spacecraft Propulsion Systems and Integration: Enabling Technologies for Space Exploration [35]	Czysz, P. Et al.	2018	Book
6	Development of the Vehicle Configuration Compendium: A Comprehensive Data-Information-Knowledge System to Aid in High-Speed Vehicle Design [19]	Simon, S.	2021	Master's Thesis
7	Fundamentals of Aircraft and Airship Design. Volume I – Aircraft Design [20]	Nicolai, L. M. Carichner, G.	2010	Book
8	Hypersonic Convergence: Background and Methodology [36]	Ledford, T. Harris, C.	2023	Guest Lecture
9	Solution-Space Screening of a Hypersonic Endurance Demonstrator [37]	Chudoba, B. Et al	2012	Journal Article
10	Computational Methods in Hypersonic Aerodynamics [38]	Murthy, T.K.S	1991	Book
11	Aerodynamic Problems of Hypersonic Vehicles (AGARD) [39]	Enkenhus, K. Et al.	1972	Lecture Series
12	Hypersonic Flow [40]	Rasmussen, M.	1994	Book
13	Hypersonic and High-Temperature Gas Dynamics [41].	Anderson, J.	2006	Book

### 2.3.1 Fundamentals of Aerodynamics by John D. Anderson [31].

Chapter 14 of this text covers the basics of hypersonic aerodynamics. This resource can be especially useful to develop a background in this field before attempting to find a suitable methodology. The key takeaway from this chapter was understanding that the word hypersonic does not necessarily relate to Mach 5.0. There is nothing special about this number. The drag does not dramatically increase at Mach 5 when compared to the exponential rise at Mach 1.0. Many other factors go into characterizing hypersonic flow.

### 2.3.2 Development of the Vehicle Configuration Compendium, Simon. S [19]

This thesis is an excellent resource for getting started with the parameters required, and understanding the roles of a discipline in PS, CL, and CE. It is easy to get lost in a literature search when trying to design a novel airplane concept such as hypersonic transport. This thesis gives classifications for wing-body (WB), all-body (AB), and blended-body (BB) configurations. There are many hypersonic aircraft from the past that help identify the body configuration such as Sanger II, X-43A, and SR-71. A compilation of comparisons between such aircraft is made as an example for the development of their Vehicle Configuration Compendium (VCC) software. For the Aerodynamics team, this is a great starting point for the parameters of interest and how they are required by other disciplines.

### 2.3.3 Future Spacecraft Propulsion Systems and Integration [35]

In the PS phase, the Synthesis team has opted to use Hypersonic Convergence as their methodology. This book, along with Scramjet Propulsion by Czysz. P and Jean. V gives a lot of information on the equations needed for the convergence logic. For the Aerodynamics team, it gives a way to estimate an initial maximum lift-to-drag (L/D) based on the Mach number and the zero lift-drag coefficient. It becomes very useful for hypersonic vehicles where information is scarce very early in the design process.

### 2.3.4 Hypersonic Research Facilities Study Phase 2 Parametric Studies

This resource along with Gary Coleman's thesis on parametric methodology are considered for the estimation of aerodynamic coefficients. Specifically, there are methods for estimating the lift-to-drag ratio, lift estimation method, and lift-curve-slope empirical relations for delta WB combinations. Additionally, a drag estimation method is presented for high Mach number vehicle concepts.

### 2.3.5 Various Design Texts for PS: Raymer, Nicolai, Anderson

## 3 Conceptual Design Breakdown

The aircraft design pyramid starts with Conceptual Design (CD) at the top, followed by Preliminary Design (PD) and Detailed Design (DD). Since this project will be taking a multi-disciplinary approach to designing the hypersonic aircraft, it becomes essential to lay down the groundwork for the chosen convergence methodology.

	<b>SENIOR DESIGN:</b> <b>MAE 4351 Project</b>	Ref.: MAE 4351-001-2021 Date: 09. Jul. 2023 Name: <b>Gayathri Kola</b> Status: In Progress
---	--	---

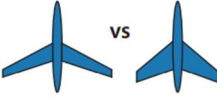
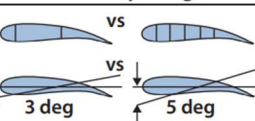
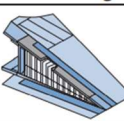
Phase 1 Conceptual Design		Phase 2 Preliminary Design	Phase 3 Detail Design
	vs		
<b>Known</b>	Basic Mission Requirements Range, Altitude, & Speed Basic Material Properties $\sigma/p$ $E/p$ $S/lb$	Aeroelastic Requirements Fatigue Requirements Flutter Requirements Overall Strength Requirements	Local Strength Requirements Producibility Functional Requirements
<b>Results</b>	Geometry Airfoil Type $R$ $t/c$ $\lambda$ $\Delta$	Design Objectives Drag Level Weight Goals Cost Goals	Basic Internal Arrangement Complete External Configuration <i>Camber &amp; Twist Distribution</i> <i>Local Flow Problems Solved</i> Major Loads, Stresses, Deflections
<b>Output</b>	Feasible Design	Mature Design	Shop Designs
<b>TRL</b>	2 – 3	4 – 5	6 – 7

Fig. 12 Aircraft design phases [20].

### 3.1 Parametric Sizing

In order to design an aircraft, we must first know the size of what is trying to be built. If the aircraft will be a fighter jet or a passenger transport. In the Parametric Sizing (PS) process, the aircraft is grossly sized using a method to converge to a solution. A solution space is created giving a visualization for the list of feasible designs. These feasible designs will be given to all disciplines. The Synthesis team has chosen to use Hypersonic Convergence as their sizing method.

#### 3.1.1 Hypersonic Convergence

Traditional convergence methods require defining many constraints to come up with a solution space. One such method is Loftin Sizing, where constraints such as stall speed, takeoff, and landing field length, and climb gradients are made. To size the aircraft, usually, first, the wing and engines are sized, and the empennage is added in the end. However, to design high-speed hypersonic aircraft, the sizing for wings, engines, and control efforts must be fully integrated to ensure optimal performance. For that reason, transitional methods become redundant as convergence becomes difficult. Hypersonic Convergence is a method that streamlines this process by fully integrating multiple design aspects into two main convergence equations. Before utilizing these equations (Fig.), the gross vehicle geometry must be known. Two new variables are introduced: slenderness ratio  $\tau$  and area ratio  $k_w$ . These parameters relate to the volume, planform area, and wetted area of the vehicle. The convergence process is iterated for a range of slenderness ratios to obtain an estimate of the Takeoff-Gross-Weight (TOGW), and the ratio of volume available to volume from variables OEW (Operating-Empty-Weight) and OWE (Operating-Weight-Empty). After the iteration process, and landing constraint is given, and a solution space is generated. For this, the Synthesis team will be creating a solution space code to output baseline design parameters such as TOGW, planform area, wing area, slenderness ratio, weight (OEW), and volume (OWE) budgets [36].

With these parameters, the disciplines can start to define the approximate wing area, engine size, horizontal and vertical tail areas, aspect ratios, components weights, overall aircraft weight, C.G. location, internal aircraft structure and loads, Thermal-Protection-System (TPS) weights, and approximate cost of the aircraft.

Several of the constants given in the equations in Fig. are estimated based on the type of aircraft being built, whether it is a Single-Stage-To-Orbit (SSTO) or Two-Stage-To-Orbit (TSTO).

	<b>SENIOR DESIGN:</b> <b>MAE 4351 Project</b>	Ref.: MAE 4351-001-2021 Date: 09. Jul. 2023 Name: <b>Gayathri Kola</b> Status: In Progress
---	--	---

### Weight budget

$$W_{OEW} = \frac{I_{str} K_w S_{pln} + C_{sys} + \frac{(T/W)_{Max} W_R}{E_{TW}} (W_{pay} + W_{crew}) + W_{cprv}}{1 + \mu_a - f_{sys}}$$

Structure      Geometry      Systems      Propulsion      Mission Requirements

### Volume budget

$$W_{OWE} = \frac{\tau S_{pln}^{1.5} (1 - k_{vv} - k_{vs}) - v_{fix} + N_{crw} (v_{crw} - k_{crw}) - W_{pay}/\rho_{pay}}{\frac{W_R - 1}{\rho_{ppl}} + (k_{ve} (T/W)_{Max} W_R)}$$

### Where:

$$W_{OWE} = W_{OEW} + W_{pay} + W_{crew}$$

**Fig. 13 Weight and volume budgets for convergence [36].**

Responsibilities of the Aerodynamics team in PS:

- Calculating L/D and giving it to the Performance/Propulsion team so they can calculate thrust requirements that will go into the Synthesis convergence logic. Additionally, to compute the lift and drag coefficients.

Responsibilities of the Stability/Control team in PS:

- Stability/Control is not involved in PS because this stage involves grossly sizing a vehicle, most variables (from Geometry, Weights, Thrust) are unknown to perform stability analysis.

### 3.2 Configuration Layout

Once a list of feasible designs is obtained from the PS phase, along with values for weight and volume to be allocated, the designs can be made in the CL phase. Here, the creativity of the multi-disciplinary design process comes into play. Each discipline will give its input on how best the geometry can be made based on mission criteria. For example, the Aerodynamics team may suggest having delta wings or modified versions of highly swept wings when laying a hypersonic aircraft. Then, the Propulsion team may suggest optimal engine placements and if the fuselage length needs to be extended based on the engine dimensions available. The Stability and Control team may input how many control effectors are needed based on historical data. A few designs are made with tweaks in geometries and placement of essential features. These designs are then evaluated in the final CE phase.

Responsibilities of the Aerodynamics team in CL:

- Coming up with a wing design: defining leading-edge sweep angles, shock angles, and fuselage length.
- Maximum lift coefficient,  $c_l_{max}$
- Estimating the wing area, canard area, horizontal tailplane area, and fuselage area ruling.
- Center of pressure location (or neutral point) in percent chord.
- Aerodynamic center in percent chord.

Responsibilities of the Stability/Control team in CL:

- Choosing control surfaces: number, layout, and placement.
- Common method using the Volume coefficient approach: looking through historical aircraft and making comparisons to gauge an approximate size of control effectors – output areas to Geometry & Synthesis.
- Computing maximum control surface deflection ranges.

The following in Fig. 14 is the Stability and Control IDA for CL.

	<b>SENIOR DESIGN:</b> MAE 4351 Project	Ref.: MAE 4351-001-2021 Date: 09. Jul. 2023 Name: <b>Gayathri Kola</b> Status: In Progress
---	---	---

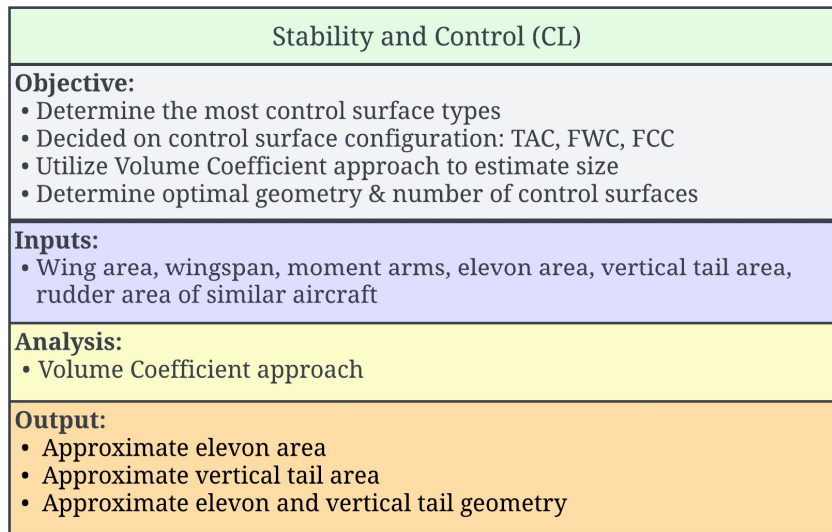


**Fig. 14 Stability and Control IDA for CL.**

### 3.3 Configuration Evaluation

The outputs from the CL phase are a list of feasible designs available. These designs will be evaluated for the entire mission profile during the CE phase. Many teams will be interacting with one another to meet different aspects of their discipline requirements. For example, the Stability and Control team must interact with the Propulsion team for thrust data and the WB team for C.G. location and placement to ensure adequate stability for the takeoff phase. Usually, the control surfaces will be sized based on the inputs provided by these teams for asymmetric thrust conditions, etc. Higher fidelity methods are typically used in CE to complete this analysis with the best accuracy. Finally, the Synthesis team will decide which discipline is important at a particular flight phase while meeting all basic discipline requirements.

Responsibilities of the Aerodynamics team in CE:

- Computing the total lift and drag forces, lift and drag coefficients, and induced drag coefficient.
- Lift-curve slopes, zero-lift drag coefficient.

Responsibilities of the Stability/Control team in CE:

- Assess the stability of the aircraft throughout the mission profile for all flight phases.
- Consider speed regimes to calculate longitudinal, lateral, and directional stability derivatives.
- Consider critical conditions as per MIL-SPEC requirements to size control surfaces.

The following in Fig. 15 is the CE IDA for Stability and Control discipline. Additional details will be added once method verification has been completed. The IDA template is credited to David Mexquitic [42].



Stability and Control (CE)	
<p><b>Takeoff</b></p> <p><b>Objective:</b></p> <ul style="list-style-type: none"> <li>• <b>Critical conditions:</b> OEI, Trim Drag, Takeoff Rotation</li> <li>• Interact with Propulsion, W&amp;B, Geometry, Aerodynamics, Synthesis to size control surfaces</li> <li>• Determine maximum elevon and rudder deflections</li> <li>• Assess static stability</li> </ul> <p><b>Inputs:</b> Propulsion: Thrust, Engine drag W&amp;B: C.G location Aerodynamics: neutral point or aerodynamic center Geometry &amp; Synthesis: TOGW, planform area, aircraft dimensions</p> <p><b>Analysis:</b></p> <ul style="list-style-type: none"> <li>• Longitudinal: Nicolai, Raymer</li> <li>• Lateral: Nicolai</li> <li>• Directional: Nicolai</li> </ul> <p><b>Output:</b></p> <ul style="list-style-type: none"> <li>• Maximum elevon and rudder deflection angles</li> <li>• Stability derivatives once stability is achieved</li> </ul>	<p><b>Climb</b></p> <p><b>Objective:</b></p> <ul style="list-style-type: none"> <li>• <b>Critical conditions:</b> Trim Drag</li> <li>• Interact with Synthesis, Geometry, Aerodynamics, W&amp;B to ensure less trim drag</li> <li>• Determine elevon and rudder deflections to trim</li> <li>• Assess static stability</li> </ul> <p><b>Inputs:</b> Aerodynamics: neutral point or aerodynamic center W&amp;B: C.G location Geometry: aircraft dimensions</p> <p><b>Analysis:</b></p> <ul style="list-style-type: none"> <li>• Longitudinal: Nicolai, Raymer</li> <li>• Lateral: Nicolai</li> <li>• Directional: Nicolai</li> </ul> <p><b>Output:</b></p> <ul style="list-style-type: none"> <li>• Maximum elevon and rudder deflection angles</li> <li>• Stability derivatives once stability is achieved</li> </ul>
<p><b>Cruise</b></p> <p><b>Objective:</b></p> <ul style="list-style-type: none"> <li>• <b>Critical conditions:</b> Trim Drag, One-Engine-Inoperative (OEI)</li> <li>• Interact with Propulsion, Synthesis, Geometry, Aerodynamics, W&amp;B to check for adequate control authority</li> <li>• Determine maximum elevon and rudder deflections</li> <li>• Assess static stability</li> </ul> <p><b>Inputs:</b> Propulsion: Thrust, Engine drag W&amp;B: C.G location Aerodynamics: neutral point or aerodynamic center Geometry &amp; Synthesis: TOGW, planform area, aircraft dimensions</p> <p><b>Analysis:</b></p> <ul style="list-style-type: none"> <li>• Longitudinal: Nicolai, Raymer</li> <li>• Lateral: Nicolai</li> <li>• Directional: Nicolai</li> </ul> <p><b>Output:</b></p> <ul style="list-style-type: none"> <li>• Maximum elevon and rudder deflection angles</li> <li>• Stability derivatives once stability is achieved</li> </ul>	<p><b>Landing</b></p> <p><b>Objective:</b></p> <ul style="list-style-type: none"> <li>• <b>Critical conditions:</b> Trim Drag, Crosswind landing</li> <li>• Interact with Propulsion, Synthesis, Geometry, Aerodynamics, W&amp;B to check for adequate control authority</li> <li>• Determine elevon and rudder deflections to trim</li> <li>• Assess static stability</li> </ul> <p><b>Inputs:</b> Aerodynamics: neutral point or aerodynamic center W&amp;B: C.G location Geometry: aircraft dimensions</p> <p><b>Analysis:</b></p> <ul style="list-style-type: none"> <li>• Longitudinal: Nicolai, Raymer</li> <li>• Lateral: Nicolai</li> <li>• Directional: Nicolai</li> </ul> <p><b>Output:</b></p> <ul style="list-style-type: none"> <li>• Maximum elevon and rudder deflection angles</li> <li>• Stability derivatives once stability is achieved</li> </ul>

**Fig. 15 Stability and Control CE IDA.**

## 4 Stability and Control

### 4.1 Background

Before beginning with any methodology, it is important to give some background on stability and control, and its role in aircraft design. The stability of an aircraft can be broken down into four main speed regimes, namely subsonic, transonic, supersonic, and hypersonic. It also depends on the kind of body configuration we are looking at; whether it is a wing-body, all-body, or a blended body. Most information is available for calculating the stability derivatives of the subsonic regime. Additionally, aircraft stability can be split into two main categories: static stability and dynamic stability.

	<b>SENIOR DESIGN:</b> <b>MAE 4351 Project</b>	Ref.: MAE 4351-001-2021 Date: 09. Jul. 2023 Name: <b>Gayathri Kola</b> Status: In Progress
---	--	---

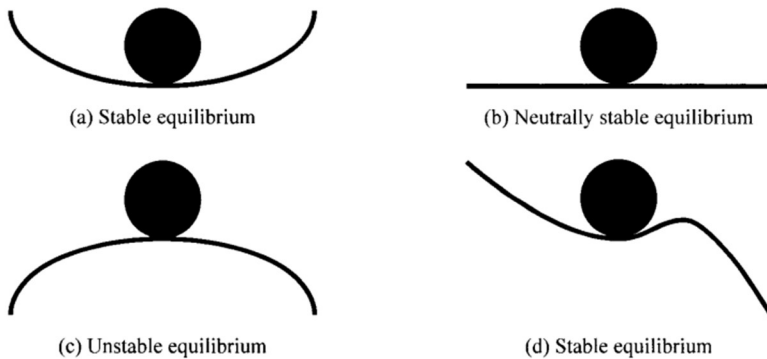


**Fig. 16 Stable, unstable, and neutral equilibrium [27].**

Static stability relates to when an aircraft inherently returns to its equilibrium position when disturbed by external forces due to its weight distribution. When an aircraft continues to deviate from equilibrium, meaning it is unstable in straight-line flight, it is known to have static instability. Most transport aircraft are designed to have static stability and these requirements are given in documents such as FAR 23, FAR 25, and MIL-SPEC-1797.

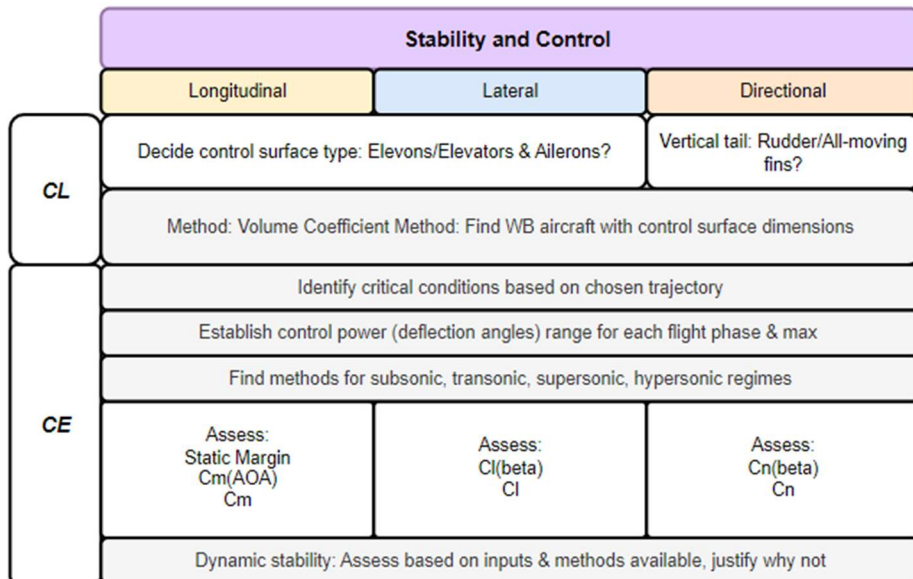


**Fig. 17 Stability and Control overview.**

During conceptual design phase, static stability will be of primary consideration. Dynamic stability analysis requires more detailed data and accuracy is limited this early in design phase.

After looking at the basics of Stability and Control, it is essential to look into the various kinds of tail configuration options available to the designer. The following Fig. shows the various types of tail configurations in general.

TAC	T ail-A ft C onfiguration	sym m etric
TFC	T ail-F irst C onfiguration	sym m etric
TSC	T hree-S urface C onfiguration	sym m etric
FWC	F lying-W ing C onfiguration	sym m etric
OWC	O blique-W ing C onfiguration	asym m etric
OFWC	O blique F lying-W ing C onfiguration	asym m etric

Tail-Aft Configuration	Tail-First Configuration	Three-Surface Configuration	Flying-Wing Configuration	Oblique-Wing Configuration	Oblique-Flying-Wing Configuration
					

Fig. 18 Types of tail configurations available to the designer [29].

The most common stability derivatives are given below in table:

**Table 4. Important longitudinal and lateral stability derivatives**

Symbol	Parameter Name	Category
$C_{L\alpha}$	Variation of lift coefficient with angle of attack	Longitudinal
$C_{D\alpha}$	Variation of drag coefficient with angle of attack	Longitudinal
$C_{m\alpha}$	Variation of pitching moment coefficient with angle of attack	Longitudinal
$C_{Lq}$	Variation of lift coefficient with pitch rate	Longitudinal
$C_{mq}$	Variation of pitching moment coefficient with pitch rate	Longitudinal
$C_{Y\beta}$	Variation of sideforce coefficient with angle of sideslip	Directional
$C_{l\beta}$	Variation of rolling moment coefficient with angle of sideslip	Lateral
$C_{n\beta}$	Variation of yawing moment coefficient with angle of sideslip	Directional
$C_{Yp}$	Variation of sideforce coefficient with roll rate	Lateral
$C_{lp}$	Variation of rolling moment coefficient with roll rate	Lateral
$C_{np}$	Variation of yawing moment coefficient with roll rate	Lateral
$C_{Yr}$	Variation of sideforce coefficient with yaw rate	Directional
$C_{lr}$	Variation of rolling moment coefficient with yaw rate	Directional
$C_{nr}$	Variation of yawing moment coefficient with yaw rate	Directional

#### 4.2 Volume Coefficient Approach

One of the most common methods used to estimate the size of control surfaces is by a method known as the volume coefficient method. In this method, similar aircraft are chosen where control surface dimensions are available. It gives a means of comparison to get a base estimate when the C.G. location of the aircraft is unknown in CL phase. The following is the way to calculate volume coefficient below [23].

$$\bar{c}_{HT} = \frac{S_{HT} l_{HT}}{S_{ref} b} \quad (1)$$

$$\bar{c}_{VT} = \frac{S_{VT} l_{VT}}{S_{ref} b} \quad (2)$$

	<b>SENIOR DESIGN:</b> <b>MAE 4351 Project</b>	Ref.: MAE 4351-001-2021 Date: 09. Jul. 2023 Name: <b>Gayathri Kola</b> Status: In Progress
---	--	---

The following are the aircraft that are the most similar to the mission. Hypersonic vehicles with wing-body configuration are rare and difficult to find. Supersonic vehicles with WB configurations such as Concorde and XB-70 were considered for comparison purposes as well.

**Table 5. Similar aircraft control surface dimensions [19,43–45].**

Aircraft Name	Speed (M)	Body Type	Tail Volume (VT)	Tail Volume (HT)	Elevon Area [ft <sup>2</sup> ]	Vertical Tail Area [ft <sup>2</sup> ]	Wingspan [ft]	Fuselage Length [ft]
Concorde	2.1	WB	0.045	0.095	172.20	365.00	83.80	184.50
TU-144	2.1	WB				717.80	94.50	215.50
XB-70	3.0	WB	0.031	0.037	197.70	233.96	150.00	185.75
Space Shuttle	25	WB	0.078	0.154	210.00	413.25	78.06	122.26
SR-71	3.0	BB	0.051	0.084	91.50	150.76	55.70	107.42

\*NASP X-30 was originally intended to be Mach 25 capability vehicle that was cancelled due to cost increments [19]. Note, the dimensions obtained are for space shuttle elevon area is for single side [44]. Similarly, for the SR-71, the elevon area is the combination of the inboard and outboard areas of a single side. The vertical tail area is for a single tail [46].

#### 4.3 Control Surface Sizing

The control surface sizing is done in the CE phase once a rough geometry is obtained from CL. Once the horizontal tail volume coefficient is known, the elevons or other combinations can be decided. Most high-speed aircraft use elevons, a dual control capability control effector. It can control the lateral and longitudinal motion to vary pitch and roll.

Questions to address for control surface sizing:

- The question becomes what types of control surfaces are needed and why? How many are required?
- Type of control surface: elevons
- Number of elevons
- Elevon geometry
- Type of control surface: ailerons. Why not?
- Canards? Why not?
- Types of control surface: Vertical tails
- Number of vertical tails
- Vertical tail dihedral angle

##### 4.3.1 Canards

There are different types of tail configurations. One of them is Tail-Forward-Configuration (TFC). This includes canards that are used for either control or trim. Having a canard serves to modify the longitudinal stability and decrease the angle of attack during takeoff and landing for delta winged aircraft. One drawback of high sweep for an aircraft is the decrease in the maximum lift coefficient which usually occurs at high angles of attack. This means the aircraft may stall at a higher angle of attack, which is very beneficial, but it reduces the maximum lift at given speed. Having canards on the forward fuselage negates this imbalance by reducing the landing angle of attack. For pitch stability, this can reduce the stability of an aircraft. This is desirable especially in overly stable flight such as hypersonic aircraft. The following in the Fig. 19 are some aircraft canard designs for reference.



(a) XB-70 Fixed Canards



(b) TU-144 Retractable Canards

**Fig. 19 Canard designs on supersonic aircraft.**

In the **Fig. 19** above, the XB-70 features a fixed canard that can be used for control. The Tupolev TU-144 has retractable canards that are mainly used for trim and reducing the angle of attack at landing [43]. The retractable nature of these devices makes them more useful for supersonic speeds where the drag can be reduced. Chines are another form of longitudinal stability feature. Although more applicable for adding directional stability, the addition of chines on the SR-71 also significantly prohibited the aft movement of neutral point at high supersonic speeds [21]. Adding too much of a blend between the fuselage and wings can change the aircraft design to a Blended-Body configuration.

#### 4.3.2 Elevons

The elevons are dual control effectors used for pitch and roll control, used by many famous supersonic and hypersonic aircraft designs. The manner of their movement dictates whether the aircraft will pitch or roll. If the elevons are deflected up or down simultaneously on either side, the aircraft will change pitch. If the elevons are deflected in opposite directions, the aircraft will roll. Most design texts are resources that do not give a separate method to calculate the control power for elevons, except Nicolai. Usually, the control power for ailerons and elevators are calculated and sized based on which movement requires greater control authority. A method to calculate the trim of aircraft using elevons is given in section 4.4.3. The following are example aircraft featuring elevons in **Fig. 20**.



(a) Concorde



(b) SR-71



(c) XB-70

**Fig. 20 Elevons features in supersonic and hypersonic aircraft.**

Notice the three different designs for elevons. The SR-71 and Concorde have both inboard and outboard elevons and the XB-70 just features outboard elevons. The elevons are inboard when they are placed in between engines location and fuselage centerline. The large delta wing of Concorde has straight elevons that are extension of the wing itself. For SR-71, the elevons have a rather distinct geometry with curvature near the engines. The elevons are also rounded at the edges. The XB-70's elevons do not extend throughout the wingspan. A sub-section of elevons are a part of the drooped wing section and each are smaller in size.

#### 4.3.3 Twin Vertical tails

For twin tails, the dihedral angle determines the kind of lateral stability the aircraft will have. If the tails are canted inwards such as for SR-71, the increase lateral stability during high-speed flight. Having outward dihedral is effective for maneuverability, most commonly found of fighter aircraft. The Hermeus Halcyon design features twin vertical

tails with an outward dihedral. Having a single large tail for a hypersonic aircraft may produce a lot of drag compared to twin tails of smaller size. Following are examples of twin tail high-speed aircraft in



(a) SR-71



(b) XB-70



(c) Halcyon (concept)

**Fig. 21 High-speed aircrafts with twin vertical tails.**

Note that the Halcyon is currently still a conceptual aircraft and many design iterations are expected to be made in the future. The hypersonic aircraft X-43A Hyper X also features straight, no-dihedral twin vertical tails. The number of tails will be a trade to be explored in the CL phase. Tail dihedral is another trade being used of CL. If twin vertical tails are used, they must be placed behind the passenger cabin for safety.

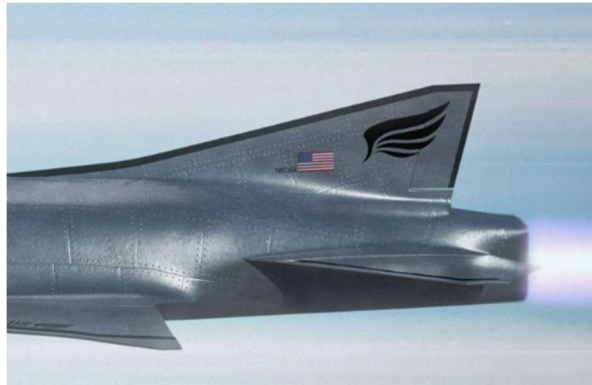
An advantage of twin vertical tails is that the aircraft directional controllability is improved compared to a long-span vertical tail. The added dihedral helps with roll control. Since the vertical tails are typically placed some distance away from the fuselage centerline, they are not obstructed by the fuselage wake region. However, twin vertical tails are slightly heavier than commonly used single vertical tails [23].

#### 4.3.4 Single Vertical tail

The two supersonic commercial transports, Concorde and TU-144 both feature a single vertical tail with two rudders aligned vertically. Having a single tail has the benefit of less maintenance since it is a common feature. However, large vertical tails require stronger structural support compared to smaller twin vertical tails. The Hermeus Quarterhorse, unmanned plane features a single, highly swept vertical tail as well. Following are example designs of single vertical tail in Fig. 22.



(a) Concorde



(b) Quarterhorse (Concept 2023)

**Fig. 22 Single vertical tail used in high-speed aircraft.**

The Concorde has a large vertical stabilizer with two rudders, mainly for redundancy. They are connected to two separate systems, so if one fails, the other can be used instead. The Quarterhorse uses a single tail, however, notice the high sweep. This could decrease aerodynamic drag at hypersonic speeds. The Quarterhorse is also currently just a conceptual design and may have design alterations in the future.

#### 4.4 Flight Conditions to address

When it comes to control surface sizing, these areas are sized to have enough control authority during critical flight conditions. For longitudinal control, these conditions are takeoff rotation, trim drag at cruise, high-g maneuver, and low speed at high angle of attacks. Since the concept is for a hypersonic passenger transport vehicle, the longitudinal control is assessed primarily for takeoff rotation and trim drag. For directional control, critical conditions such as crosswind landings, asymmetric thrust due to one-engine-inoperative (OEI) and adverse yaw must be taken into consideration for the sizing process. For lateral control, the deflections of elevons or ailerons will not be adding to lateral stability of the aircraft. They only function of roll control. The roll stability comes from the wing, vertical tail and fuselage configuration [20]. However, the elevon can be sized for lateral control requirements of roll performance given in MIL-HDBK-1797. The document MIL-HDBK-1797 is a handbook that gives guidelines on aircraft handling; however, it is not a military standard. The actual military standard specifications document named MIL-SPEC-1797 is currently classified. From MIL-HBDK-1797, our hypersonic concept aircraft will fall into Class III, meaning heavy transport requiring low-to-medium maneuverability. For a Class III aircraft, the roll performance requirements are 300 in 1.5 seconds [20]. This report will detail the longitudinal control aspects. The lateral controllability will be covered by fellow S&C engineer, Carlos Carmona and directional control by Oscar Ariza.

#### 4.4.1 Takeoff rotation

Many disciplines are involved for this critical condition. First, the P&T team determines the angle of attack at takeoff. The W&B team provides the C.G. location to the Structures team who determines the appropriate placement of landing gear so that the aft end does not strike the ground and damage any engine. This is determined by a ground clearance requirement. Notice, most commercial airplanes have an angled fuselage at the aft for the same purpose. For takeoff rotation, the location of the main landing gear is directly related to the most aft C.G. location.

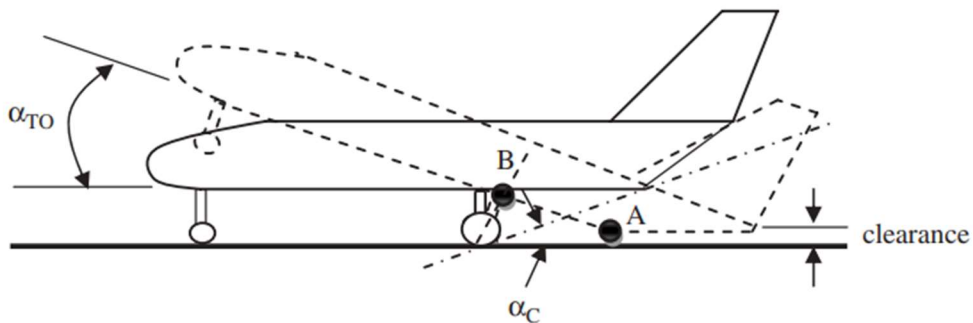


**Fig. 23 Ground clearance required for takeoff rotation [23].**

In terms of S&C, takeoff rotation is a longitudinal control requirement. The elevons must have enough control power to rotate the aircraft about the main landing gear such that the nose lifts up at 80% take-off speed. The methodology for takeoff rotation is adapted from reference [23] due to detailed steps given for the process. A more detailed Quasi-steady-state process is given by reference [47], however, it may be too complex to compute for the given time available. The elevon deflection needed to rotate the aircraft about the main landing gear is given by the following:

$$\delta_e = -\frac{C_{L\alpha} C_{m_0} + C_{m_\alpha} C_L}{C_{L\alpha} C_{m\delta_e} - C_{L\delta_e} C_{m\alpha}} \quad (3)$$

Note, most of the input comes from within S&C team and Aerodynamics team. A detailed procedure for locating the main landing gear position is given in the same reference. Here, the rotation point is about the main landing gear, and the initial acceleration has to have a value of 4-6 deg/s<sup>2</sup>. This requirement is for a tricycle landing gear arrangement. The overall takeoff rotation should not exceed 3-5 seconds for a large transport. The following gives the main forces and moments related to takeoff rotation. The moments about the C.G. location must be overcome by elevon deflection at takeoff rotation, given in the equation below.

$$\sum M_{cg} = I_{yy\ mg} \ddot{\theta} = -M_W + M_D - M_T + M_{Lwf} + M_{acwf} + M_{Lh} + M_a \quad (4)$$

The forces and distances associated with the moments are given below in **Fig. 24**. As mentioned, the initial acceleration  $\ddot{\theta}$  value for a large transport must be within 4-6 deg/s<sup>2</sup>. The entire process will be coded to find the maximum elevon deflection for takeoff rotation. The moment of inertia  $I_{yy}$  of the landing gear is an input from W&B team.

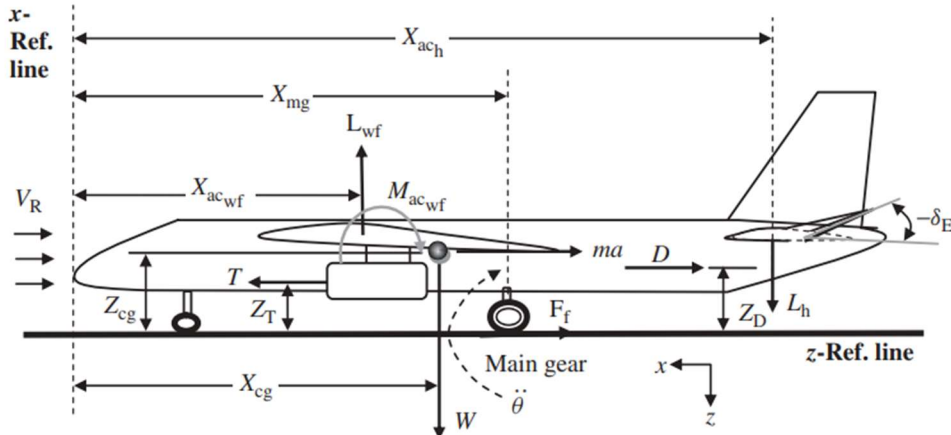


**Fig. 24 Forces and moments during takeoff rotation [23]**

#### 4.4.2 Trim drag

Trim drag is caused due to excessive force required to trim an aircraft. Usually, an overly stable aircraft flying at high speeds will experience large amounts of trim drag when pitch control effectors are used. One way to minimize this trim drag is by moving the neutral point forward, either closer to the aircraft C.G. or ahead of it. This destabilizes the aircraft enough that large control deflections producing trim drag are avoided. The procedure to estimate the elevon deflection angle is given in Eq. (5). A generic method to calculate trim drag is given below in Eq. (6) [20].

$$D_{trim} = \eta_T q_\infty S_T K_T C_{LT}^2 \quad (7)$$

The term  $C_{LT}$  is the lift coefficient of the tail. The trim drag must not be more than 10% of the total drag. If this is the case, moving the C.G. near the neutral point, or increasing the tail aspect ratio can help reduce trim drag. Increasing the control effector size can also reduce trim drag since less force will be needed for deflection.

#### 4.4.3 Trim of tailless aircraft

Following are the elevon trim equations for a tailless aircraft, similar to the WB configuration being considered [20]. The following equations are for a load factor  $n = 1$ . A load factor of 1 represents straight and level flight, meaning lift on the body is equal to its weight.

$$0 = C_{Ma.c.w} - \frac{x_w}{\bar{c}} C_L + \frac{Tz_T}{q_\infty S_{ref} \bar{c}} \quad (8)$$

For a deflected elevon:

$$0 = \left( \frac{dC_{Ma.c.}}{d\delta_e} \right) \delta_e - \frac{x_w}{\bar{c}} \left[ \left( \frac{dC_L}{d\alpha} \right)_w \alpha + \left( \frac{dC_L}{d\delta_e} \right) \delta_e \right] + \frac{Tz_T}{q_\infty S_{ref} \bar{c}} \quad (9)$$

Can be re-written as:

$$\delta_e = \frac{\left(\frac{x_w}{c}\right) \left(\frac{dC_L}{d\alpha}\right)_w \alpha - \left(\frac{Tz_T}{q_\infty S_{ref} c}\right)}{-\left(\frac{x_w}{c}\right) C_{L\delta} + C_{M\delta}} \quad (10)$$

The geometric parameters in the Eq. (11-12) are illustrated in Fig. 31.

#### 4.4.4 Asymmetric thrust

One of the most critical conditions to size for occurs at takeoff when an engine fails. This critical condition is also known as One-Engine-Inoperative (OEI). However, if there are two engines on one side of the aircraft, the possibility of both engines failing must be considered as well. Another flight phase where OEI can be evident is in the case of inlet unstarts at cruise. This was most notable in SR-71 Blackbird's case where the SAS would also manage control movements in such small time spans. For such a case, knowing the maximum rudder or vertical tail deflection range is essential.

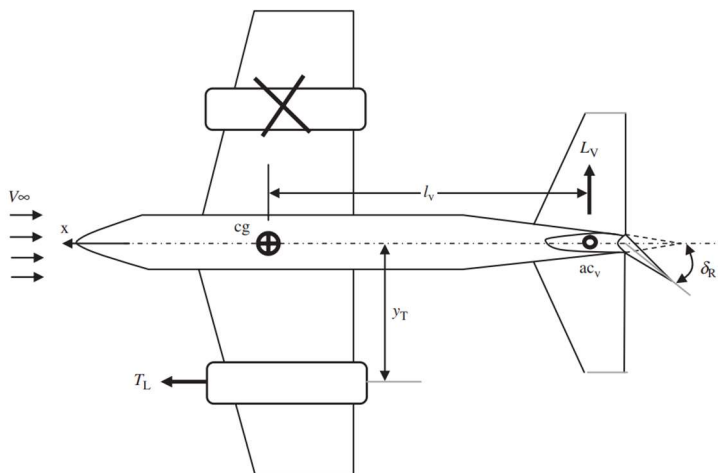


**Fig. 25 Asymmetric thrust condition [23]**

The maximum rudder deflection at OEI can be estimated using the following relation below in Eq. (13). The following assumptions can be made, first, the yawing moment bias  $C_{n_0}$  can be assumed to be zero for a symmetric aircraft. Then, the elevon deflection is assumed to be zero, along with sideslip angle  $\beta$ . If there are more than two engines on the aircraft, then the thrust for additional engines must be considered along with distance from fuselage centerline  $y_T$ .

$$\delta_r = \frac{T_L y_T}{-\bar{q} S_{ref} b C_{n\delta_r}} \quad (14)$$

Most parameters for this calculation come from the Propulsion, Geometry and S&C teams.

#### 4.4.5 Crosswind landings

There were two methods found for sizing for crosswind landings. A simple method was given in Nicolai and a more detailed method was obtained from reference [23]. The method given from Nicolai to size. Nicolai recommends a sideslip of  $\beta = 11.5^\circ$  for the analysis. The crosswind condition is given by the following relation from Nicolai [20]:

$$C_n = 0 = C_{n\beta} \beta + C_{n\delta_r} \delta_r \quad (15)$$

A summary of all critical conditions to size for given below in **Fig. 26**.

	<b>SENIOR DESIGN:</b> MAE 4351 Project	Ref.: MAE 4351-001-2021 Date: 09. Jul. 2023 Name: <b>Gayathri Kola</b> Status: In Progress
---	---	---

Takeoff Rotation	Asymmetric Thrust (or OEI)
<i>Flight phase: Takeoff</i>	<i>Flight phase: Takeoff, Cruise</i>
<b>Main Inputs:</b> Geometry: $z_t, S_{ref}$ <b>Propulsion:</b> Thrust <b>S&amp;C:</b> $C_{m_0}, C_{L_1}, C_{L_0}, C_{m_\alpha}, C_{m_{\delta_e}}, C_{L_{\delta_e}}$ <b>Aerodynamics:</b> $C_{L_\alpha}$	<b>Main Inputs:</b> Geometry: $y_t, S_{ref}, b$ <b>Propulsion:</b> Thrust <b>S&amp;C:</b> $C_{n_{\delta_r}}$ <b>Aerodynamics:</b> $C_{L_{\alpha_{VT}}}$
<b>Analysis:</b> Methodology: Conceptual Design, A Systems Engineering Approach, M. Sadraey, 2013.	<b>Analysis:</b> Methodology: Conceptual Design, A Systems Engineering Approach, M. Sadraey, 2013.
<b>Outputs:</b> Maximum elevon deflection angle $\delta_e$	<b>Outputs:</b> Maximum rudder deflection angle $\delta_r$
Trim Drag	Crosswind Landing
<i>Flight phase: Cruise, Climb</i>	<i>Flight phase: Approach</i>
<b>Main Inputs:</b> Geometry: $z_t, S_{ref}, \bar{c}$ <b>W&amp;B:</b> C.G. location <b>Aerodynamics:</b> Neutral point	<b>Main Inputs:</b> P&T: $V_{TO}$ <b>S&amp;C:</b> $C_{n_{\delta_r}}, C_{n_\beta}$ <b>Aerodynamics:</b> $C_{L_{\alpha_{VT}}}$
<b>Analysis:</b> Methodology: Fundamentals of Aircraft and Airship Design, Nicolai & Carichner, 2010	<b>Analysis:</b> Methodology: Fundamentals of Aircraft and Airship Design, Nicolai & Carichner, 2010
<b>Outputs:</b> Trim drag at cruise, climb. Static Margin (SM)	<b>Outputs:</b> Maximum rudder deflection angle $\delta_r$ for a sideslip of $\beta = 11.5^\circ$

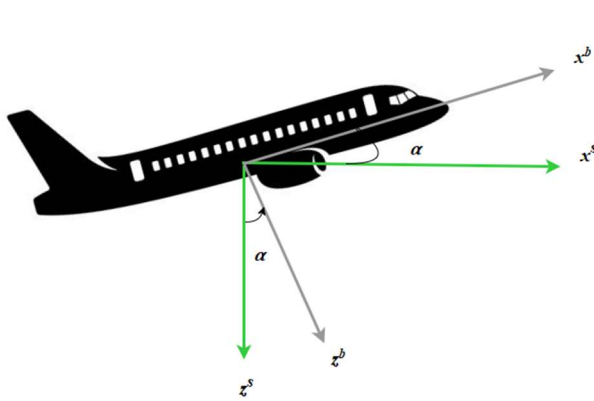
Fig. 26 Control surface sizing IDA for CE

#### 4.5 Axis systems

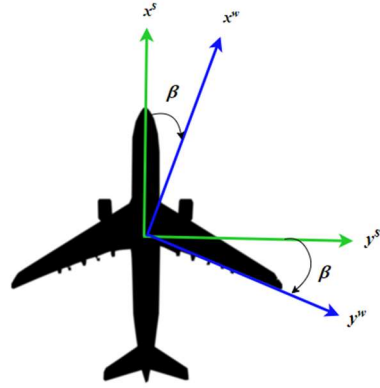
This section presents the various axis systems involved in stability determination. The aircraft system generally used is the body axis which is fixed to the aircraft C.G. location with x-axis positive toward the nose, y-axis positive towards the right wing and z-axis positive towards the ground station on Earth. This axis system is fixed with the body of the aircraft.

The stability axis system is similar to the body axis system; however, it is independent on angle of attack. The stability axis system is rotated by right hand rule about the y-axis of body axis by some value of angle of attack as in Fig. 27 (a). A transformation matrix is used to move from stability frame to body frame using angle of attack.

Similarly, another axis system known as the wind axis is used for lateral stability. The wind axis is rotated by a sideslip angle  $\beta$  from the stability axis, as seen from top view.



(a) Stability Axis



(b) Wind Axis

**Fig. 27 Axis Systems with body frame**

#### 4.6 Static Stability

Static stability refers to the condition when an aircraft inherently returns to its equilibrium position when disturbed. This is also known as positive static stability when the aircraft returns to equilibrium after experiencing some decreasing oscillations. In the case of neutral static stability, the disturbance (such as wind) changes the attitude of the aircraft after which it stays on the same path. If the aircraft starts to deviate from the equilibrium position after a minor disturbance, the aircraft is said to have negative static stability, often undesirable for stability design.

Since our aircraft will be carrying passengers, it will be considered a transport aircraft. According to FAR 25, the document ascribing flying qualities for transport aircraft, the aircraft must have static stability in all directions:

*“The airplane must be longitudinally, directionally, and laterally stable. In addition, the airplane must show suitable stability and control “feel” (static stability) in any condition normally encountered in service” [20].*

The Fig. 28 gives an overview on static stability requirements in general. Static stability is measured by three common derivatives based on longitudinal, lateral, and directional sections. For longitudinal static stability, pitching moments as a function of angle of attack  $C_{m_a}$  and static margin  $SM$  are of primary importance. For most aircraft, the lateral and directional movements are coupled; a yawing motion induced a rolling motion inherently since the aircraft must bank a little. They are influenced by the wind axis, hence a sideslip angle  $\beta$  is considered for lateral-directional moments. The sign conventions that assure stability are given in the Fig. 28 below. The primary objective is to have our aircraft statically stable. Lateral modes such as spin resistance and roll reversal will be omitted from our analysis.

Criterion	Description
<b>Longitudinal</b> $C_{m_\alpha} = -(SM)C_{L_\alpha} < 0$	When satisfied, any disturbance in pitch will result in a restoring pitching moment. This requirement may be relaxed to improve performance or maneuverability.
<b>Directional</b> $C_{n_\beta} > 0$	When satisfied, any disturbance in side-slip will result in a restoring yawing moment. Primarily effected by the vertical lifting surface.
$C_{l_\beta} < 0$	When satisfied, any disturbance in side-slip will result in a restoring rolling moment. Primarily effected by the dihedral effect.
<b>Lateral (spin resistance and roll reversal)</b> $C_{n_{\beta_{dyn}}} = C_{n_\beta} - C_{l_\beta} \frac{I_{zz}}{I_{xx}} \tan \alpha > 0$ $LCSP = C_{n_\beta} - C_{l_\beta} \frac{C_{n_\delta}^{LaCE}}{C_{l_\delta}^{LaCE}} > 0$	Provides an approximation for aircraft spin resistance during non-rolling maneuvers, no control inputs. Usually important for fighter and high-speed aircraft. Lateral Control Spin Parameter provides an approximation for roll reversal. Adverse yaw induced by the aileron combined with low directional stability can produce a natural roll reversal. Usually important for fighter and high-speed aircraft.

Fig. 28 Static stability requirements overview [30]

#### 4.7 Dynamic Stability

In dynamic stability, the time, and oscillations of the aircraft before returning to the equilibrium state are considered. If an aircraft has positive dynamic stability, the aircraft return to equilibrium through a sequence of decreasing oscillations. For neutral dynamic stability, the aircraft will keep oscillating with the frequency until another disturbance occurs. For a negative dynamic stability, the aircraft will have increasing oscillations making it unstable. For an aircraft to have dynamic stability, it must first have positive static stability. Hence static stability analysis is conducted first.

#### 4.8 Longitudinal Stability

Longitudinal stability consists of assessing the pitching motion of an aircraft. To maintain a steady-level flight, the net moments along the longitudinal axis of an aircraft must be zero at a given angle of attack. If there is a positive pitching moment, it causes the aircraft to pitch up (nose up). If the moment is negative, it causes a nose down moment. Either of these moments, be it pitch up or down, are undesirable beyond a certain limit. After an aircraft crosses the sonic barrier ( $M = 1$ ), the center of pressure (point where lift and drag forces act) also known as the neutral point shifts backward aft the center of gravity. This over-stabilizes an aircraft at high speeds prohibiting its maneuverability. If the aircraft were to solely rely on its pitch control effectors such as elevons to pitch up, the aircraft will experience large amounts of *trim drag*. Trim drag is the drag that occurs to trim an aircraft.

The most common and important longitudinal stability parameters are the following:

- Pitching moment as a function of angle of attack,  $c_{m_\alpha}$
- Static Margin (SM)

The static margin gives an assessment of the level of stability an aircraft has, it is calculated using the formula below:

$$SM = (\bar{X}_{np} - \bar{X}_{cg}) = -\frac{C_{m_\alpha}}{C_{L_\alpha}} \quad (16)$$

Note, the location of neutral point and center of gravity must be normalized values. If the SM is negative, that means the aircraft is unstable and a positive value of SM indicates stability. A higher positive value of SM indicates that the vehicle might be overly stable. Most fighter aircraft are designed to have relaxed static stability, where their static margins are from 0 to -15% which allows them to maneuver easily. The Flight-Control-System (FCS) is used to automatically stabilize these aircraft, significantly reducing trim drag [25]. The aerodynamic center is calculated by

the Aerodynamics team and given to the Weights & Balance (W&B) member. The W&B member will calculate the C.G location and provide it to S&C for SM calculations.

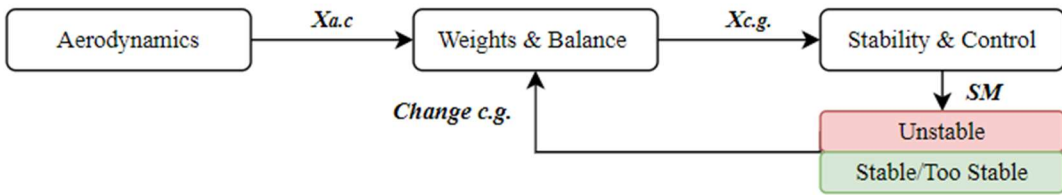


**Fig. 29 Interactions between disciplines for longitudinal stability.**

To estimate the pitching moment, the following relation can be used:

$$C_m = C_{m_0} - \frac{1}{c} C_{L\alpha} \alpha (x_{cp} - x_{cg}) \quad (17)$$

Where  $C_{m_0}$  is pitching moment independent of angle of attack. The relation above is valid for Mach number less than 5 [28]. Where the  $C_{L\alpha}$  is the wing-body lift curve slope.

And the longitudinal stability derivative can be written as [20]:

$$C_{m\alpha} = -SM C_{L\alpha} \quad (18)$$

**Table 6. Sign requirements for main stability derivatives [20].**

Sub-section	Derivative	Derivative Name	Stable	Unstable
Longitudinal	$C_{m\alpha}$	Pitching moment as a function of angle of attack	Negative	Positive
Lateral	$C_{l\beta}$	Rolling moment due to side slip angle	Negative	Positive
Directional	$C_{n\beta}$	Yawing moment due to side slip angle	Positive	Negative

#### 4.9 Methodology for Stability and Control derivatives

Now that there is some background given, the methodology used for calculating stability and control derivatives will be split into four different segments: subsonic, transonic, supersonic, and hypersonic Mach numbers. The following is the checklist for choosing a method to calculate stability derivatives:

- Wing-body configuration.
- Fewer geometric inputs.

This report will be covering the calculation of longitudinal stability derivatives. If time permits, dynamic stability will be assessed. The following is a helpful roadmap for static stability assessment.

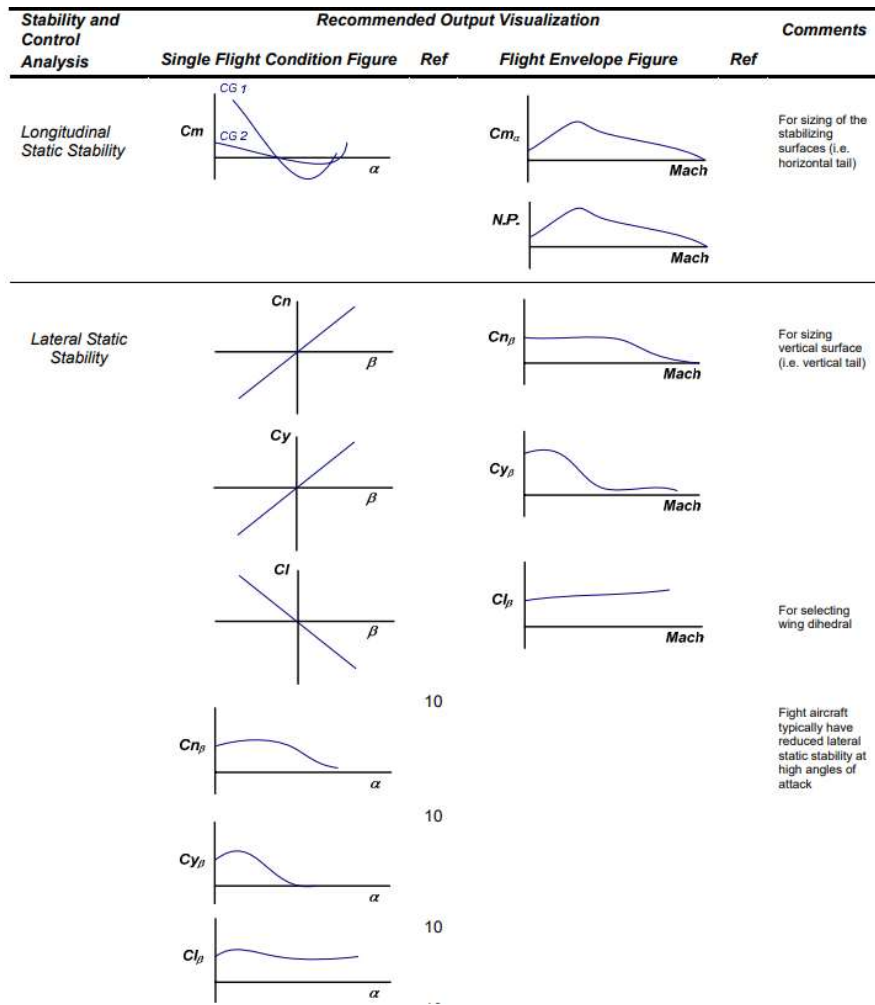


Fig. 30 Static stability assessment roadmap [30].

Simplified trim equations of motion are given below from Eq. (19-20):

Longitudinal trim:

$$0 = C_{m_0} + C_{m_\alpha}(\alpha) + C_{m_{\delta_e}}(\delta_e) + C_{m_{\delta_r}}(\delta_r) \quad (21)$$

Lateral trim:

$$0 = C_{l_0} + C_{l_\beta}(\beta) + C_{l_{\delta_e}}(\delta_e) + C_{l_{\delta_r}}(\delta_r) \quad (22)$$

Directional trim:

$$0 = C_{n_0} + C_{n_\beta}(\beta) + C_{n_{\delta_e}}(\delta_e) + C_{n_{\delta_r}}(\delta_r) \quad (23)$$

Please note that the derivatives due to stabilizer incidence have not been included in the equations above. Most of the derivatives can be found from Jan Roskam's design series within the subsonic regime. For supersonic and transonic regime, DATCOM methods are more applicable. A detailed overview is given in the Jan Roskam's design section.

	<b>SENIOR DESIGN:</b> MAE 4351 Project	Ref.: MAE 4351-001-2021 Date: 09. Jul. 2023 Name: <b>Gayathri Kola</b> Status: In Progress
---	---	---

*Chudoba, Cook Method – Trim Equations of Motion for Steady State Straight-line flight [48].*

This paper gives a generic method to assess stability for symmetric and asymmetric aircraft. For stability assessment in conceptual design phase, a complete 6 DOF assessment is essential for characterizing a vehicle's stability. This analytical method allows for control power assessment in 6 DOF and allowing for trim analysis. There are two papers in this series – one covers steady state straight-line flight, and the other focuses on dynamic stability analysis involving turning flight, pull-up, and push over maneuvers [47]. For the dynamic analysis, perturbed EOMs are used instead of steady state EOMs. Due to the fully coupled 6 DOF analysis, there are 6 equations and multiple assumptions must be made to simplify the analysis. Following are 6 DOF steady state trim EOMs given:

$$0 = -mg \sin \theta + X_A + X_T \quad (24)$$

$$0 = mg \sin \phi \cos \theta + Y_A + Y_T \quad (25)$$

$$0 = mg \cos \theta \cos \phi + Z_A + Z_T \quad (26)$$

$$0 = L_A + L_T \quad (27)$$

$$0 = M_A + M_T \quad (28)$$

$$0 = N_A + N_T \quad (29)$$

Here,  $\phi, \theta, \psi$  are Euler angles denoting roll, pitch, and yaw. The variables  $L, M$  and  $N$  are external moments about the center of gravity. Meaning, rolling, pitching, and yawing moments. Finally, the variables  $X, Y$ , and  $Z$  are the resultant force components. The full description of equations is not mentioned here due to length. The equations follow these assumptions:

- The Earth is a flat surface and rests in the inertial space with rotational velocity ignored.
- Uses a body axis system with origin at the C.G. of the aircraft.
- The aircraft must be a rigid body, meaning the inertia matrix will be zero.
- Wind velocity is neglected.

The paper gives many critical condition cases where the controllability can be evaluated and adds the simplifying assumptions that can be made. For longitudinal stability, the following cases were suggested:

- Cruise trim drag utilizing aerodynamic control effectors – for symmetric thrust.
- Trim drag during straight sideslip – for symmetric thrust.
- Trim drag during OEI cruise – for asymmetric thrust.

Upon deliberation, it was decided amongst the team to first conduct a de-coupled stability analysis and if time permits, to move to a more complex analysis. If this method is chosen, methods for individual coefficients must be decided, and a MATLAB script will be written to perform the analysis. More detailed inputs from W&B and Propulsion team are required, specifically moments of inertia and thrust incidence angles.

*Nicolai – Pitching moments about C.G. [20]*

For longitudinal derivatives, Nicolai gives a method to estimate pitching moments for a tailless aircraft, similar to the geometry our team is considering for CL. The axis system for the wing-body tailless aircraft is given in the Fig. 31. To calculate the pitching moments about the C.G. location, following relation can be used for a tailless aircraft:

$$C_{m_{c.g.}} = -C_L \frac{x_w}{\bar{c}} + C_D \frac{z}{\bar{c}} + C_{m_{a.c.w}} + \frac{T z_T}{q_\infty S_{ref} \bar{c}} - C_{m_{c.g.inlet}} \quad (30)$$

Where,  $C_L$  and  $C_D$  need to be functions of Mach number  $M$  and angle of attack  $\alpha$ . The Aerodynamics team can give MATLAB functions of the same. This resource is also being used for lateral rolling moment build-up by team member Carlos Carmona. A more general method for calculation of the coefficient in Eq. (31) is given in Raymer [25]. For a trimmed condition, the Eq. (32) is set to zero.

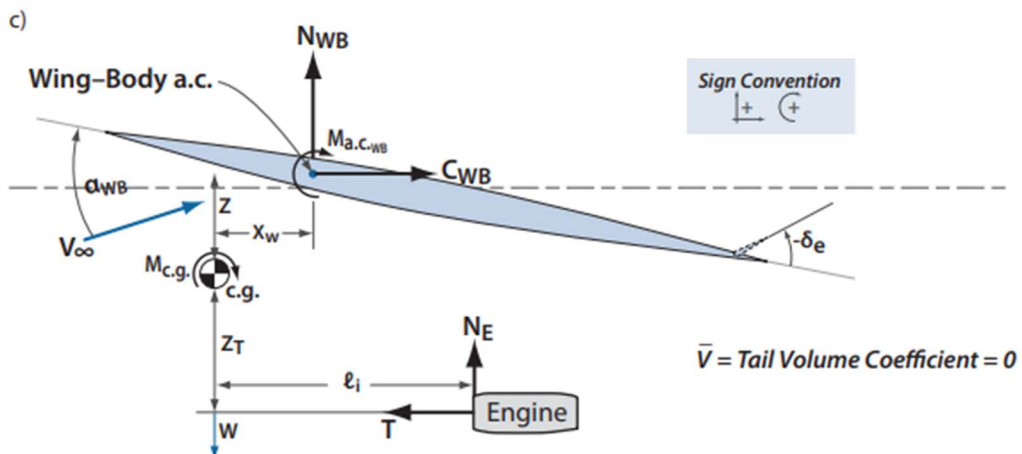
Similarly, to find the pitching moment as a function of angle attack  $C_{m\alpha}$ , the following relation can be used. The  $C_{m\alpha}$  is important because it gives the angle of attack for trim condition. Additionally, if the term has constant values when the C.G. location is changed, the neutral point can be estimated, as in  $C_{m\alpha}$  will be zero.

$$C_{m\alpha} = -\frac{x_w}{c} m_w + C_{m\alpha I} \quad (33)$$

$$m_w = (C_{L\alpha})_{WB} \quad (34)$$

$$C_{m\alpha I} \approx \frac{2\dot{m}_0 \beta l_i}{\rho V_\infty S_{ref} c} \frac{d\beta}{d\alpha} \text{ (per radian)} \quad (35)$$

The exact geometric parameter definitions are illustrated in the Fig. 31 below. The last multiplier term in Eq. (36) can be assumed to be 1 for inlet placement beneath the wing. Most parameters are required from the Aerodynamics and Propulsion teams. A similar, a more general method was found in Raymer, however, it seemed for applicable for traditional subsonic commercial aircraft present today with an aft tail. Hence, the method given in Nicolai was chosen for analysis.



All distances are positive as shown  
 $\epsilon_T$  = tail downwash angle due to wing downwash  $w_T$  at the tail a.c.  
 For small  $a$  we can assume  
 $N$  = normal force =  $L = C_L q S_{ref}$   
 $C$  = chord force =  $D = C_D q S_{ref}$

Fig. 31 Axis system and forces acting on a tailless wing-body [20]

#### Jan Roskam Design Series

As mentioned in the literature section, the Jan Roskam design texts give a simplified method to calculate many of the stability and control derivatives. The following table summarizes methods available for the derivatives involved.

Table 7. Stability and Control derivatives in Jan Roskam [15,32,49]

Derivative Symbol	Subsonic	Transonic	Supersonic	Hypersonic	Assumptions
Longitudinal Stability Derivatives					
Steady-state derivatives					
$C_{L1}$	✓	✓	✓	✓	
$C_{D1}$	✓	✓	✓	✓	
$C_{M1}$	✓	✓	✓	✓	

	<b>SENIOR DESIGN:</b> <b>MAE 4351 Project</b>	Ref.: MAE 4351-001-2021 Date: 09. Jul. 2023 Name: Gayathri Kola Status: In Progress
---	--	--

$C_{T_x}$	✓	✓	✓	✓	
$C_{M_{T_x}}$	✓	✓	✓	✓	
<b>Speed derivatives</b>					
$C_{L_u}$	✓	✓	✓		
$C_{D_u}$	✓	✓	✓	✓	
$C_{M_u}$	✓	✓	✓	✓	
$C_{T_x u}$	✓	✓	✓	✓	Gliders, RBCC = 0
$C_{M_{T_x} u}$	✓	✓	✓	✓	
<b>Angle of attack derivatives</b>					
$C_{L_\alpha}$	✓	✓	✓		
$C_{D_\alpha}$	✓	✓	✓	✓	
$C_{M_\alpha}$	✓	✓	✓		
$C_{M_{T_\alpha}}$					
<b>Rate of angle of attack derivatives</b>					
$C_{L_{\dot{\alpha}}}$	✓				
$C_{D_{\dot{\alpha}}}$	0	0	0	0	Neglect
$C_{M_{\dot{\alpha}}}$	✓				
<b>Lateral-Directional Stability Derivatives</b>					
<b>Sideslip derivatives</b>					
$C_{Y_\beta}$	✓				
$C_{l_\beta}$	✓				
$C_{n_\beta}$	✓				
$C_{n_{T_\beta}}$	✓				
<b>Rate of sideslip derivatives</b>					
$C_{Y_\dot{\beta}}$	✓				
$C_{l_\dot{\beta}}$	✓				
$C_{n_\dot{\beta}}$	✓				
<b>Roll rate derivatives</b>					
$C_{Y_p}$	✓				
$C_{l_p}$	✓				
$C_{n_p}$	✓				
<b>Pitch rate derivatives</b>					
$C_{D_q}$	✓				
$C_{L_q}$	✓				
$C_{m_q}$	✓				
<b>Yaw rate derivatives</b>					
$C_{Y_r}$	✓				
$C_{l_r}$	✓				
$C_{n_r}$	✓				
<b>Control Derivatives</b>					
<b>Control: Elevator derivatives</b>					
$C_{D_{\delta_e}}$	✓				
$C_{L_{\delta_e}}$	✓				
$C_{M_{\delta_e}}$	✓				
<b>Control: Aileron derivatives</b>					
$C_{Y_{\delta_a}}$	✓				
$C_{l_{\delta_a}}$	✓				
$C_{n_{\delta_a}}$	✓				
<b>Control: Rudder derivatives</b>					
$C_{Y_{\delta_r}}$	✓				
$C_{l_{\delta_r}}$	✓				
$C_{n_{\delta_r}}$	✓				

As seen from the table above, most methodology available from this resource is applicable for subsonic regime, this is case for lateral and directional stability derivatives and control derivatives. Roskam recommends DATCOM for calculating lateral-directional derivatives for supersonic and hypersonic regimes. However, most methodology in

	<b>SENIOR DESIGN:</b> MAE 4351 Project	Ref.: MAE 4351-001-2021 Date: 09. Jul. 2023 Name: <b>Gayathri Kola</b> Status: In Progress
---	---	---

DATCOM is complex so simplifications must be made before using the resource. Jan Roskam series also has methodology to calculate control derivatives for canards, differential stabilizers, and spoilers.

#### *Jan Roskam Flight Dynamics – Pitching control derivatives [26]*

This text gives formulas for the majority of control derivatives that can be used while evaluating trim conditions. The Eq. (37) gives the derivatives essential for calculating longitudinal trim. Notice, the pitching moment due to stabilizer incidence  $C_{m_{i_h}}$  is being neglected here to simplify the analysis.

$$C_{m_0} \approx C_{m_{a.c}} + C_{L_0}(\bar{x}_{cg} - \bar{x}_{ac-e}) \quad (38)$$

$$C_{m_{\delta_e}} = -C_{L_a} \eta_h \frac{S_e}{S_{ref}} (\bar{x}_{ac-e} - \bar{x}_{cg}) \tau_e \quad (39)$$

Note, the pitching moment due to rudder deflection  $C_{m_{\delta_r}}$  is neglected since its effect is negligible on longitudinal stability. The term  $C_{m_0}$  is often referred to as pitching moment bias, where the angle of attack and elevon deflection are zero. The term  $C_{L_0}$  is the lift coefficient at same assumptions. Since there is no aft tail, the dynamic pressure can be assumed to be the same at the elevons, thereby making the term  $\eta_h$  equal to 1. Finally, the term  $\tau_e$  is the angle of attack effectiveness parameter of the elevon. These methods will be used in conjunction with Nicolai to estimate trim and control surface deflections needed at each flight phase.

#### 4.10 Validation methods

Most verification data is available for Space Shuttle orbiter, SR-71 and XB-70. Following is the table listing all the resources with useful verification plots for S&C analysis.

**Table 8. Stability and Control Verification Literature.**

Aircraft	Year	Literature Name
SR-71	2012	SR-71 Flight Manual [46].
Space Shuttle	1975	Results of Investigations on a 0.010 scale 140A/B configuration space shuttle orbiter model 72-0 [50].
Space Shuttle	1974	Space Shuttle Orbiter and Subsystems [44].
XB-70	1973	Summary of stability and control characteristic of the XB-70 airplane [51].
XB-70	1973	Comparisons of predictions of the XB-70-1 longitudinal stability and control derivatives [52].

#### 4.11 Results, Verification and Discussion for S&C.

This section is intended to present the results obtained from converged vehicle analysis.

## 5 Aerodynamics

Aerodynamics is one of the primary disciplines in aircraft design. The flow of air around an aircraft determines how it will fly. For that reason, understanding the key concepts such as how lift is generated, where drag is beneficial and where it is unnecessary can help with better, efficient designs. Lift is the byproduct of uneven pressure distribution on an aircraft.

### 5.1 Background

#### 5.1.1 Hypersonic Aerodynamics

One of the most common misconceptions that author John D. Anderson discusses in the book “Fundamentals of Aerodynamics” is that flow becomes hypersonic at Mach 5. For most aircraft, crossing the sound barrier at Mach 1, the aircraft must overcome significant drag buildup. The drag increases exponentially at the sonic limit, and to counter this various design features can be incorporated to reduce that drastic increment. The region of Mach 0.8 to 1.2,

	<b>SENIOR DESIGN:</b> MAE 4351 Project	Ref.: MAE 4351-001-2021 Date: 09. Jul. 2023 Name: <b>Gayathri Kola</b> Status: In Progress
---	---	---

transonic speeds, the aircraft experiences shock wave induced flow separation that severely alters the aerodynamic characteristics of the design. To reduce this, the critical Mach number of the aircraft must be increased to delay flow separation on the wings. This can be done by decreasing wing thickness ratio ( $t/c$ ), increasing leading edge sweep angle of the wing, decreasing aspect ratio or using a supercritical airfoil [20].

Intuitively, having rectangular wings at hypersonic speeds does not seem feasible. The drag will be significantly high, and due to the heat, there are potential safety concerns. The key term is having a low aspect ratio. Additionally, the vehicle cannot be very heavy since at hypersonic speeds the aircraft will be flying at high altitude where the air is less dense. At the same time, the airframe must be strong enough to withstand the extremely high temperatures and keep the passengers cool inside.

At hypersonic speeds, the aerodynamics of the aircraft significantly changes since there is another variable that has to be taken into account: temperature. John Anderson illustrates this by giving the example of a blunt body during re-entry into Earth's atmosphere at Mach 36. The blunt bottom causes a bow shock wave, with the temperature behind the normal portion of bow shock reaching up to 65,248 K (approximately 65,000 °C). The air must be assumed to be calorically perfect for this case. However, at such high temperatures, the density is not constant due to chemical reactions, and the air is not considered calorically perfect anymore (specific heat  $\gamma$  keeps changing). So the actual temperature is approximately around 11,000 K (or around 10,700 °C). Around 9000 K, the Nitrogen and Oxygen molecules would have both dissociated into ions; the resulting shock layer will be partly ionized plasma [31].

The density is no longer stable, its changing due to boundary layer formation and its interaction with the surface of the aircraft. This viscous phenomenon increases skin friction drag. Additionally, there are shock waves that form at sharp edges of the aircraft such as the nose cone, inlets, vertical tails, etc. This creates wave drag. It must be taken into account to estimate drag for supersonic and hypersonic speeds.

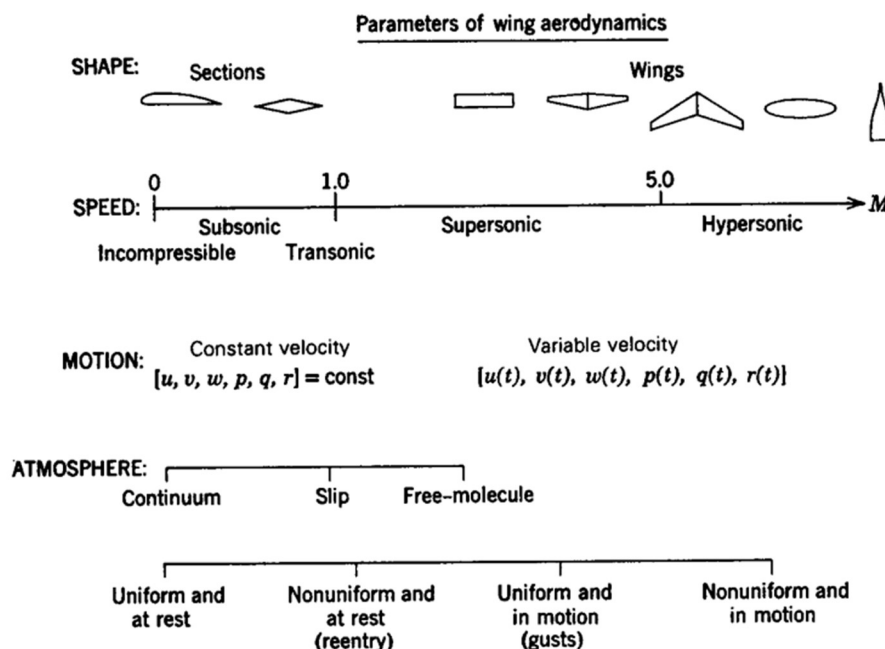


Fig. 32 Spectrum of aerodynamic issues to address [53].

### 5.1.2 Hypersonic Convergence and Aerodynamics

This portion will explain the role of the Aerodynamics team within the Synthesis convergence methodology to be adopted. A brief review of the Hypersonic Convergence methodology is given in section 3.1. To start the PS process, an estimate for the maximum lift-to-drag ratio must be known of a given aircraft. Since our aircraft will be a hypersonic, wing-body configuration with an air-breathing propulsion system, looking into similar aircraft can give an approximate for starters.

For the PS phase, the Kuchemann relation can be used to estimate the lift-to drag ratio as seen below [35].

$$\left(\frac{L}{D}\right)_{max} = \frac{A}{M}(M + B) = \frac{4}{M}(M + 3) \quad (40)$$

Where constant A and B are taken to for future state-of-the-art (SoA) aircraft. Hence, as given in the text by Czysz. P, the constants are A = 4 and B = 3 as seen in the Eq. (41). To calculate the zero-life drag coefficient, the following relation can be used for initial estimates:

$$\beta C_{D_0} = 0.05772 \cdot e^{0.4076} \quad (42)$$

Where,

$$\beta = \sqrt{M^2 - 1} \quad (43)$$

So, for the three conceptual vehicles of Mach numbers 5, 7.5 and 10, the following are the initial estimates to be given to the Synthesis team.

**Table 9. Concept vehicles aerodynamic estimates for PS phase.**

Vehicle Mach, M	Constant A	Constant B	$\beta$	$(L/D)_{max}$	$C_{D_0}$
5.0	4	3	4.89	6.4	0.01771
7.5	4	3	7.43	5.6	0.01167
10.0	4	3	9.95	5.2	0.00872

### 5.1.3 Wings for hypersonic aircraft

Highly swept wings are suitable for high-speed flight. Intuitively, swept wings are less likely to obstruct airflow than rectangular wings. Hence, a hypersonic Spirit of St. Louis with rectangular wings is not feasible from an aerodynamics standpoint. The goal with the concept of hypersonic Spirit of St. Louis is to maximize range. By using highly swept wings such as the delta wings, the goal for Aerodynamics is to minimize drag at hypersonic speeds. The following are many variations of delta wings in Fig. 33.

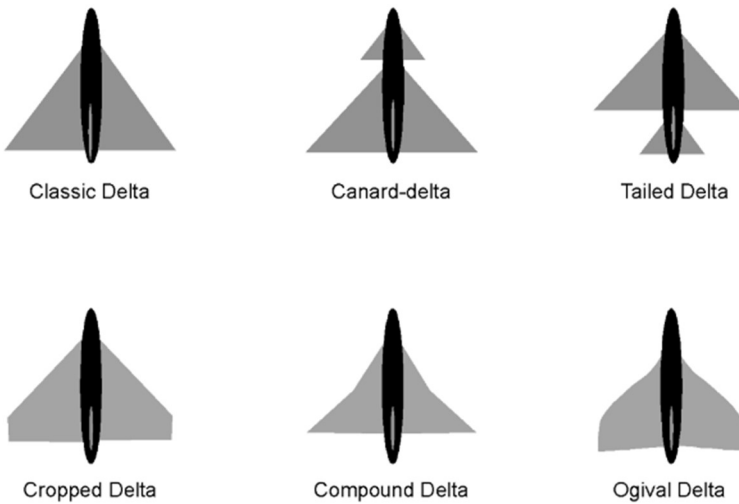


**Fig. 33 Common types of delta wings [54]**

One of the main reasons to have a canard is to destabilize the aircraft, which is much needed since the neutral point shifts backward. Supersonic aircraft such as the experimental plane by NASA – the XB-70 Valkyrie had a canard with trim capability. The Russian supersonic transport Tupolev TU-144 featured retractable canards. The compound delta

wings, also known as double delta, aid in generating strong free vortices along the wing intersection allowing for low-speed efficiency. The Ogive wing has a similar effect to the double delta wings. Most supersonic transports have an extended fuselage where the vertical tail is placed. A tailed delta wing might not be suitable for controllability since strong downwash at high-speed may render the tail end useless. Cropped delta wing has the benefit of low induced drag due to trailing edge vortices. A wing-body aircraft typically has a higher aspect ratio than an All-body aircraft, which increases viscous drag known as parasite drag. The term is a culmination of skin friction drag, wave drag, interference drag, pressure drag (form drag), miscellaneous drag, etc. The high drag may create thick boundary layers, where viscous interaction phenomena take place, specifically in hypersonic flow. Therefore, the aircraft must have strong airframe material and TPS to safeguard its passengers. The Concorde, TU-144, XB-70 are good examples of delta wing variations, although they are built for supersonic speeds. The Hermeus Halcyon has similarities between the space shuttle orbiter and XB-70 with its drooped wings and wing geometry.

For additional lift, devices like Leading Edge Extensions (LEX), fuselage strakes can be incorporated into the wing, provided they are able to withstand hypersonic heating. These devices can create tiny free vortices that propel energized air through suction on a boundary layer. This can prevent boundary layer separation.

#### 5.1.4 Shape of the Nose

The shape of the nose determines the type of shock wave the aircraft will encounter during flight. Oblique shock waves are weaker in nature. The flow after the shock is supersonic. Normal shock waves are very strong, leading to subsonic flow after. Normal shock waves are used in engine intakes to slow the flow from supersonic to subsonic as the air flows to the combustor. Typically, engines need to be placed within the Mach cone produced by a sharp nose. If placed outside the cone, the flow may interfere with flow at engine intakes.

The leading-edge shape of the aircraft has significant effects on the airflow around the body. It becomes important to explore the types of noses suitable for hypersonic travel. Sharp cone noses reveal an oblique shock wave, blunt noses as in the case of X-43A (AB configuration) yield a bow shock.

Benefits of bow shock:

The X-43A has a spatula nose geometry, similar to one chosen for our concept hypersonic plane during PS phase. A spatula nose is primarily beneficial for propulsion integration. With a more flatter nose, the airframe has increased wingspan to accommodate either a larger engine or higher number of engines. Additionally, the bow shock wave created at the nose at high speeds has its own benefits.

### 5.2 Methodology for Aerodynamics in PS

#### 5.2.1 Lift

The lift generated by a delta wing will be non-linear due to crossflow and formation of free vortices at the upper edges of the wing. The crossflow is the spanwise flow of air. The velocity component for crossflow increases in the spanwise direction leading to flow separation near wing tips at high speeds. Thus, for low aspect ratio (AR) bodies such as a delta wing, it becomes important to account for the non-linearity of lift. Following in the Fig. 34 below is the flow pattern for the slender bodies.

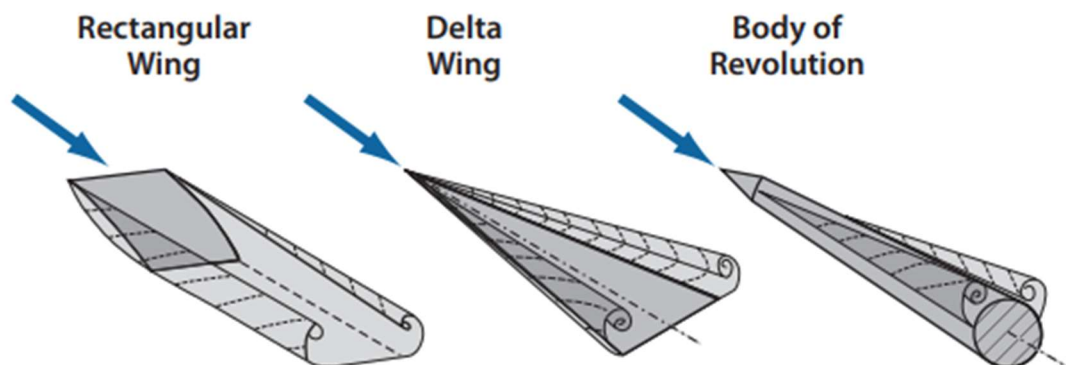


Fig. 34 Lift formation due to free vortices on various aircraft bodies [Nicolai].

*Nicolai's method – CL max*

Following the information presented, the methodology given below can be used to estimate the lift coefficient for subsonic, slender bodies of low aspect ratios [20]:

$$\frac{dC_L}{d\alpha} = C_{L\alpha} = \frac{2\pi AR}{2 + \sqrt{4 + AR^2\beta^2(1 + \left[ \left( \frac{\tan^2 \Lambda_{LE}}{\beta^2} \right) \right])}} \quad (44)$$

Where,

$$\beta = \sqrt{1 - M^2} \quad (45)$$

The non-linear lift coefficient will be:

$$C_L = \left( \frac{dC_L}{d\alpha} \right)_{\alpha=0} \alpha + C_1 \alpha^2 \quad (46)$$

To obtain the coefficient  $C_1$ , the following chart can be used once AR is known, specifically for a delta planform. The pitching moment can also be estimated in similar fashion for an estimate during PS phase.

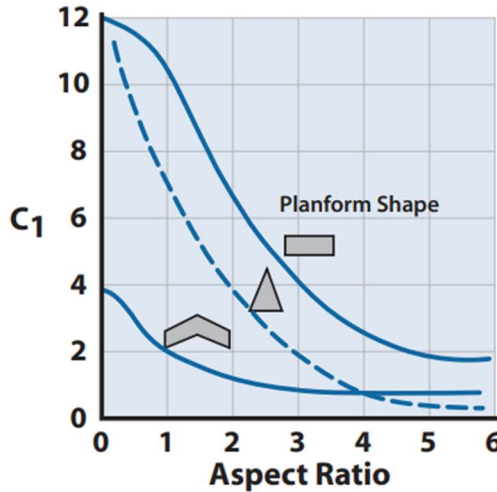


**Fig. 35 Chart for determining constant for non-linear lift coefficient [20].**

This method by Nicolai was tested to obtain  $C_{L_{max}}$ , details are presented in Section 5.4. The lift-curve-slope  $C_{L\alpha}$  was calculated first, then the angle of attack was varied while extracting constants from Fig. 35 for delta wing. Aspect ratios ranging from 1.5 to 3.0 were chosen. This resulted in a non-linear plot, however, there is no indication of stalling. Usually, predicting stall point using analytical models is difficult, wind tunnel tests give a much more accurate depiction of flow behavior. Another option can be to select a maximum angle of attack  $\alpha_{max}$ , to find the corresponding maximum lift coefficient. Another method from Raymer was also considered and given below.

For a generic estimate of the lift-curve-slope  $C_{L\alpha}$  during the PS phase, the following approximating for wing-body configuration can also be used, outlined in Roskam [55]. However, the author will be using Nicolai's method since it is more applicable to delta planforms.

$$\left( \frac{dC_L}{d\alpha} \right)_{WB} = \left[ 1 + \frac{1}{4} \left( \frac{d}{b} \right) - \frac{1}{40} \left( \frac{d}{b} \right)^2 \right] \left( \frac{dC_L}{d\alpha} \right)_w \quad (47)$$

	<b>SENIOR DESIGN:</b> MAE 4351 Project	Ref.: MAE 4351-001-2021 Date: 09. Jul. 2023 Name: <b>Gayathri Kola</b> Status: In Progress
---	---	---

To compare the results, similar transport and high-speed WB aircraft are chosen. The Synthesis team has provided an initial aircraft weight of 500,000 lb. Following in the table below are chosen aircraft and their geometric features.

**Table 10. Aircraft with similar TOGW as our conceptual vehicles**

Aircraft Name	TOGW [lb]	$\Lambda_{LE}$ [deg]	$\Lambda_{2ND}$ [deg]	AR
Concorde	408,010			1.85
TU-144	456,357	76.00	57.00	1.66
XB-70	542,000	65.57	-	1.75
Sanger 2	559,000	83.00	67.00	2.40
Space Shuttle Orbiter	242,508	81.00	45.00	2.27

*Raymer's method – CL max [25]*

The text also provides a way to estimate  $C_{Lmax}$  for low aspect ratio wings. The difference from the method above is that Raymer recommends estimating this value assuming maximum lift at takeoff occurs at Mach 0.5. There is no clear explanation for why this speed was chosen. Two leading edge sweep angles were chosen based on a study done by NASA in 1966 for low-speed delta and double delta wings. It was concluded that the strake portion of a double delta wing increased the strength of vortices over the wing [56]. Following assumptions were made to test the method:

- No taper delta wings ( $\lambda = 0$ )
- Mach number = 0.5
- Low aspect ratio
- Two leading edge sweep angles:  $\Lambda_{LE} = 75^\circ$  and  $\Lambda_{LE} = 62^\circ$

Upon choosing the necessary variables, the maximum low aspect ratio was determined:

$$AR \leq \frac{3}{(C_1 + 1)(\cos \Lambda_{LE})} \quad (48)$$

The constant  $C_1$  is a function of taper ratio, must be determined empirically. From the empirical charts,  $C_1$  will be zero. Using additional empirical charts given for this process,  $C_{Lmax}$  and  $\alpha_{max}$  are estimated.

$$term\ 1 = (C_1 + 1) \frac{AR}{\sqrt{1 - M^2}} \cos \Lambda_{LE} \quad (49)$$

$$term\ 2 = (C_2 + 1) AR \tan \Lambda_{LE} \quad (50)$$

The maximum lift coefficient is given by:

$$C_{Lmax} = (C_{Lmax})_{base} + \Delta C_{Lmax} \quad (51)$$

And its corresponding maximum angle of attack is given by:

$$\alpha_{C_{Lmax}} = (\alpha_{C_{Lmax}})_{base} + \Delta \alpha_{C_{Lmax}} \quad (52)$$

Here, the first term of Eq. (53-54) can be found using the empirical charts given below:

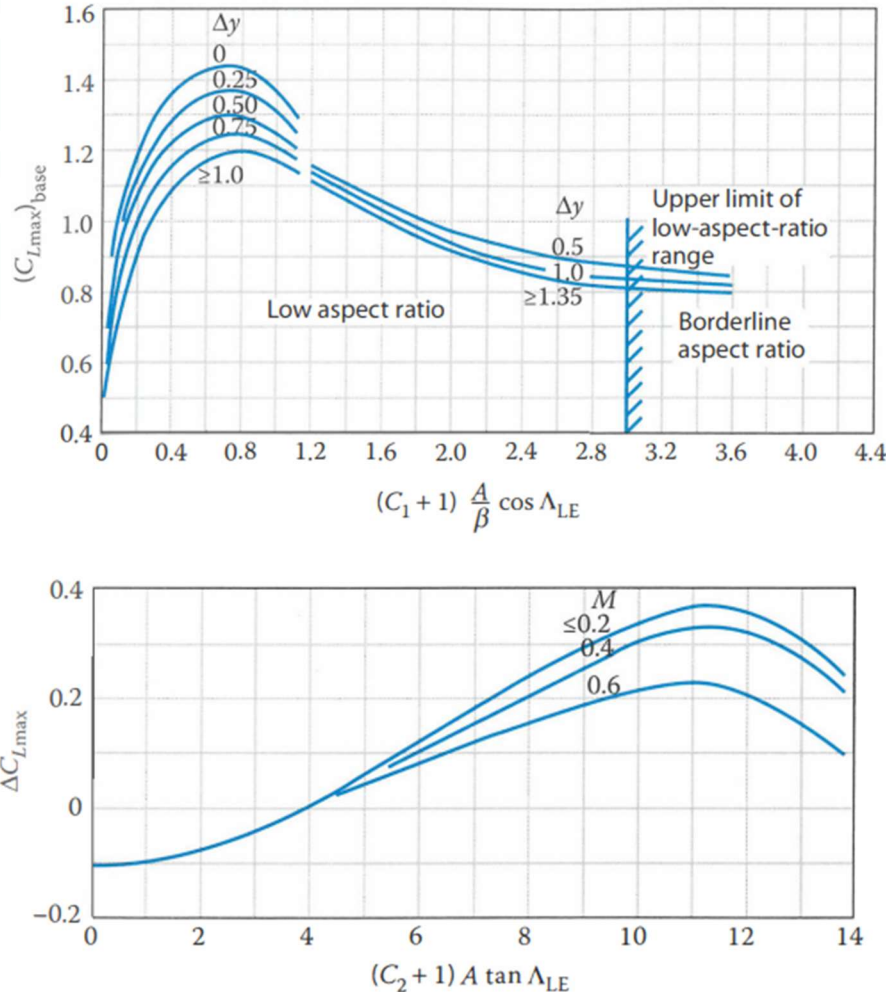


**Fig. 36 Empirical charts to estimate maximum lift coefficient [25]**

Following was the data produced from this process in the Table 11. The term  $\Delta y$  is the leading-edge slenderness parameter. For this analysis, a value of 11.8 t/c for a biconvex airfoil was chosen, with a thickness-to-chord ratio (t/c) of 0.05. This gives the term  $\Delta y = 0.56$ .

**Table 11. Data using Raymer's method for subsonic maximum lift coefficient [57].**

Leading edge sweep angles $\Lambda_{\text{LE}}$ [deg]	AR	Term 1	Term 2	$(C_{L\max})_{\text{base}}$	$\Delta C_{L\max}$	$C_{L\max}$	$(\alpha_{C_{L\max}})_{\text{base}}$	$\Delta \alpha_{C_{L\max}}$	$\alpha_{\max}$
62	4.45	3.46	-4.88	0.85	-0.1	0.75	22	-10	12
63	3.04	3.46	0.52	0.85	-0.1	0.75	22	-8	14
70	4.74	3.46	5.79	0.85	0.1	0.95	22	-10	12
75	3.25	3.46	-1.37	0.85	-0.1	0.75	22	-10	12

As seen in the table above, there is no clear trend seen amongst the values obtained. The angles were converted to radians before using the equations. Although, the maximum lift coefficient and angle of attack fall in the right ballpark values. For a known airfoil, the 2D lift-curve-slope can be obtained from which a 2D maximum lift coefficient  $C_{l\max}$  can be estimated. From that, for moderate sweep angles the following can be used:

$$C_{L_{max}} = 0.9 C_{l_{max}} \cos \Lambda_{0.25c} \quad (55)$$

#### *HYFAC method – Supersonic $C_{L_\alpha}$*

The supersonic lift-curve-slope can be estimated from the following correlation for delta planforms of a WB configuration. This chart is obtained from HYFAC document where it gives lift estimation method for hypersonic vehicle concepts. Most of these vehicles are Hydrogen fuel based. For a double-delta wing, an effective leading-edge angle must be calculated to obtain the  $C_{L_\alpha}$ . The geometric parameters needed are provided in the chart, are the inputs needed from Geometry team.

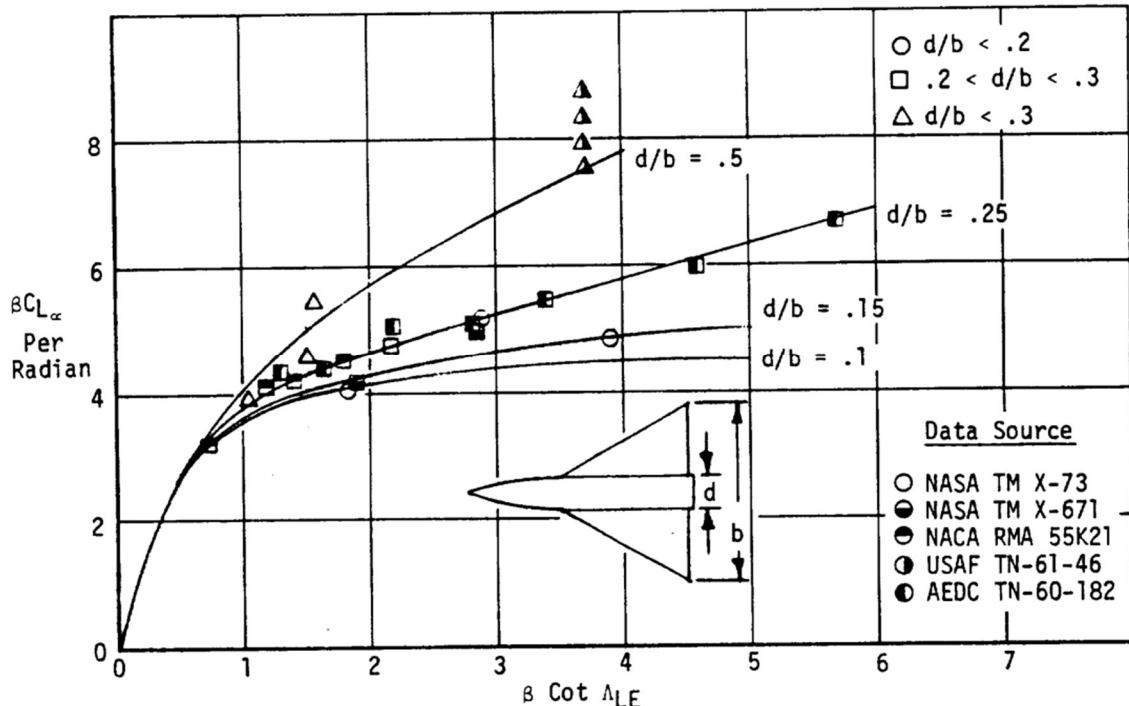


Fig. 37 Correlation for supersonic lift-curve-slope of delta wing-body configuration [HYFAC]

#### 5.2.2 Drag: Induced Drag and Wave Drag

For the drag build-up, many analytical and empirical methods can be used to give the Synthesis & Performance teams with approximate values. General analytical methods for wave drag coefficients may have large errors since wave drag depends on shock waves produced at different Mach numbers. This is dependent on the aircraft geometry for which higher fidelity methods can be used for accuracy. For PS, these coefficients are heavily based on empirical estimates.

The total drag of an aircraft can be calculated by the following relation:

$$C_{D_{total}} = C_{D_0} + L' C_L^2 \quad (56)$$

The first term  $C_{D_0}$  is known as the zero lift drag coefficient. It accounts for all the viscous effects of drag including skin friction drag, pressure drag, wave drag, base drag, interference drag, and engine drag. The second term accounts for drag due to lift, an inviscid phenomenon.

#### *HYFAC method – Drag Coefficient at subsonic speeds*

	<b>SENIOR DESIGN:</b> MAE 4351 Project	Ref.: MAE 4351-001-2021 Date: 09. Jul. 2023 Name: <b>Gayathri Kola</b> Status: In Progress
---	---	---

A method to estimate skin friction drag is given in HYFAC. This is the Von Karman-Schoenherr equation which assumes incompressible flow along a smooth flat plate. For temperature conditions less than Mach 5.0, adiabatic gas condition is assumed.

$$\log 10 (R_N C_F) = \frac{0.242}{\sqrt{C_F}} \quad (57)$$

To account for the thickness of the body at subsonic speeds, relations for the ratio between the wing and flat plate are given. The same is done for the body of the aircraft using the following relations below:

$$\frac{C_{F_{Body}}}{C_{F_{Flat plate}}} = 1 + 1.5 \left( \frac{d}{l} \right)^{\frac{3}{2}} + 7 \left( \frac{d}{l} \right)^3 \quad (58)$$

$$\frac{C_{F_{Wing}}}{C_{F_{flat plate}}} = 1 + 2 \left( \frac{t}{c} \right) + 60 \left( \frac{t}{c} \right)^4 \quad (59)$$

Here, the skin friction coefficient for the body takes body diameter and length into account. For the wing, the ratio of thickness and chord are used. These correction factors are not applicable for supersonic speeds.

#### *P. Czysz and HYFAC methods – Subsonic/Supersonic Induced Drag Factor*

The drag and drag polar estimations are split into three speed regimes: subsonic, transonic, supersonic/hypersonic. The methods for drag polars are summarized in Gary Coleman's thesis paper [33]. These empirical methods are pulled from different sources namely HYFAC reports and "Hypersonic Convergence" publication by Paul Czysz. These methods given below are applicable to both WB and BB configurations. These methods are specifically for hypersonic cruise vehicles, which is a bonus.

For the subsonic drag polar of a highly swept WB planform, empirical relations are used to estimate the maximum L/D and induced drag factor  $L'$ . The induced drag factor can be found using the equation below [33]. These are just used for baseline estimates for PS phase.

$$L' = \frac{1}{4C_{D_0} \left( \frac{L}{D} \right)^2} \quad (60)$$

For the supersonic/hypersonic drag polar of WB or BB configuration, the same method above can be used for Mach numbers up to 12. The thesis gives empirical relations for Mach numbers 2, 5, 12. For our case of Mach numbers 7.5 and 10, the empirical data can be interpolated to estimate the maximum L/D for a given slenderness ratio. The Synthesis team has requested equations that directly relate to geometric changes which could be integrated into the convergence code instead of empirical relations.

Add cleaner empirical charts.

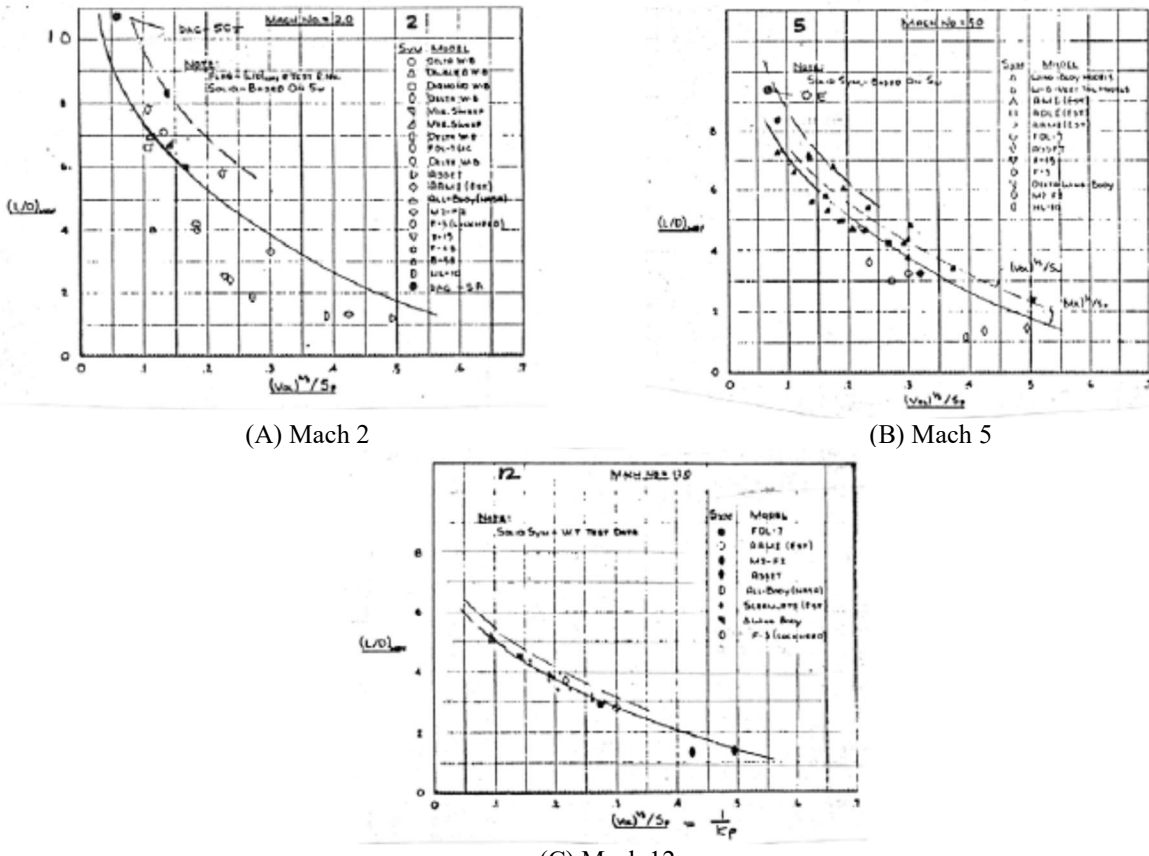


**Fig. 38 Lift-to-drag relations for Mach numbers 2, 5 and 12.**

*Coleman's thesis – Transonic/Supersonic Wave Drag Coefficient [33]*

A method to estimate wave drag at transonic regime (transonic drag rise) is also given in the thesis. This method applies to highly swept WB and BB planforms. This correlation is made based on the aircraft's frontal area  $S_{front}$ . This method is applicable to speeds up to Mach 2.0 and requires frontal area and total aircraft length as inputs. There are two criteria for estimating the wave drag:

1. If  $S_{front}/L^2 < 0.015$ , the wave drag coefficient is:

$$(C_{Dwave})_{max} = \frac{S_{front}}{S_{pln}} \left[ 1.3862 \left( \frac{S_{front}}{L^2} \right) + 0.067 \right] \quad (61)$$

2. If  $S_{front}/L^2 > 0.015$ , the wave drag coefficient is:

$$(C_{D_{wave}})_{max} = \frac{S_{front}}{S_{pln}} \left[ 0.9536 \left( \frac{S_{front}}{L^2} \right)^3 - 1.916 \left( \frac{S_{front}}{L^2} \right)^2 + 1.3651 \left( \frac{S_{front}}{L^2} \right) + 0.1119 \right] \quad (62)$$

The question then becomes, what is the limit for maximum wave drag at transonic, supersonic, and hypersonic speeds.

Aprovitola, et. al Method – Supersonic Wave Drag [58]

The wave drag for the supersonic regime can be estimated using the Sears-Hack body concept. This method is used to minimize drag at high-speed flight. This method was used for Concorde aerodynamic analysis [58].

$$C_{D_w} = \frac{24V}{L^3} \frac{S_{max}}{S_{ref}} = \frac{9\pi^2}{2} \left( \frac{R_{max}}{L} \right) \frac{S_{max}}{S_{ref}} = \frac{4.69}{4} \left[ \left( \frac{R_{max}}{2l_N} \right)^2 + \left( \frac{R_{max}}{2l_T} \right)^2 \right] \frac{S_{max}}{S_{ref}} \quad (63)$$

Here, the parameter  $S_{ref}$  is the reference area, also known as the planform area  $S_{pln}$ . The  $R_{max}$  is the maximum body radius,  $S_{max}$  is the maximum cross-sectional area also known as the frontal area  $S_{front}$  used in our convergence logic. The variables  $l_N$  and  $l_T$  are the nose and tail lengths as illustrated in the Fig. 39 below. Lastly,  $L$  is the entire body length. While the exact dimensions were not found, Tupolev TU-144 data was obtained from [43].

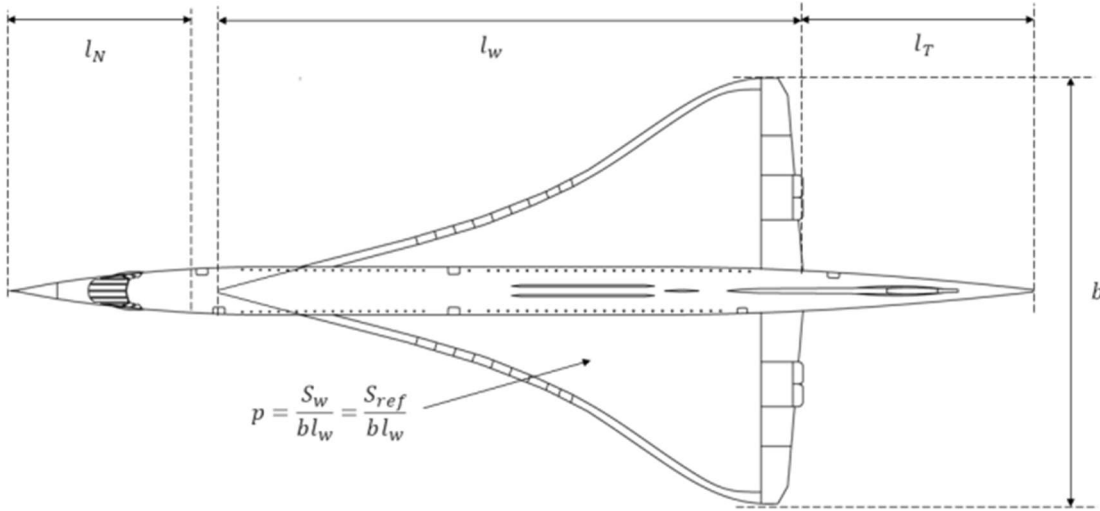


**Fig. 39 Concorde aerodynamic analysis geometric parameters [58].**

#### *Raymer's method – Supersonic skin friction and wave drag coefficient [25]*

Raymer gives a method for estimating supersonic parasite drag. For supersonic speeds, the wave drag becomes a lot dominant due to shock wave formation. First, a method to estimate skin friction drag is presented, followed by the area-ruling method for wave drag. Area ruling is a method to strategically allocate volume between wing and fuselage with an aim to minimize wave drag during transonic and supersonic speeds. Most area-ruled aircraft have tapered fuselage towards the end and the subsequent area is filled by the wing. The buildup of all component areas from the nose up to the end must give a Sears-Hack distribution. Note, no aircraft will have a perfect Sears-Hack distribution. The goal is to arrange components in such a way that there are no significant spikes in the area distribution. An area-ruled aircraft may be more efficient at certain Mach numbers than all.

The parasite drag is a culmination for all viscous drags experienced by the aircraft. At certain speeds, certain combinations of drag are more dominant than others. Parasite drag typically increases with speed. To estimate parasite drag, the following relation can be used:

$$C_{D_0} = C_{D_f} + C_{D_w} + C_{D_{misc}} + C_{D_{L&P}} \quad (64)$$

The last two terms of miscellaneous drag and leakage & protuberance drag are neglected for PS estimates. Only the wave drag coefficient and skin friction drag coefficient are estimated for the parasite drag portion.

To estimate the skin friction drag for supersonic regime, turbulent flow is considered, and includes a Mach number correction. The same method is also presented in Nicolai [20].

	<b>SENIOR DESIGN:</b> MAE 4351 Project	Ref.: MAE 4351-001-2021 Date: 09. Jul. 2023 Name: <b>Gayathri Kola</b> Status: In Progress
---	---	---

$$C_f = \frac{0.455}{(\log_{10} R)^{2.58} (1 + 0.144M^2)^{0.65}} \quad (65)$$

The Reynold number cutoff from the Eq. (66) above is given by the following relation for supersonic or transonic regimes:

$$R = 44.62 \left( \frac{l}{k} \right)^{1.053} M^{1.16} \quad (67)$$

Where  $k$  is the skin roughness factor and  $l$  is the characteristic length of the body, meaning from nose to aircraft end. For our analysis, the skin roughness value was assumed to be  $0.0000133 \text{ ft}^2$  for production sheet metal.

$$\left( \frac{D}{q} \right)_{wave-SH} = \frac{9\pi}{2} \left( \frac{S_{front}}{l} \right)^2 \quad (68)$$

Notice that equation above does not directly give the wave drag coefficient for a Sears-Hack distribution.

$$\left( \frac{D}{q} \right)_{wave} = E_{WD} \left[ 1 - 0.2(M - 1.2)^{0.57} \left( 1 - \frac{\pi \Lambda_{LE-deg}^{0.77}}{100} \right) \right] \left( \frac{D}{q} \right)_{wave-SH} \quad (69)$$

Note, the terms above are not the actual drag coefficient. In fact, the Eq. (70) above must be divided by planform area to obtain correct values.

#### *Leading Edge Suction Method – Supersonic Induced Drag Factor [25]*

There are two methods presented in Raymer to estimate the induced drag factor for supersonic regimes. One is a function of Mach number and leading-edge sweep angle  $\Lambda_{LE}$ , and the other is simply the inverse of  $C_{L\alpha}$ . Raymer recommends using the second method for more accuracy; it's based on the leading-edge suction method. The relation below can be used for a quick estimate of  $K$ :

$$K = \frac{AR(M^2 - 1) \cos \Lambda_{LE}}{(4AR\sqrt{M^2 - 1}) - 2} \quad (71)$$

$$K = \frac{\alpha C_L}{C_L^2} = \frac{\alpha}{C_L} = \frac{1}{C_{L\alpha}} \quad (72)$$

#### 5.2.3 Lift-to-Drag Ratio

The lift-to-drag ratio also known as the “aerodynamic efficiency” is the simple ratio of overall lift and drag for a given speed. The following is the relation:

$$\frac{L}{D} = \frac{C_L}{C_D} \quad (73)$$

This ratio can also be estimated using empirical relations given in Fig. 38 with interpolated values for Mach numbers in between for the PS phase.

Additionally, some analytical methods to calculate L/D are given in the book “Hypersonic Flow” by Maurice Rasmussen. These pertain to a caret waverider, wedge-derived waverider and general cone derived waverider. There are methods to estimate base drag, wave drag, skin friction drag for supersonic and hypersonic flow. However,

	<b>SENIOR DESIGN:</b> MAE 4351 Project	Ref.: MAE 4351-001-2021 Date: 09. Jul. 2023 Name: <b>Gayathri Kola</b> Status: In Progress
---	---	---

these seemed more applicable for All-Body designs. If any of these geometries are considered in the future, these will be applicable.

*Newtonian flat plate theory – Hypersonic L/D estimation [54]*

$$C_L = 2 \sin^2 \alpha \cos \alpha \quad (74)$$

$$C_D = 2 \sin^3 \alpha \quad (75)$$

$$\frac{C_L}{C_D} = \frac{2 \sin^2 \alpha \cos \alpha}{2 \sin^3 \alpha} = \frac{\cos \alpha}{\sin \alpha} = \cot \alpha \quad (76)$$

*Hypersonic flow – Maurice Rasmussen [40]*

Dependent on the type of body chosen caret waveraider, general cone waveraider, wedge-derived waveraider. It is applicable for lifting bodies (AB configurations). However, the estimation process requires a lot more input and may be more tedious for PS logic.

#### 5.2.4 Oswald efficiency factor $e$ :

A simple method to estimate the Oswald efficiency factor is given by the following relation [59]:

$$\left(\frac{L}{D}\right)_{max} = \frac{1}{2} \sqrt{\frac{\pi e A R}{C_{D_0}}} \quad (77)$$

The equation above can be re-arranged for  $e$ :

$$e = \frac{4 C_{D_0}}{\pi A R} \left(\frac{L}{D}\right)_{max}^2 \quad (78)$$

Alternative methods are given in Raymer and reference [59], however, this variable is no longer required by the P&T team.

#### 5.2.5 Aerodynamic center

For the Aerodynamics team, the author will mainly focus on aerodynamic center calculations during CL and CE phase. The aerodynamic center, also known as neutral point, becomes essential for static margin calculations to assess how stable the aircraft is. The current method being considered is given in Raymer [25] and given below:

$$x_{np} = \frac{C_{L_\alpha} \bar{x}_{acw} - C_{m_{\alpha fus}} + \eta_h \frac{S_e}{S_w} C_{L_{\alpha_e}} \frac{\partial \alpha_h}{\partial \alpha} \bar{x}_{ach} + \frac{F_{p_\alpha}}{q S_w} \frac{\partial \alpha_p}{\partial \alpha} \bar{x}_p}{C_{L_\alpha} + \eta_h \frac{S_e}{S_w} C_{L_{\alpha_h}} \frac{\partial \alpha_h}{\partial \alpha} + \frac{F_{p_\alpha}}{q S_w} \frac{\partial \alpha_p}{\partial \alpha}} \quad (79)$$

Most of the derivative terms in the Eq. (80) above are given in empirical relations. Majority of inputs come from Geometry and from within Aerodynamics team. While this method can be used, other directly codable methods are needed that give similar results.

#### 5.2.6 Mission Profile for PS

The mission profile has been generated by the Synthesis and P&T team. The altitude conditions have been checked by the Propulsion team. It has been decided amongst other competing teams to have JFK airport (New York) as the

	<b>SENIOR DESIGN:</b> <b>MAE 4351 Project</b>	Ref.: MAE 4351-001-2021 Date: 09. Jul. 2023 Name: <b>Gayathri Kola</b> Status: In Progress
---	--	---

takeoff point and landing airport would Charles de Gaulle (Paris). There are three speed regimes with two vehicles designed for each: with single and double flow paths to engine intakes. For PS phase, there will be an ascent, cruise, and descent mission segments. One of the concerns raised was the single climb portion of the mission with no division for transonic region. This is a simplified trajectory specific to PS phase for gross sizing estimates. A detailed trajectory will be produced by P&T team in the CE phase.

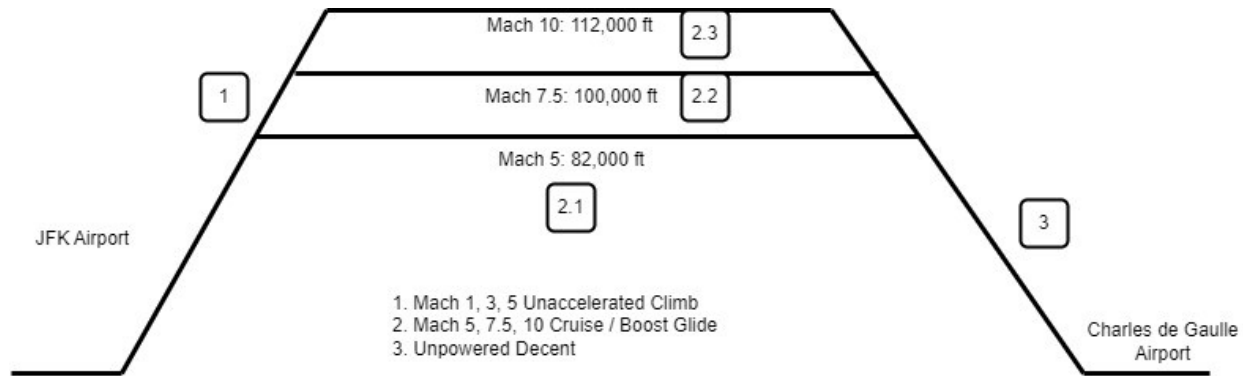


**Fig. 40 Mission profile chosen for PS phase created by Noah Blakely [12].**

### 5.3 Methodology for CL and CE

Once the aircraft geometry is defined, the lift and drag coefficients can be approximated using Oblique Shock Wave and Prandtl-Meyer Expansion wave theories. For X-43A Hyper X, an aerodynamic study was performed by *Universitat Politècnica de Catalunya* (Barcelona, Spain) by employing both analytical and Computational Fluid Dynamics (CFD) models. The study was evaluated for Mach 7 flight at 98,425 ft (30 km). For the analytical portion, several assumptions were made including steady state flow, neglecting viscous and heat transfer effects, assuming air as a calorically perfect gas. For the CFD portion, a tool named OpenFOAM was used to perform a more accurate analysis incorporating the thrust from the scramjet engine [60]. OpenFOAM is a free CFD software that is capable of solving complex fluid flow scenarios [61]. OpenVSP is another tool that is capable of solving for aerodynamic forces within the module VSPAero [62]. Based on the geometry, either of these methods can be employed using CL and CE phase for a more sophisticated analysis.

### 5.4 Validation methods

This section serves to present method verification and the results obtained for aspects that are verifiable. Methods are compared with existing data, dimensions available for similar aircraft to assess the percent error between actual and method values.

#### *Nicolai's method verification – lift curve slope for delta wings*

This method was presented in section 5.2.1, and the produce was tested for varying angle of attack to hopefully obtain a maximum lift coefficient and stall region since the method was for non-linear calculations. Three aspect ratios were chosen that fall within the range similar aircraft given in Table 10. However, as seen in the Fig. 41 below, there is no stall point. The lift coefficient values appear to be quite lower for the corresponding aspect ratio. This may not be the best method applicable for our use.

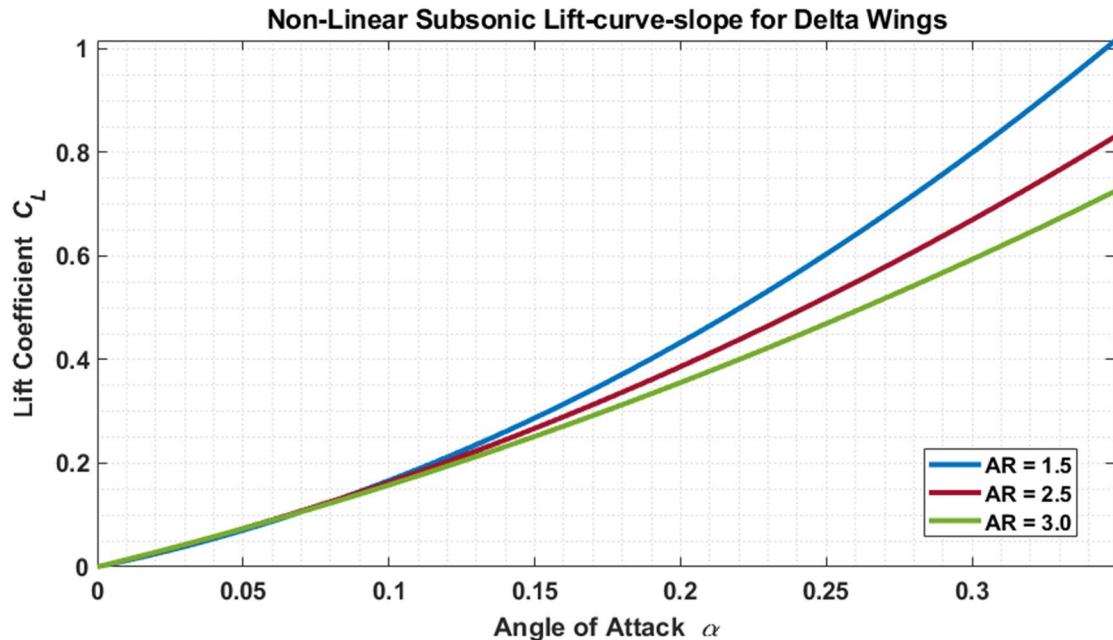


Fig. 41 Subsonic lift-curve-slope of Nicolai's method.

Raymer's method verification – supersonic zero-lift drag coefficient.

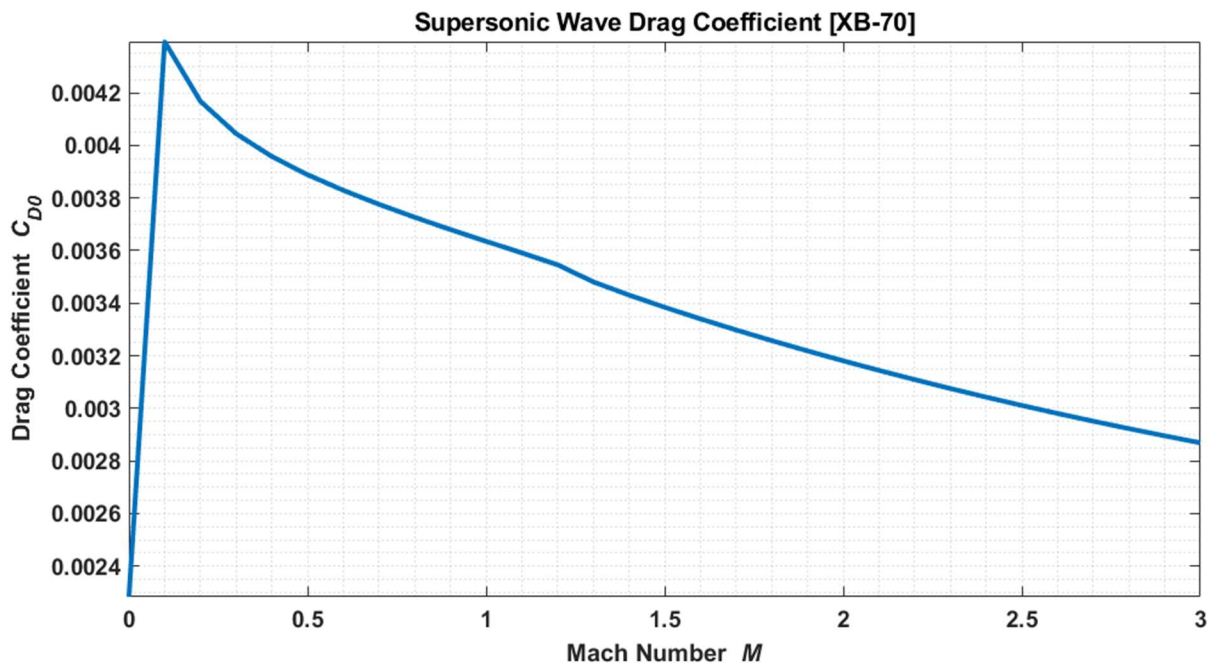


Fig. 42 XB-70 parasite drag test using Raymer's method.

The parasite drag coefficient was tested using the method given in Raymer. When compared with the Fig. 43, the method given in Raymer does not agree. The  $C_{D0}$  range is higher, around 0.005 for the XB-70. Additionally, unlike the Fig. 42, the parasite drag correctly increases around Mach 1, at the sonic speed. With the method given in Raymer, this spike occurs rather early, which is not correct. The geometric data for XB-70 was extracted from NASA technical report [57]. The following was the data used from the report, given in Table 12. Alternative methods need to be tested

for this estimation. A reason for the low values, is the supersonic wave drag efficiency factor  $E_{WD}$ . Raymer recommends a range from 1.8 to 2.2 for supersonic transport aircraft. For the plot above, a value of 1.8 was used. But increasing the value up to 2.2 does not bring a significant change either. A higher value for frontal area would increase the parasite drag. Only the fuselage frontal area was used for calculations. The XB-70's engines are also a large part of the frontal geometric area; this was neglected in the analysis. Which could be the reason for low parasite drag numbers.

**Table 12. The XB-70 data used for parasite drag verification [57].**

Parameter	Symbol	Value	Units
Frontal Area	$S_{front}$	106	inches
Fuselage Length	$l$	189	ft
Planform Area	$S_{pln}$	1184	ft
Leading edge sweep angle	$\Lambda_{LE}$	65	degrees
Mach number	$M$	0 – 3	-

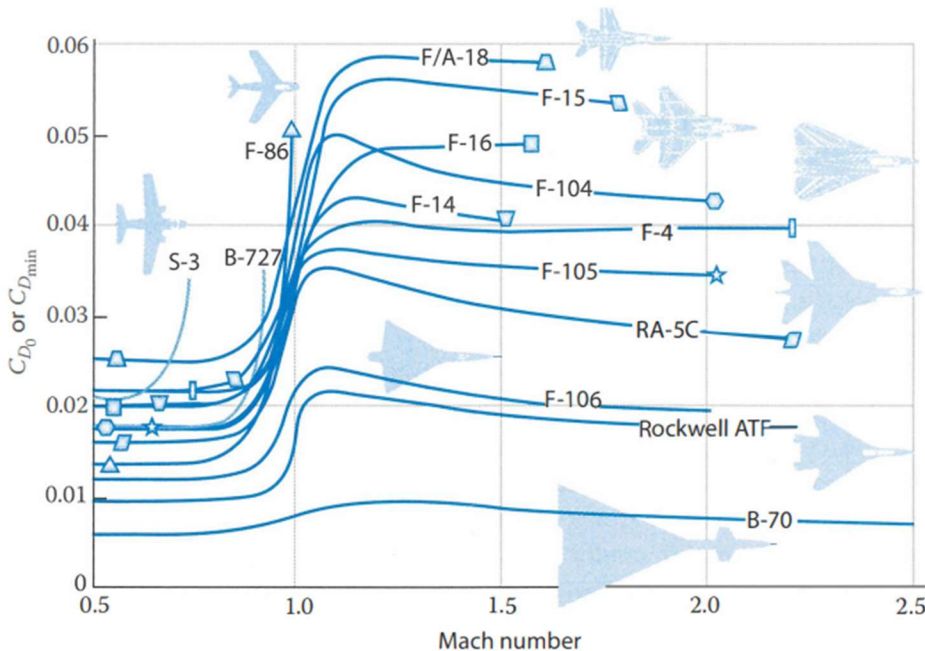


**Fig. 43 Zero-lift drag coefficient verification of XB-70 [Raymer].**

## 5.5 Results, Verification and Discussion for Aerodynamics

This section presents the results obtained from converged vehicle analysis.

## 6 Historical Development

The following section will be dedicated to weekly progress: work that was done and then work that needs to be completed for the following week.

### 6.1 Week 1

The first week was spent gathering literature suitable for each discipline and material pertaining to hypersonic aircraft after the project was launched. The basics of hypersonic aerodynamics were reviewed and understood from previous course texts. For Stability and Control, resources other than DATCOM that can be applied for hypersonic aircraft were searched. Time was spent on looking into project aircrafts such as the Spirit of St. Louis, Gulfstream G700, SR-71, Quarterhorse, Darkhorse, Halcyon, and X-43A. The team meeting included basic communication setup

	<b>SENIOR DESIGN:</b> MAE 4351 Project	Ref.: MAE 4351-001-2021 Date: 09. Jul. 2023 Name: <b>Gayathri Kola</b> Status: In Progress
---	---	---

and expectations for weekly meeting presentations. The author will be keeping track of minutes of meetings and producing written summaries for the team at the end of each meeting. The next week's goal is to identify important parameters for Aerodynamics and Stability and Control that can aid in Parametric Sizing process.

### 6.2 Week 2

The Stability and Control team decided to split responsibilities by topic: longitudinal, lateral, and directional stability and control. The author will be focusing on longitudinal stability and control. The week was spent gathering methodology for longitudinal Stability/Control for CL and CE as well as understanding the issues emerging at hypersonic speeds. The Aerodynamics team decided to look into methods for calculating wing geometry parameters needed and for coming up with a list of similar aircraft and their geometries for reference.

Next week, the goal is to write MATLAB scripts to build on the collected methodology.

### 6.3 Week 3

The week was spent understanding hypersonic aerodynamics and gathering suitable methodology for PS phase. The Synthesis and Performance team have given Aerodynamics team with the inputs required: CL at takeoff, subsonic CD, supersonic CD, hypersonic CD, maximum subsonic lift coefficient, L/D and Oswald Efficiency factor. Aircraft within similar weight class were gathered for method verification. The Synthesis team had requested analytical equations for the inputs required to code into convergence logic. However, upon further research it appears that the accurate calculation of supersonic, hypersonic wave drag requires higher fidelity software. Since the current geometry is a spatula double delta wing, it was difficult to find equations for the same. Empirical relations for WB delta wing with double delta estimation techniques were easier to find. Hence, it appears best to use empirical estimates for PS. Various design features were studied, however, there was less time to write about them. It will be included in the next report.

For Stability and Control, the majority of data was found for control surfaces of the chosen WB aircraft. Less lucky with AB aircraft. The volume coefficients have to be calculated and a database needs to be made to include in code. For next week, methodology for supersonic and hypersonic pitching moment calculation needs to be found and method verification must be done.

### 6.4 Week 4

The week was spent gathering methodology for Aerodynamics team. The initial plan was to find methodology for all parameters related to hypersonic flight by all three team members to compare the assumptions. However, later in the week, the author focused on supersonic drag build up, calculation and verification to add to Aerodynamics module in Synthesis convergence code. Three simple estimation methods were found, of which the author decided to go with the method given in Raymer since the inputs were simpler to obtain from Geometry module.

### 6.5 Week 5

The midterm week was spent gathering and organizing control sizing methodology and identifying useful methods for critical conditions in S&C. Verification literature was gathered and organized based on aircraft type. Additionally, methodology for calculating many stability and control derivatives was found in Roskam's design text and the method is being implemented in code. The code is currently under works, being written with expected completion after week 6. Control surfaces and geometries were explored by the author, however, not much information was found on elevon geometries. Geometries for vertical tail have been found. For control surface sizing code, all the methodologies have been identified, the code must be written and tested.

For Aerodynamics, additional methods for neutral point calculations were looked at, however, the author will be continuing with the method presented in Raymer unless another method is found.

## Appendix

### Appendix A

This appendix serves to give additional information on matters pertaining to Stability and Control discipline.

$\frac{x_{a.c.}}{c_r}$ (calculations based on exposed wing geometry) <ul style="list-style-type: none"> <li>1. Single wing with body (i.e., no cruciform or other multipanel arrangements)</li> <li>2. <math>M \leq 0.6</math>; however, if swept wing with <math>t/c \leq 0.04</math>, application to higher Mach numbers is acceptable</li> <li>3. Linear-lift range</li> </ul> <p><math>C_{L_\alpha}</math></p> <ul style="list-style-type: none"> <li>4. (Body diameter)/(wing span) <math>\leq 0.8</math></li> <li>5. No curved planforms</li> <li>6. Bodies of revolution</li> <li>7. Slender-body theory</li> <li>8. <math>M \leq 0.8</math>, <math>t/c \leq 0.1</math>, if swept wing with round LE</li> </ul>	$\frac{x_{a.c.}}{c_r}$ (calculations based on exposed wing geometry) <ul style="list-style-type: none"> <li>1. Straight-tapered wings</li> <li>2. Single wing with body (i.e., no cruciform or other multipanel arrangements)</li> <li>3. Symmetric airfoils of conventional thickness distribution</li> <li>4. Linear-lift range</li> </ul> <p><math>C_{L_\alpha}</math></p> <ul style="list-style-type: none"> <li>5. Bodies of revolution</li> <li>6. Slender-body theory</li> <li>7. <math>\alpha = 0</math></li> </ul>
(a) Subsonic	(b) Transonic

$\frac{x_{a.c.}}{c_r}$ (calculations based on exposed wing geometry) <ul style="list-style-type: none"> <li>1. Single wing with body (i.e., no cruciform or other multipanel arrangements)</li> <li>2. Linear-lift range</li> </ul> <p><math>C_{N_\alpha}</math></p> <ul style="list-style-type: none"> <li>3. Breaks in LE and TE at same spanwise station</li> <li>4. Bodies of revolution</li> <li>5. Slender-body theory</li> <li>6. <math>M \geq 1.4</math> for straight-tapered wings</li> <li>7. <math>1.2 \leq M \leq 3</math> for composite wings</li> <li>8. <math>1.0 \leq M \leq 3</math> for curved planforms</li> </ul>	$\frac{x_{a.c.}}{c_r}$ (calculations based on exposed wing geometry) <ul style="list-style-type: none"> <li>1. Single wing with body (i.e., no cruciform or other multipanel arrangements)</li> <li>2. Linear-lift range</li> </ul> <p><math>C_{N_\alpha}</math></p> <ul style="list-style-type: none"> <li>3. Breaks in LE and TE at same spanwise station</li> <li>4. Bodies of revolution</li> <li>5. Slender-body theory</li> <li>6. <math>M \geq 1.4</math> for straight-tapered wings</li> <li>7. <math>1.2 \leq M \leq 3</math> for composite wings</li> <li>8. <math>1.0 \leq M \leq 3</math> for curved planforms</li> </ul>
(c) Supersonic	

**Fig. 44 Assumptions to calculate pitching moment as a function of angle of attack from DATCOM [24]**

Following has been removed from the methodology in the Stability and Control section:

#### DATCOM method at subsonic speeds:

The method to calculate pitching moments at subsonic speeds for a wing body configuration is given in DATCOM [24]. The method given below is the same for *supersonic* and *transonic* regimes as well, however, the assumptions differ. The assumptions are given in the Appendix A. According to DATCOM, this method is applicable to the wing body configuration of a conical body mounted on a delta wing as seen in Fig. below. This method utilizes slender body theory, its limitations are that it does not apply to wings with sweptback trailing edges [24].

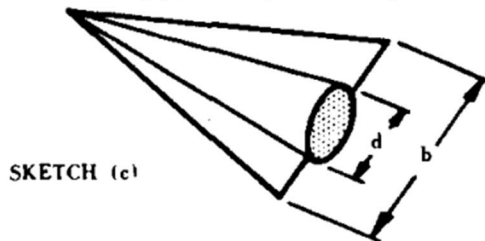


**Fig. 45 Specific wing-body geometry for calculating 3D lift-curve slope of the wing [24].**

$$C_{m\alpha} = \left( n - \frac{x_{a.c.}}{c_r} \right) \frac{c_r}{c} C_{L\alpha} \quad (81)$$

The parameters given in the Eq. (82) are shown in Fig below.

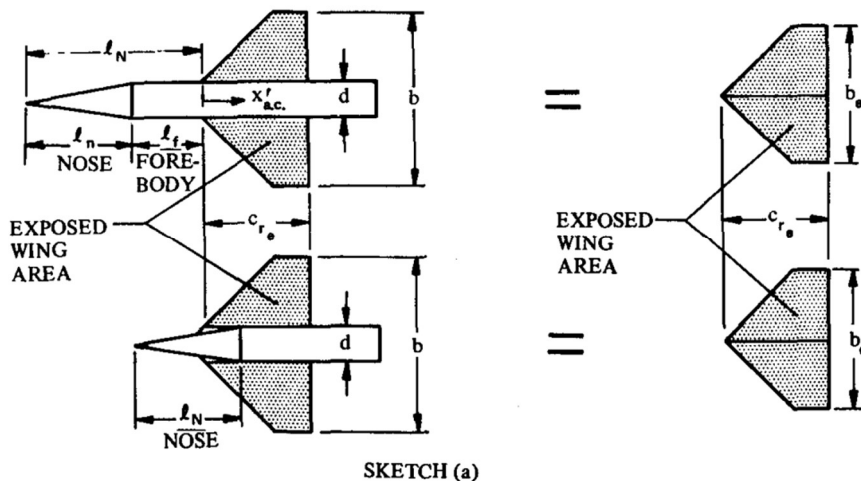


**Fig. 46 Wing geometry parameter definitions [24].**

Here, the 3D lift-curve slope for WB configuration is calculated by the following relation:

$$(C_{L\alpha})_{WB} = K_{(WB)} (C_{L\alpha})_W \quad (83)$$

Where  $K_{(WB)}$  can be estimated from the following Fig. below. It requires the diameter of the body and wingspan.

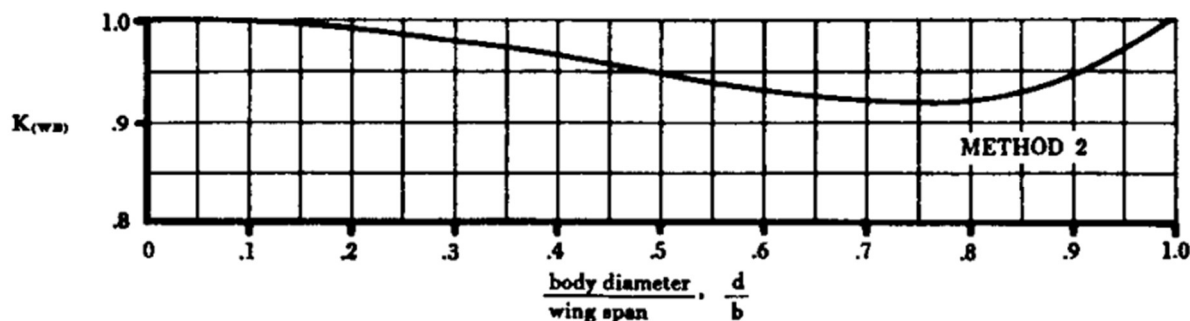


**FIGURE 4.3.1.2-12c LIFT RATIO FOR METHOD 2**

**Fig. 47 Method to find lift ratio for estimating pitching moments [24].**

To find the subsonic  $(C_{L\alpha})_W$  for just the wing, the following relation must be used for a double-delta wing. There are methods available for Ogee and Gothic wings as well. The distinction in geometry is seen below in Fig.

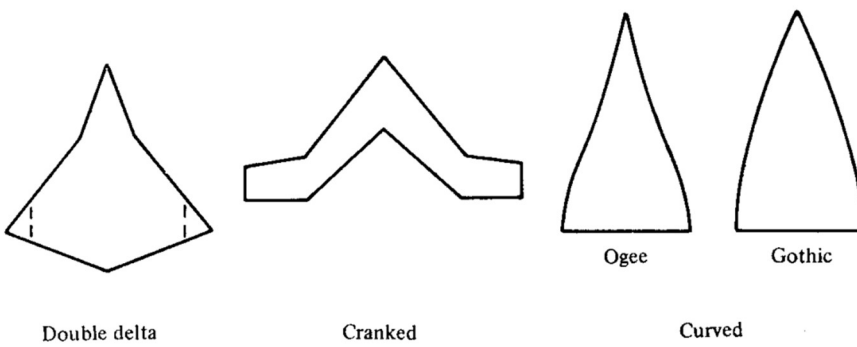


**Fig. 48 Wing geometries presented to estimate the lift-curve slope [24].**

	<b>SENIOR DESIGN:</b> MAE 4351 Project	Ref.: MAE 4351-001-2021 Date: 09. Jul. 2023 Name: <b>Gayathri Kola</b> Status: In Progress
---	---	---

As per the needs of the Aerodynamics team, any of these geometries can be chosen. Since the lift-curve slope is an output given by the Aerodynamics team, this portion will be further discussed in the section 5 once the geometry is chosen. It appears that it would be best to find the lift-curve slopes using a higher fidelity software such as OpenVSP once the geometry is known. The method laid out in DATCOM is time intensive.

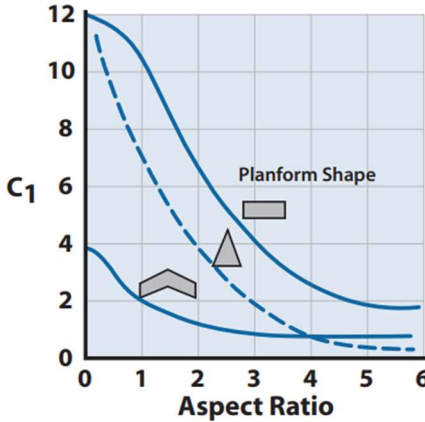
## Appendix B

This appendix serves to give additional information on matters pertaining to Aerodynamics discipline.

## Appendix C

This appendix serves to give method summary cards chosen or considered at a certain phase in the design process.

### AERODYNAMICS

Method Overview			
<b>Discipline</b> Aerodynamics	<b>Design Phase</b> Parametric Sizing (PS)	<b>Method Title</b> Subsonic lift-curve-slope for delta wings. Subsonic lift coefficient for delta wings.	<b>Author(s)</b> Nicolai
<b>Reference:</b> Nicolai, L. M., and Carichner, G. E. <i>Fundamentals of Aircraft and Airship Design</i> . Volume I AIAA 2010			
<b>Brief Description:</b> Lift-curve-slope $C_{L\alpha}$ calculation for subsonic, Low AR, delta wings with a non-linear lift correction. The constant $C_1$ is estimated from the chart given below.			
<b>Assumptions</b> <ul style="list-style-type: none"> <li>• Subsonic</li> <li>• Delta wing, planform</li> <li>• Low aspect ratio (AR)</li> <li>• Non-linear lift</li> </ul>		<b>Applicability</b> Subsonic regimes only.	
<b>Execution of Method</b>			
<b>Input</b> Mach number $M$ , leading edge sweep angle $\Lambda_{LE}$ , aspect ratio $AR$ , angle of attack $\alpha$			
<b>Analysis Description</b>			
<ol style="list-style-type: none"> <li>1. <math>\beta = \sqrt{1 - M^2}</math></li> <li>2. <math>\frac{dC_L}{d\alpha} = C_{L\alpha} = \frac{2\pi AR}{2 + \sqrt{4 + AR^2\beta^2(1 + \left[ \frac{(\tan^2 \Lambda_{LE})}{\beta^2} \right])}}</math></li> <li>3. Chart: delta planform</li> <li>4. <math>C_L = \left( \frac{dC_L}{d\alpha} \right)_{\alpha=0} \alpha + C_1 \alpha^2</math></li> </ol>			
			
<b>Output</b> $C_{L\alpha}, C_L$			
<b>Experience</b>			
<b>Accuracy</b>	<b>Time to Calculate</b>	<b>General Comments</b>	



Best for delta planforms	Fast	Estimate for PS only.
Template adapted from Gary Coleman's thesis		

Method Overview					
Discipline	Design Phase	Method Title	Author(s)		
Aerodynamics	Parametric Sizing (PS)	Supersonic lift-curve-slope: Delta wings of WB Configuration	HYFAC		
<b>Reference:</b> HYFAC					
<b>Brief Description:</b> Lift-curve-slope $C_{L\alpha}$ calculation for supersonic, WB delta wings. For a double-delta wing, an effective leading edge sweep angle must be used.					
<b>Assumptions</b> <ul style="list-style-type: none"> <li>• Supersonic</li> <li>• Delta wing, planform</li> <li>• Low aspect ratio (AR)</li> <li>• Non-linear lift</li> </ul>		<b>Applicability</b> Supersonic regimes. Delta wing & Double-Delta wings.			
<b>Execution of Method</b>					
<b>Input</b> Mach number $M$ , leading edge sweep angle $\Lambda_{LE}$ or <b>effective leading edge sweep angle <math>\Lambda_{EFF}</math> (double delta)</b> , wingspan $b$ , fuselage diameter $d$					
<b>Analysis Description</b>					
<ol style="list-style-type: none"> <li>1. <math>\beta = \sqrt{1 - M^2}</math></li> <li>2. Ratio: <math>d/b</math></li> <li>3. Calculate <math>\beta \cot \Lambda_{LE}</math></li> <li>4. Chart correlation for <math>C_{L\alpha}</math></li> <li>5. Don't forget to divide by <math>\beta</math></li> </ol> <p>The graph plots <math>\beta C_{L\alpha}</math> (Per Radian) on the y-axis (0 to 8) against <math>\beta \cot \Lambda_{LE}</math> on the x-axis (0 to 7). Four curves are shown for <math>d/b = .1</math>, <math>.15</math>, <math>.25</math>, and <math>.5</math>. Data points are represented by circles, squares, and triangles, corresponding to different <math>d/b</math> ratios: <math>d/b &lt; .2</math> (open circles), <math>.2 &lt; d/b &lt; .3</math> (open squares), and <math>d/b &lt; .3</math> (open triangles). A legend indicates the data sources: NASA TM X-73 (open circle), NASA TM X-671 (solid circle), NACA RMA 55K21 (solid square), USAF TN-61-46 (solid triangle), and AEDC TN-60-182 (solid circle).</p>					
<b>Output</b> $C_{L\alpha}$ (supersonic)					
<b>Experience</b>					
<b>Accuracy</b> Best for delta planforms. Can be used for double-delta planforms		<b>Time to Calculate</b> Fast	<b>General Comments</b> Estimate for PS only.		
Template adapted from Gary Coleman's thesis					

<b>ATLANTIX</b>		SENIOR DESIGN: MAE 4351 Project	Ref.: MAE 4351-001-2021 Date: 09. Jul. 2023 Name: <b>Gayathri Kola</b> Status: In Progress
-----------------	---	------------------------------------	---

Method Overview					
Discipline	Design Phase	Method Title	Author(s)		
Aerodynamics	Parametric Sizing (PS)	Subsonic skin friction coefficient (analytical)	HYFAC		
<b>Reference:</b> HYFAC					
<b>Brief Description:</b> Calculation of skin friction coefficient for subsonic speeds using the Von-Schoenherr equation. First assuming a flat plate, then adding a correction for a wing and body.					
<b>Assumptions</b> <ul style="list-style-type: none"> <li>• Subsonic</li> <li>• Incompressible flow over a smooth flat plate</li> <li>• Adiabatic gas (air) for Mach numbers less than 5.0</li> </ul>		<b>Applicability</b> Subsonic regimes. WB configuration			
<b>Execution of Method</b>					
<b>Input</b> Reynolds number $R_e$ , wing thickness $t$ , chord length $c$ , fuselage diameter $d$ , fuselage length $l$					
<b>Analysis Description</b>					
$1. \frac{C_{F_{Body}}}{C_{F_{Flat\ plate}}} = 1 + 1.5 \left(\frac{d}{l}\right)^{\frac{3}{2}} + 7 \left(\frac{d}{l}\right)^3$ $2. \frac{C_{F_{Wing}}}{C_{F_{flat\ plate}}} = 1 + 2 \left(\frac{t}{c}\right) + 60 \left(\frac{t}{c}\right)^4$ 3. Not sure how to use this yet: $\log 10 (R_N C_F) = \frac{0.242}{\sqrt{C_F}}$					
<b>Output</b> $C_F$ (subsonic)					
<b>Experience</b>					
<b>Accuracy</b> Not the most accurate.	<b>Time to Calculate</b> Fast	<b>General Comments</b> Estimate for PS only.			
Template adapted from Gary Coleman's thesis					

Method Overview			
Discipline	Design Phase	Method Title	Author(s)
Aerodynamics	Parametric Sizing (PS)	Transonic wave drag coefficient for WB, BB Supersonic wave drag coefficient for WB	Paul Czysz Gary Coleman
<b>Reference:</b>			
1. Coleman, G. <i>Aircraft Conceptual Design – An Adaptable Parametric Sizing Methodology</i> . 2. Aprovitola, A., Dyblenko, O., Pezzella, G., and Viviani, A. “ <i>Aerodynamic Analysis of a Supersonic Transport Aircraft at Low and High Speed Flow Conditions</i> ”.			
<b>Brief Description:</b>			

	<b>SENIOR DESIGN:</b> MAE 4351 Project	Ref.: MAE 4351-001-2021 Date: 09. Jul. 2023 Name: <b>Gayathri Kola</b> Status: In Progress
---	---	---

Calculation of skin friction coefficient for subsonic speeds using the Von-Schoenherr equation. First assuming a flat plate, then adding a correction for a wing and body.

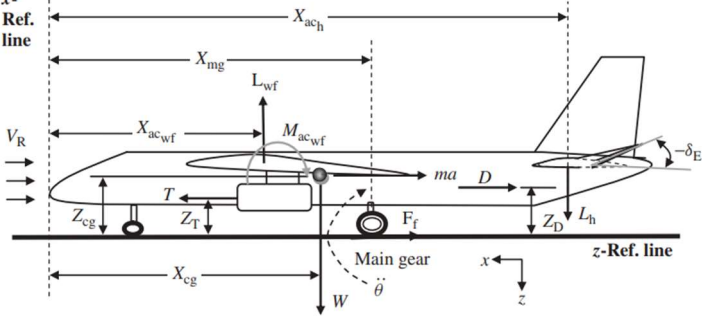
<b>Assumptions</b> <ul style="list-style-type: none"> <li>Transonic (<math>0.8 &lt; M &lt; 1.2</math>), supersonic</li> <li>Incompressible flow over a smooth flat plate</li> <li>Adiabatic gas (air) for Mach numbers less than 5.0</li> </ul>	<b>Applicability</b> Subsonic and supersonic regime. For supersonic, the equation comes method for Concorde analysis.	
<b>Execution of Method</b>		
<b>Input</b>		
Transonic: Aircraft frontal area $S_{front}$ , aircraft length $L$ , planform area $S_{pln}$ , Supersonic: Maximum body radius $R_{max}$ , Maximum cross-sectional area $S_{max}$ ( $S_{front}$ ), Planform area $S_{ref}$ , nose length $l_N$ , tail length $l_T$ , body length $L$		
<b>Analysis Description</b>		
<p><b>Transonic:</b></p> <ol style="list-style-type: none"> <li>If <math>S_{front}/L^2 &lt; 0.015</math></li> </ol> $(C_{Dwave})_{max} = \frac{S_{front}}{S_{pln}} \left[ 1.3862 \left( \frac{S_{front}}{L^2} \right) + 0.067 \right]$ <ol style="list-style-type: none"> <li>If <math>S_{front}/L^2 &gt; 0.015</math></li> </ol> $(C_{Dwave})_{max} = \frac{S_{front}}{S_{pln}} \left[ 0.9536 \left( \frac{S_{front}}{L^2} \right)^3 - 1.916 \left( \frac{S_{front}}{L^2} \right)^2 + 1.3651 \left( \frac{S_{front}}{L^2} \right) + 0.1119 \right]$		
<p><b>Supersonic:</b></p> <ol style="list-style-type: none"> <li><math>C_{Dw} = \frac{24V}{L^3} \frac{S_{max}}{S_{ref}} = \frac{9\pi^2}{2} \left( \frac{R_{max}}{L} \right) \frac{S_{max}}{S_{ref}} = \frac{4.69}{4} \left[ \left( \frac{R_{max}}{2l_N} \right)^2 + \left( \frac{R_{max}}{2l_T} \right)^2 \right] \frac{S_{max}}{S_{ref}}</math></li> </ol>		
<b>Output</b>		
$C_{Dw}$ (Transonic), $C_{Dw}$ (Supersonic)		
<b>Experience</b>		
<b>Accuracy</b>	<b>Time to Calculate</b> Fast	<b>General Comments</b> Estimate for PS only.
Template adapted from Gary Coleman's thesis		

Raymer: CD supersonic – Pg. 432.

HYFAC: Induced drag factor, Vol 2 – Part 2.

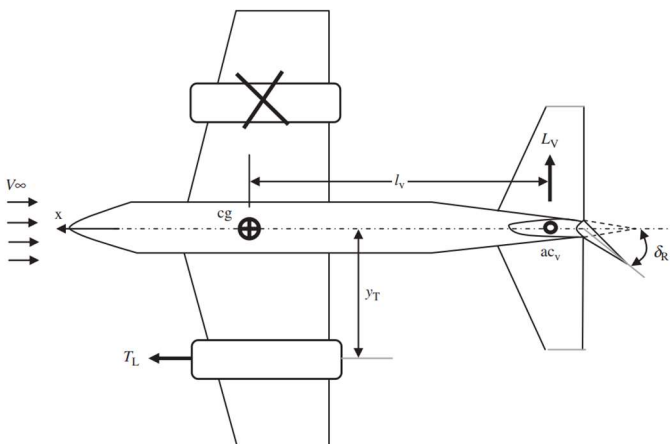
## STABILITY AND CONTROL

Method Overview			
Discipline	Design Phase	Method Title	Author(s)
Stability and Control	Configuration Evaluation (CE)	Takeoff Rotation	M. Sadraey
<b>Reference:</b>			
Sadraey, M. H. <i>Aircraft Design: A Systems Engineering Approach</i> . Wiley, Chichester, West Sussex, U.K, 2013.			
<b>Brief Description:</b>			
Provides a way to find the maximum elevator deflection angle to rotate about the main landing gear during takeoff. Has detailed methodology for estimating takeoff acceleration.			
<b>Assumptions</b>		<b>Applicability</b>	
<ul style="list-style-type: none"> <li>Large transport aircraft</li> <li>0.2V<sub>TO</sub> (takeoff speed)</li> </ul>		Transport aircraft	

Execution of Method				
Input				
Lift-curve-slope $C_{L\alpha}$ , lift coefficient $C_L$ , control derivatives $C_{L\delta_e}$ and $C_{m\delta_e}$ , Stability derivatives $C_{m\alpha}$ and $C_{m_0}$				
Analysis Description				
$5. \quad \delta_e = -\frac{C_{L\alpha}C_{m_0} + C_{m\alpha}C_L}{C_{L\alpha}C_{m\delta_e} - C_{L\delta_e}C_{m\alpha}}$ $6. \quad \sum M_{cg} = I_{yy_mg} \ddot{\theta} = -M_W + M_D - M_T + M_{Lwf} + M_{acwf} + M_{Lh} + M_a$				
				
Output	$\ddot{\theta}$ for takeoff, $\delta_e$ for different trim conditions (same code)			
Experience				
Accuracy	Time to Calculate	General Comments		
Unsure		Will go into the Control Surface Sizing code.		
Template adapted from Gary Coleman's thesis				

Method Overview								
Discipline	Design Phase	Method Title	Author(s)					
Stability and Control	Configuration Evaluation (CE)	Trim Drag	Nicolai & Carichner					
Reference:								
Fundamentals of Aircraft and Airship Design (Vol 1), Nicolai & Carichner 2012.								
Brief Description:								
Gives a way to calculate trim drag for TAC configuration that can be adapted to tailless aircraft with elevons. Will be using this method unless a better method is found.								
Assumptions		Applicability						
<ul style="list-style-type: none"> <li>Load factor <math>n = 1</math>, most applicable for subsonic regimes.</li> <li>Extended to supersonic &amp; hypersonic regimes.</li> </ul>		Mostly applicable to TAC aircraft.						
Execution of Method								
Input	Tail efficiency $\eta_T$ , tail area $S_T$ , tail lift coefficient $C_{L_T}$ , wing lift-curve-slope $C_{L\alpha}$ , thrust $T$ (all engines), z-location of thrust line $z_T$ , wing area $S_{ref}$ , stability derivatives $C_{m\delta}$ and $C_{L\delta}$ (from empirical relations).							
Analysis Description								
$7. \quad \delta_e = \frac{\left(\frac{x_w}{c}\right)\left(\frac{dC_L}{d\alpha}\right)_w \alpha - \left(\frac{Tz_T}{q_\infty S_{ref} c}\right)}{-\left(\frac{x_w}{c}\right)C_{L\delta} + C_{M\delta}}$ $8. \quad D_{trim} = \eta_T q_\infty S_T K_T C_L^2 T$								
Output	$D_{trim}$ , $\delta_e$ for different trim conditions (same code)							

Experience		
Accuracy	Time to Calculate	General Comments
Unsure		Will go into the Control Surface Sizing code.  Template adapted from Gary Coleman's thesis

Method Overview					
Discipline	Design Phase	Method Title	Author(s)		
Stability and Control	Configuration Evaluation (CE)	Takeoff Rotation	M. Sadraey		
<b>Reference:</b>					
OEI: Sadraey, M. H. <i>Aircraft Design: A Systems Engineering Approach</i> . Wiley, Chichester, West Sussex, U.K, 2013. Crosswind Landing: Fundamentals of Aircraft and Airship Design (Vol 1), Nicolai & Carichner 2012.					
<b>Brief Description:</b>					
The two books above will be used to first find the maximum rudder deflection for OEI. If there is more than one engine on a single side of the plane, the book gives methods for multiple engines as well. For crosswind landing, simpler method is being used given in Nicolai compared to Sadraey, due to time constraints.					
<b>Assumptions</b>		<b>Applicability</b>			
OEI:		Transport aircraft			
<ul style="list-style-type: none"> <li><math>C_{n_0} = 0</math> (Symmetric aircraft)</li> <li>Twin engines</li> <li>No elevon deflection <math>\delta_e = 0</math></li> <li>sideslip angle <math>\beta = 0</math></li> </ul>					
Crosswind landing:					
<ul style="list-style-type: none"> <li>Sideslip angle <math>\beta = 11.5^\circ</math></li> <li><math>0.2V_{TO}</math> crosswinds</li> </ul>					
<b>Execution of Method</b>					
<b>Input</b>					
OEI: Thrust from both engines $T_L$ , y-location of engines from fuselage centerline $y_T$ , wing area $S_{ref}$ , wingspan $b$ , control derivative $C_{n_{\delta_r}}$ , vertical tail area $S_{VT}$					
Crosswind landing: $V_{TO}$ , $C_{n_\beta}$ , $C_{n_{\delta_r}}$ . Vary rudder deflection angle $\delta_r$ and fix sideslip angle $\beta$ .					
<b>Analysis Description</b>					
<ol style="list-style-type: none"> <li>OEI:  <math display="block">\delta_r = \frac{T_L y_T}{-\bar{q} S_{ref} b C_{n_{\delta_r}}}</math> </li> <li>Crosswind Landing  <math display="block">C_n = 0 = C_{n_\beta} \beta + C_{n_{\delta_r}} \delta_r</math> </li> </ol>					
					
<b>Output</b>					
Maximum rudder deflection angle $\delta_r$					



Experience		
Accuracy	Time to Calculate	General Comments
Unsure		Will go into the Control Surface Sizing code.
Template adapted from Gary Coleman's thesis		

## Appendix D

This appendix serves to give codes written by the author.

### AERODYNAMICS

Supersonic parasite drag estimation module given in Raymer. This has been included in Aeromodule.m of Synthesis code.

```
% Verifying Supersonic Parasite drag with XB-70 dimensions:  
% Reference: Base Pressure Measurements on the XB-70 Airplane at Mach 0.4 to 3.0, NASA-TM-X-1612.  
  
%[ft^2] Frontal area:  
Sfront = pi*((106/12)/2)^2;  
  
%[ft] Fuselage length:  
l = 189;  
  
%[-] Mach Number range  
M = 0:0.1:3;  
  
%[ft^2] Planform area  
Spln = 1184;  
  
%[deg] leading edge sweep angle:  
SweepLE = 65;  
  
%[-] Extracting supersonic drag coefficient from the function:  
for i = 1:length(M)  
    [CDo(i), CDw(i), Cdf(i)] = CDSupersonic(Sfront, l, M(i), SweepLE, Spln);  
end  
  
%% Initiates nicer colors for plots:  
% Plot settings code kindly provided by David Mexquitic  
Color = get(gcf, 'DefaultAxesColorOrder');  
brown = Color(4,:); gold = Color(3,:);  
cielo = Color(6,:); red = Color(7,:);  
green = Color(5,:); blue = Color(1,:);  
orange = Color(2,:);  
  
Lw = 3; % Line width, used in plot command  
fSize = 15; % Text size, used in X & Y label  
  
% Plotting Commands  
legs = {'C_D_0', 'C_D_w', 'C_D_f'};  
figure('Name', 'FigureName', 'NumberTitle', 'off')  
plot(M, CDo(:), 'linewidth', Lw, 'Color', blue)  
% hold on  
% plot(M, CDw(:), 'linewidth', Lw, 'Color', green)  
% hold on  
% plot(M, Cdf(:), 'linewidth', Lw, 'Color', orange)  
% hold on  
box on; % adds a box i guess  
grid minor  
% legend(legs)  
set(gca, 'FontWeight', 'bold', 'FontSize', 14) % Sets the axis and fonts to bold  
set(gcf, 'Color', 'W') % Sets the figure background to white
```



```
title('Supersonic Wave Drag Coefficient [XB-70]') % Title of the plot
ylabel('Drag Coefficient {\it C_D_0}', 'FontSize', fSize) % Y axis label
xlabel('Mach Number {\it M}', 'FontSize', fSize) % X axis label
ylim([-inf inf])
xlim([-inf inf])
ax = gca; % axes handle
ax.YAxis.Exponent = 0;

% Sets nicer grid lines, i think AIAA does not use grids
% set(gca, 'YMinorGrid', 'On','XMinorGrid', 'On')

function [CDo_ss, CDwave_ss, CSkinFriction_ss] = CDSupersonic(Amax, l, M, SweepLE, Splt)
% METHOD: RAYMER, Pg. 420, 432, 433
% ASSUMPTIONS: Supersonic regime

% INPUTS >>
% Amax [ft^2] - Maximum Cross-sectional area
% l [ft] - body length: from nose to end.
% M [-] - Mach number
% SweepLE [deg] - Leading Edge sweep angle
% Supersonic wave drag:

%[ft] Skin Roughness Value [Production sheet metal]
k = 1.33E-5;

%[-] Cut-off Reynolds Number of Supersonic: [flat plate + Mach correction factor]
R_ss = 44.62 * ((l/k)^1.053) * (M^1.16);

%[-] Supersonic skin friction drag:
CSkinFriction_ss = (0.455) / ((log10(R_ss)^2.58)*((1+0.144*(M^2))^0.65));

%[-] Sears Hack Wave Drag Coefficient:
CDWave_SHack = (9*pi/2) * (Amax/l)^2;

%[-] Wave drag efficiency factor: (Supersonic factor from 1.8 - 2.2)
EWD = 1.8;

%[-] Area ruled wave drag coefficient: !! Sweep in degrees
CDwave_ss = (EWD * (1 - (0.2*(M-1.2)^0.57)*(1 - (pi*(SweepLE^0.77)/100))) * CDWave_SHack) / Splt;

%[-] Estimated parasite drag coefficient
CDo_ss = CSkinFriction_ss + CDwave_ss;

end
```

---

Subsonic lift-curve-slope – Nicolai method test  
% METHOD: NICOLAI, Pg. 46-49  
% ASSUMPTIONS: Subsonic, delta wing, low-aspect ratio.

```
% INPUTS >>
% AR [-] - Aspect ratio
% M [-] - Mach number
% SweepLE [deg] - Leading Edge sweep angle

clc
clear
close

%[-] Mach Number
M = 0.5;

%[-] Aspect Ratio
AR1 = 1.5;
```



```
AR2 = 2.5;
AR3 = 3;

%[-] Constant for AR of delta wing
C1 = 5;
C2 = 3;
C3 = 2;

%[-] Some parameter
Beta = sqrt(1 - M^2);

%[rad] Leading edge sweep
SweepLE = 75 * (pi/180);

%[-] lift-curve-slope for delta wing
CLAlpha1 = (2*pi*AR1) / (2 + sqrt(4 + ((AR1^2*Beta^2)*(1 + (tan(SweepLE)^2/Beta^2))))));
CLAlpha2 = (2*pi*AR2) / (2 + sqrt(4 + ((AR2^2*Beta^2)*(1 + (tan(SweepLE)^2/Beta^2))))));
CLAlpha3 = (2*pi*AR3) / (2 + sqrt(4 + ((AR3^2*Beta^2)*(1 + (tan(SweepLE)^2/Beta^2))))));

% %[rad] angle of attack
% alpha = 1 * (pi/180);

%[-] Lift coefficient
CL1 = @(alpha) (CLAlpha1 * alpha) + (C1 * alpha^2);
CL2 = @(alpha) (CLAlpha2 * alpha) + (C2 * alpha^2);
CL3 = @(alpha) (CLAlpha3 * alpha) + (C3 * alpha^2);

% Initiates nicer colors for plots:
% Plot settings code kindly given by David Mexquitic
Color = get(groot, 'DefaultAxesColorOrder');
brown = Color(4,:); gold = Color(3,:);
cielo = Color(6,:); red = Color(7,:);
green = Color(5,:); blue = Color(1,:);
orange = Color(2,:);

Lw = 3;      % Line width, used in plot command
fSize = 15; % Text size, used in X & Y label

%% Plotting Commands
legs = {'AR = 1.5', 'AR = 2.5', 'AR = 3.0'};

figure('Name','FigureName','NumberTitle','off')
fplot(CL1, deg2rad([0 20]), 'linewidth', Lw, 'Color', blue)
hold on
fplot(CL2, deg2rad([0 20]), 'linewidth', Lw, 'Color', red)
hold on
fplot(CL3, deg2rad([0 20]), 'linewidth', Lw, 'Color', green)
box on; % adds a box i guess
legend(legs)
grid minor
set(gca, 'FontWeight', 'bold', 'FontSize', 14) % Sets the axis and fonts to bold
set(gcf, 'Color','W') % Sets the figure background to white
title('Non-Linear Subsonic Lift-curve-slope for Delta Wings') % Title of the plot
ylabel('Lift Coefficient {\it C_L}', 'FontSize', fSize) % Y axis label
xlabel('Angle of Attack {\it \alpha}', 'FontSize', fSize) % X axis label
ylim([-inf inf])
xlim([-inf inf])

% Sets nicer grid lines, i think AIAA does not use grids
% set(gca, 'YMinorGrid', 'On','XMinorGrid', 'On')
```

---

## STABILITY AND CONTROL

	<b>SENIOR DESIGN:</b> MAE 4351 Project	Ref.: MAE 4351-001-2021 Date: 09. Jul. 2023 Name: <b>Gayathri Kola</b> Status: In Progress
---	---	---

Adapting Jan Roskam's PART VI methodology for calculating longitudinal stability derivatives for the subsonic, supersonic, and extended to hypersonic regimes. Code in progress.

```

%% Stability and Control: CE Analysis
%% WRITTEN BY: Gayathri Kola
%% METHOD >> JAN ROSKAM (PART 6)
%% INPUTS >>

% STEADY-STATE DERIVATIVES
%-----

[CD1, CL1, CM1, CTX1, CMT1] = SteadyState_Derivatives(inputs);

% STABILITY: SPEED DERIVATIVES
%-----

[CDu, CLu, CMu, CTXu, CMTu] = Speed_Derivatives(inputs);

% STABILITY: ANGLE OF ATTACK DERIVATIVES
%-----

[CDaoa, CLaoa, CMaoa, CMTaoa] = AOA_Derivatives(inputs);

% STABILITY: RATE OF ANGLE OF ATTACK DERIVATIVES
%-----

[CD_Raoa, CL_Raoa, CM_Raoa] = RateAOA_Derivatives(inputs);

% STABILITY: ANGLE OF SIDESLIP DERIVATIVES
%-----

[CYbeta, Clbeta, Cnbeta, CnTbeta] = BETA_Derivatives(inputs);

% STABILITY: RATE OF ANGLE OF SIDESLIP DERIVATIVES
%-----

[CY_Rbeta, Cl_Rbeta, Cn_Rbeta] = RateBETA_Derivatives(inputs);

% STABILITY: ROLL RATE DERIVATIVES
%-----

[CYp, Clp, Cnp] = RollRate_Derivatives(inputs);

% STABILITY: PITCH RATE DERIVATIVES
%-----

[CDq, CLq, CMq] = PitchRate_Derivatives(inputs);

% STABILITY: YAW RATE DERIVATIVES
%-----

[CYr, Clr, Cnr] = YawRate_Derivatives(inputs);

% CONTROL: STABILIZER CONTROL DERIVATIVES
%-----

% CONTROL: ELEVATOR CONTROL DERIVATIVES
%-----

[CDDeltaE, CLDeltaE, CMDeltaE] = ControlElevator_Derivatives(inputs);

% CONTROL: AILERON CONTROL DERIVATIVES
%-----

[CYDeltaA, ClDeltaA, CnDeltaA] = ControlAileron_Derivatives(inputs);

```



```
% CONTROL: RUDDER CONTROL DERIVATIVES
%-----
[CYDeltaR, ClDeltaR, CnDeltaR] = ControlRudder_Derivatives(inputs);

%=====
% Longitudinal Aerodynamic Matrix
longMatrix = [...
    -(CdU + 2*CD1) (-CDaoa + CL1) -CD_Raoa -CDq -CDDeltaE;...
    -(ClU + 2*CL1) (-CLaoa - CD1) -Cl_Raoa -CLq -CLDeltaE;...
    (CMu + 2*CM1) CMaoa CM_Raoa CMq CMDeltaE];

% Lateral-Directional Aerodynamic Matrix
LatDirMatrix = [...
    CYbeta CY_Rbeta CYp CYr CYDeltaA CYDeltaR;...
    Clbeta Cl_Rbeta Clp Clr ClDeltaA ClDeltaR;...
    Cnbeta Cn_Rbeta Cnp Cnr CnDeltaA CnDeltaR];
```

Function files: (to be updated :/ )

```
function [CL_Raoa, CD_Raoa, CM_Raoa] = RateAOA_Derivatives(Xbar_ach, Xbar_cg, Sh, Sref, inputs)
    % STABILITY: RATE OF ANGLE OF ATTACK DERIVATIVES

    % Horizontal tail volume coefficient:
    VBarh = (Xbar_ach - Xbar_cg) * (Sh / Sref);

    % DRAG DUE TO RATE OF ANGLE OF ATTACK: [NEGLECT]
    CD_Raoa = 0;

    % LIFT DUE TO RATE OF ANGLE OF ATTACK:
    CL_Raoa = 2 * CLaoah * nuh * VBarh * (de_daoa);

    % PITCHING MOMENT DUE TO ANGLE OF ATTACK:
    CM_Raoa = -2 * CLaoah * nuh * VBarh * (Xbar_ach - Xbar_cg) * de_daoa;
end

function [CYbeta, Clbeta, Cnbeta] = BETA_Derivatives(Dihedral, Sref, Sv, SweepC4, zw, zf, AR, CLaoav, inputs)
    % STABILITY: ANGLE OF SIDESLIP DERIVATIVES

    % Sideforce wing contribution:
    CYbeta_w = -0.00573 * abs(Dihedral);

    % Sideforce fuselage contribution:
    CYbeta_f = -2 * Ki * (So / Sref);

    % term: (1 + dSigma_dBeta) * nuv :
    termASD1 = 0.724 + (3.06 * ((Sv / Sref) / (1 + cos(SweepC4)))) + (0.4 * (zw / zf)) + (0.009 * AR);

    % Sideforce (Single) vertical tail contribution:
    CYbeta_v = -kv * CLaoav * termASD1 * nuv * (Sv / Sref);

    % Sideforce (Twin) vertical tails contribution:
    % CYbeta_v = -2 * (CYbeta_v_wf / CYbeta_v_eff) * CYbeta_v_eff * (Sv / Sref);

    % SIDEFORCE DUE TO SIDESLIP:
    CYbeta = CYbeta_w + CYbeta_f + CYbeta_v;

    % Rolling moment due to sideslip - wing & fuselage contribution:
    Clbeta_wf = 57.3 * ( CL_wf * ((Clbeta_CL_SweepC4 * kmSweep * kf) + Clbeta_CL_AR) + )
```

	<b>SENIOR DESIGN:</b> MAE 4351 Project	Ref.: MAE 4351-001-2021 Date: 09. Jul. 2023 Name: <b>Gayathri Kola</b> Status: In Progress
---	---	---

```
% Rolling moment due to horizontal tail contribution:  

Clbeta_h = Clbeta_hf * (Sh * bh / Sref * b);  

% Rolling moment due to vertical tail contribution:  

Clbeta_v = CYbeta * ((zv * cos(aoa)) - (lv * sin(aoa)) / b);  

% ROLLING MOMENT DUE TO SIDESLIP: [DIHEDRAL EFFECT]  

Clbeta = Clbeta_wf + Clbeta_h + Clbeta_v;  

% Yawing moment due to sideslip - wing contribution:  

Cnbeta_w = 0;  

% Yawing moment due to sideslip - fuselage contribution:  

Cnbeta_f = -57.3 * KN * Krl * (Sfs * lf / Sref * b);  

% Yawing moment due to sideslip - vertical contribution:  

Cnbeta_v = -CYbeta_v * ((lv * cos(aoa)) + (zv * sin(aoa))) / b;  

% YAWING MOMENT DUE TO SIDESLIP:  

Cnbeta = Cnbeta_w + Cnbeta_f + Cnbeta_v;  

end
```

## References

- [1] 1927 Spirit of St. Louis | Fantasy of Flight. *Fantasy of Flight*. <https://www.fantasyofflight.com/collection/aircraft/currently-not-showing-in-museum/golden-age/1927-spirit-of-st-louis/>. Accessed Jun. 11, 2023.
- [2] Hall, N. "The Spirit of St. Louis." *Advanced Materials & Processes*, Vol. 161, No. 11, 2003, pp. 43–46.
- [3] New Aircraft: Gulfstream G700 | Private Jet Charter®. *Private Jet Charter*. <https://privatejetcharter.com/gulfstream-g700-private-jet-charter/>. Accessed Jun. 11, 2023.
- [4] Miller, L. S. SR-71 RSO Tells the Story of When His Blackbird Photographed All of the SA-2 SAM Sites in North Korea in One Mission before Doing an Emergency Landing in South Korea Because of an Engine Failure. *The Aviation Geek Club*. Accessed Jun. 11, 2023.
- [5] Hermeus. Quarterhorse. *Hermeus*. <https://www.hermeus.com/quarterhorse>.
- [6] Hermeus. Darkhorse. *Hermeus*. <https://www.hermeus.com/darkhorse>.
- [7] DARKHORSE. *Hermeus*. <https://www.hermeus.com/darkhorse>. Accessed Jun. 11, 2023.
- [8] Hermeus. Halcyon. *Hermeus*. <https://www.hermeus.com/halcyon>.
- [9] HALCYON. *Hermeus*. <https://www.hermeus.com/halcyon>. Accessed Jun. 11, 2023.
- [10] Chudoba, D. B. Design Project: Hypersonic Spirit of St. Louis. Jun 06, 2023.
- [11] Junell, W. *Designing a Wing Body Hypersonic Spirit of St. Louis: Detailed Analysis of Vehicle Synthesis and Geometry*. University of Texas at Arlington, Arlington, TX, 2023.
- [12] Blakely, N. *Trans-Atlantic Hypersonic Transport Aircraft: Reimagining the Spirit of St. Louis*. University of Texas at Arlington, Arlington, TX, 2023.
- [13] Leone, D. Tu-144 Vs Concorde: The Concordski Was Bigger and Faster than Its Anglo-French Counterpart, but Its Glory Was Quite Short. Here's Why. *The Aviation Geek Club*. <https://theaviationgeekclub.com/tu-144-vs-concorde-the-concordski-was-bigger-and-faster-than-its-anglo-french-counterpart-but-its-glory-was-quite-short-heres-why/>. Accessed Jun. 23, 2023.
- [14] Chudoba, B. *Stability and Control of Conventional and Unconventional Aerospace Vehicle Configurations: A Generic Approach from Subsonic to Hypersonic Speeds*. Springer International Publishing, Cham, 2019.
- [15] Roskam, D. J. *Airplane Design Part VII: Determination of Stability, Control and Performance Characteristics*. Design, Analysis and Research Corporation, Lawrence, Kansas, 2017.
- [16] Moes, T. R. *Stability and Control Estimation Flight Test Results for the SR-71 Aircraft With Externally Mounted Experiments*. National Aeronautics and Space Administration, Dryden Flight Research Center, 2002.
- [17] Moes, T., Cobleigh, B., Cox, T., Conners, T., Iliff, K., and Powers, B. Flight Stability and Control and Performance Results from the Linear Aerospike SR-71 Experiment (LASRE). Presented at the 23rd Atmospheric Flight Mechanics Conference, Boston, MA, U.S.A., 1998.

	<b>SENIOR DESIGN:</b> MAE 4351 Project	Ref.: MAE 4351-001-2021 Date: 09. Jul. 2023 Name: <b>Gayathri Kola</b> Status: In Progress
---	---	---

- [18] Cox, T. H., and Marshall, A. "Longitudinal Handling Qualities of the Tu-144LL Airplane and Comparisons With Other Large, Supersonic Aircraft." *National Aeronautics and Space Administration, Dryden Flight Research Center*, 2000, p. 44.
- [19] Simon, S. *Development of the Vehicle Configuration Compendium: A Comprehensive Data-Information-Knowledge System to Aid in High-Speed Vehicle Design*. University of Texas at Arlington, 2022.
- [20] Nicolai, L. M., and Carichner, G. E. *Fundamentals of Aircraft and Airship Design*. American Institute of Aeronautics and Astronautics, Inc., Reston, Virginia, 2010.
- [21] Anderson, J. D. *Aircraft Performance & Design*. McGraw-Hill Education, 1999.
- [22] Yechout, T. R., Hallgren, W. F., Morris, S. L., and Bossert, D. E. *Introduction to Aircraft Flight Mechanics Performance, Static Stability, Dynamic Stability, and Classical Feedback Control*. American Institute of Aeronautics and Astronautics, Reston, UNITED STATES, 2003.
- [23] Sadraey, M. H. *Aircraft Design: A Systems Engineering Approach*. Wiley, Chichester, West Sussex, U.K, 2013.
- [24] USAF (United States Air Force) *Stability and Control DATCOM (Data Compendium)*.
- [25] Raymer, D. P. *Aircraft Design: A Conceptual Approach*. American Institute of Aeronautics and Astronautics, Inc, Reston, VA, 2018.
- [26] Roskam, J. *Airplane Flight Dynamics and Automatic Flight Controls*. DARcorporation, 1998.
- [27] Warren Phillips. *Mechanics of Flight*. John Wiley & Sons, Inc., 2004.
- [28] Coleman, C. C., and Faruqi, F. A. "On Stability and Control of Hypersonic Vehicles."
- [29] Coleman, G., and Chudoba, B. A Generic Stability and Control Tool for Conceptual Design, Prototype Styem Overview. In *45th AIAA Aerospace Sciences Meeting and Exhibit*, American Institute of Aeronautics and Astronautics, 2007.
- [30] Coleman, G. J. "A Generic Stability And Control Tool For Flight Vehicle Conceptual Design: Aeromech Software Development." 2007.
- [31] Anderson, Jr, J. D. *Fundamentals of Aerodynamics*. McGraw-Hill Education, 2017.
- [32] Roskam, J. *Airplane Design VI: Preliminary Calculation of Aerodynamic, Thrust and Power Characteristics*. DARcorporation, 1987.
- [33] Coleman, G. *AIRCRAFT CONCEPTUAL DESIGN – AN ADAPTABLE PARAMETRIC SIZING METHODOLOGY*. Dissertation. University of Texas at Arlington, Arlington, TX, 2010.
- [34] Czysz, P., and Vandekerckhove, J. Transatmospheric Launcher Sizing. In *Scramjet Propulsion*, American Institute of Aeronautics and Astronautics (AIAA), 2001.
- [35] Czysz, P., Bruno, C., and Chudoba, B. *Future Spacecraft Propulsion Systems and Integration: Enabling Technologies for Space Exploration*. Springer, Berlin, Heidelberg, 2018.
- [36] Ledford, T., and Harris, C. Hypersonic Convergence. Background and Methodology. Aerospace Vehicle Design (AVD) Laboratory, Feb 08, 2023.
- [37] Chudoba, B., Coleman, G., Oza, A., Gonzalez, L., and Czysz, P. *Solution-Space Screening of a Hypersonic Endurance Demonstrator*. Publication NF1676L-14425. 2012.
- [38] Murthy, T. K. S. *Computational Methods in Hypersonic Aerodynamics*. Springer Dordrecht, 1991.
- [39] Enkenhus, K., Wendt, J. F., and Pankhurst, R. C. *Aerodynamic Problems of Hypersonic Vehicles*. Advisory Group for Aerospace Research and Development (AGARD), 1972.
- [40] Rasmussen, M. *Hypersonic Flow*. Wiley, 1994.
- [41] Anderson Jr., J. D. *Hypersonic and High-Temperature Gas Dynamics, Second Edition*. American Institute of Aeronautics and Astronautics, Reston ,VA, 2006.
- [42] Mexquitic, D. *Designing a Wing-Body Hypersonic Spirit of St. Louis: Aerodynamics, Cost/Market*. University of Texas at Arlington, Arlington, TX, 2023.
- [43] Bartley, S., Urquidi, N., and Lurie, D. XB-70, SR-71, and TU-144: Large Supersonic Transports. Mar 22, 2006.
- [44] Whitman, D. G. "Space Shuttle Orbiter And Subsystems."
- [45] Gordon. Concorde SST. NASA, , 2017.
- [46] Lockheed Martin. *SR-71 Flight Manual*. 1989.
- [47] Chudoba, B., and Cook, M. Trim Equations of Motion for Aircraft Design: Turning Flight, Pull-Up and Push-Over. Presented at the AIAA Atmospheric Flight Mechanics Conference and Exhibit, Austin, Texas, 2003.
- [48] Chudoba, B., and Cook, M. Trim Equations of Motion for Aircraft Design: Steady State Straight Line Flight. Presented at the AIAA Atmospheric Flight Mechanics Conference and Exhibit, Austin, Texas, 2003.

	<b>SENIOR DESIGN:</b> MAE 4351 Project	Ref.: MAE 4351-001-2021 Date: 09. Jul. 2023 Name: <b>Gayathri Kola</b> Status: In Progress
---	---	---

- [49] Roskam, J. *Airplane Design Part I-VII*. DARcorporation, 2002.
- [50] Hawthorne, P. J. *Results of Investigations on a 0.010-Scale 140A/B Configuration Space Shuttle Vehicle Orbiter Model 72-0 in the NASA/Langley Research Center Continuous Flow Hypersonic Tunnel (OA90)*. Publication NASA-CR-141805. 1975.
- [51] Wolowicz, C. H., and Yancey, R. B. *Summary of Stability and Control Characteristics of the XB-70 Airplane*. Publication NASA-TM-X-2933. 1973.
- [52] Wolowicz, C. H., and Yancey, R. B. *Comparisons of Predictions of the XB-70-1 Longitudinal Stability and Control Derivatives with Flight Results for Six Flight Conditions*. Publication NASA-TM-X-2881. 1973.
- [53] Dynamics of Flight: Stability and Control, 3rd Edition | Wiley. *Wiley.com*. <https://www.wiley.com/en-us/Dynamics+of+Flight%3A+Stability+and+Control%2C+3rd+Edition-p-9780471034186>. Accessed Jun. 18, 2023.
- [54] Leishman, J. G. “Flying Fast – Supersonic & Hypersonic Flight.” 2023. <https://doi.org/10.15394/eaglepub.2022.1066.n43>.
- [55] Roskam, J. *Airplane Design: Preliminary Sizing of Airplanes*. DARcorporation, 1985.
- [56] Mc Mahon, M. C., and Wentz, W. H. *An Experimental Investigation of the Flow Fields about Delta and Double-Delta Wings at Low Speeds*. Publication NASA-CR-521. 1966.
- [57] Goecke, S. A., Pembo, C., and Saltzman, E. J. *Base Pressure Measurements on the XB-70 Airplane at Mach Numbers from 0.4 to 3.0*. Publication NASA-TM-X-1612. 1968.
- [58] Aprovitola, A., Dyblenko, O., Pezzella, G., and Viviani, A. “Aerodynamic Analysis of a Supersonic Transport Aircraft at Low and High Speed Flow Conditions.” *Aerospace*, Vol. 9, No. 8, 2022, p. 411. <https://doi.org/10.3390/aerospace9080411>.
- [59] Samoylovitch, O., and Strelets, D. “Determination of the Oswald Efficiency Factor at the Aeroplane Design Preliminary Stage.” *Aircraft Design*, 2000.
- [60] Aerodynamic Study of the NASA’s X-43A Hypersonic Aircraft. <https://www.mdpi.com/2076-3417/10/22/8211>. Accessed Jun. 23, 2023.
- [61] OpenFOAM. <https://www.openfoam.com/>. Accessed Jun. 23, 2023.
- [62] OpenVSP. <https://openvsp.org/>. Accessed Jun. 23, 2023.